

Air Force Institute of Technology

AFIT Scholar

Theses and Dissertations

Student Graduate Works

12-1995

Analysis and Interpretation of Ion Data Associated with Neutral Gas Releases in the Earth's Ionosphere

Timothy M. Shadid

Follow this and additional works at: <https://scholar.afit.edu/etd>



Part of the [Atmospheric Sciences Commons](#), and the [Electromagnetics and Photonics Commons](#)

Recommended Citation

Shadid, Timothy M., "Analysis and Interpretation of Ion Data Associated with Neutral Gas Releases in the Earth's Ionosphere" (1995). *Theses and Dissertations*. 6134.

<https://scholar.afit.edu/etd/6134>

This Thesis is brought to you for free and open access by the Student Graduate Works at AFIT Scholar. It has been accepted for inclusion in Theses and Dissertations by an authorized administrator of AFIT Scholar. For more information, please contact AFIT.ENWL.Repository@us.af.mil.



DTIC
SELECTED
JAN 22 1996
S D
G

ANALYSIS AND INTERPRETATION OF ION DATA
ASSOCIATED WITH NEUTRAL GAS RELEASES
IN THE EARTH'S IONOSPHERE

THESIS

Timothy M. Shadid, Captain, USAF

AFIT/GAP/ENP/95D-12

19960118 038

DEPARTMENT OF THE AIR FORCE
AIR UNIVERSITY
AIR FORCE INSTITUTE OF TECHNOLOGY

DTIC QUALITY INSPECTED 3

Wright-Patterson Air Force Base, Ohio

DISTRIBUTION STATEMENT A

Approved for public release;
Distribution Unlimited

AFIT/GAP/ENP/95D-12

ANALYSIS AND INTERPRETATION OF ION DATA
ASSOCIATED WITH NEUTRAL GAS RELEASES
IN THE EARTH'S IONOSPHERE

THESIS

Timothy M. Shadid, Captain, USAF

AFIT/GAP/ENP/95D-12

Accession For	
NTIS CRA&I	<input checked="" type="checkbox"/>
DTIC TAB	<input checked="" type="checkbox"/>
Unannounced	<input type="checkbox"/>
Justification	
By	
Distribution /	
Availability Codes	
Dist	Avail and/or Special
A-1	

Approved for public release; distribution unlimited

DTIC QUALITY INSPECTED 3

AFIT/GAP/ENP/95D-12

ANALYSIS AND INTERPRETATION OF ION DATA
ASSOCIATED WITH NEUTRAL GAS RELEASES
IN THE EARTH'S IONOSPHERE

THESIS

Presented to the Faculty of the School of Engineering

Air Education and Training Command

In Partial Fulfillment of the

Requirement for the Degree of

Master of Science

Timothy M. Shadid, B.S.

Captain, USAF

December 1995

Approved for public release; distribution unlimited

AFIT/GAP/ENP/95D-12

ANALYSIS AND INTERPRETATION OF ION DATA
ASSOCIATED WITH NEUTRAL GAS RELEASES
IN THE EARTH'S IONOSPHERE

Timothy M. Shadid, B.S.
Captain, USAF

Approved:



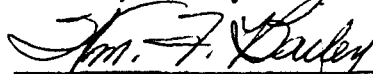
Paul J. Wolf, Lt Col, USAF
Chairman, Advisory Committee

1 DEC 95



Donald E. Hunton
Member, Advisory Committee

1 Dec 95



William F. Bailey
Member, Advisory Committee

1 Dec 95

Acknowledgments

I first would like to thank my thesis advisor, Lieutenant Colonel Paul J. Wolf. His invaluable guidance throughout the spring, summer, and fall enabled me to progress from wondering how a thesis and thesis research are accomplished to actually arriving at this finished product. My sponsor was Dr. Donald E. Hunton of the Geophysics Directorate at Phillips Laboratory. His explanations and reassurances through many phone calls and electronic mail messages allowed me to make the progress presented here. The last member of my committee, Dr. William F. Bailey, has given me help and much needed encouragement not only during this research, but also throughout the preceding coursework.

Several faculty provided valuable support as well. Captain Cliff Dungey was tireless in his efforts, helping me get a thesis topic, providing advice, and yielding his office and computer to me on several occasions. Dr. David Weeks, Captain Derrill Goldizen, and Captain Jeffrey Martin also gave me generous portions of their time. The administrative help that I received was just as important. Ms. Diana Jordan was always available to help ensure a professional looking thesis and Ms. Karen Dobbyn provided "speedy" assistance on several occasions when I needed to rapidly transport or receive items to and from Phillips Laboratory.

Foremost throughout this arduous process has been the friendship given to me, from both those above as well as others. My parents, William and Nancy Shadid, received many phone calls at odd times and put up with my irritability and frustration. The rest of my family--Don, Janet, Bill, and Peggy, my friend Leslie Lash, and other close friends suffered the same. I also thank the parish of St. Paul the Apostle Orthodox Christian Church, who made a home for me here in Dayton. Most importantly, I thank God for giving me everything that allowed me to produce this work and permitting me to enter the lives of so many wonderful people.

Timothy M. Shadid

Table of Contents

	Page
Acknowledgements	iv
List of Figures	vii
List of Tables	viii
List of Notations	ix
Abstract	x
1. Introduction.....	1
1.1 Opening Description	1
1.2 Statement of Problem.....	2
1.3 History of Experiment.....	6
2. CRRES Chemical Release	7
2.1 QIMS Instrument	7
2.2 Satellite Orbital Factors	11
2.3 Release Description	12
2.4 Cloud Expansion.....	16
2.5 Transverse Motion Across Magnetic Field Lines	20
2.6 Snowplow Effect.....	23
3. Background Theory	26
3.1 Ionospheric Chemistry	26
3.2 Selection of Barium and Strontium.....	28
4. Approach to Modeling Problem.....	30
4.1 Initial Basic Model: Description and Analysis	30
4.2 Consideration of Assumptions.....	37
4.3 Validation of Initial Model and Normalization	40
4.4 Rotation of Spacecraft.....	41

5. Discussion of Results.....	44
5.1 Research into Ionization Mechanisms	44
5.1.1 Photoionization	44
5.1.2 Charge Exchange	47
5.1.3 Electron Impact.....	50
5.1.4 Associative Ionization.....	51
5.1.5 Charge Stripping.....	54
5.1.6 Thermal Ionization and Population of Metastable States from Thermite Burn.....	55
5.2 Comparison of Modeled Processes to Experimental Data.....	55
5.2.1 Photoionization	56
5.2.2 Charge Exchange	57
5.2.3 Electron Impact.....	61
5.2.4 Charge Stripping.....	64
5.3 Investigation of Twin Peaks at First Maximum.....	68
6. Synopsis.....	74
6.1 Summary of Results.....	74
6.2 Conclusions.....	75
Appendix A: Investigation into CIV.....	79
A.1 Critical Ionization Velocity.....	79
A.2 Summary of CIV Importance to CRRES Releases.....	89
Appendix B: Modeling of CRRES Data.....	91
Appendix C: Calculation of Basic Parameters.....	128
Bibliography	130
Vita.....	135

List of Figures

Figure	Page
1. CRRES G-1 and G-11b Release Locations	5
2. QIMS Ion Data.....	8
3. QIMS Position on CRRES.....	9-10
4. Terminator Crossings.....	13
5. Release Geometry	15
6. Cloud Expansion.....	18-19
7. Ratio of Ba ⁺ to Sr ⁺	21
8. Oxygen Ion Data.....	24
9. Neutral Density Plot.....	34
10. Radius in Spacecraft Reference Frame	36
11. Parallel Velocity Component.....	39
12. Normalization of Barium Model to G-1 (sunlit) Data	42
13. Barium Model with Rotation Compared to Data and Basic Model.....	42
14. Comparison of Photoionization Model with Data	57
15. Comparison of Charge Exchange Model with Data.	58-59
16. Comparison of Electron Impact Model with Data.....	62-63
17. Comparison of Charge Stripping Model with Data	65-66
18. Twin Peaks at First Maximum.....	69-70

List of Tables

Table	Page
1. Conditions for CRRES G-1 and G-11b Releases	4
2. Required Cross Sections for Charge Stripping to Match Data	67
3. Summary of CRRES Modeling Results.....	75
A-1. Summary of CRRES CIV Determining Factors.....	90

List of Notations

<u>Full Text</u>	<u>Abbreviation</u>
Combined Release and Radiation Effects Satellite.....	CRRES
Quadrupole Ion Mass Spectrometer.....	QIMS
critical ionization velocity.....	CIV
charge exchange.....	CE
electron impact ionization.....	EI
associative ionization.....	AI
barium, barium ion.....	Ba, Ba ⁺
strontium, strontium ion.....	Sr, Sr ⁺
neutral atomic oxygen.....	O
atomic oxygen ion.....	O ⁺
ultraviolet.....	UV
atomic mass unit.....	amu
centimeter.....	cm
meter.....	m
kilometer.....	km
kilogram.....	kg
second.....	s
electron volt.....	eV

Abstract

Barium and strontium release experiments were conducted throughout 1991 from the Combined Release and Radiation Effects Satellite (CRRES) to study both natural and man-made disturbances in the earth's ionosphere. A mass spectrometer mounted on the spacecraft counted the Ba and Sr ions as the cloud expanded through the satellite's path. In this study, data from the G-1 (in sunlight) and G-11b (in darkness) releases were chosen and were modeled to understand the source of the ion signals. The model appeared to reproduce the Ba⁺ sun data reasonably well assuming photoionization ($\tau = 28$ s) was the primary ionization mechanism. However, it was not able to account for the remaining ion data in sunlight or darkness: (a) Sr has a very long photoionization time constant from the ground state ($\tau = 1920$ s) and model/data comparisons showed that the Sr ionization rate must be ≈ 60 times greater than the photoionization rate to account for the observed signals. (b) The charge transfer ionization process between ground state atoms and ambient O⁺ were not sufficient to reproduce the ionization rates for Sr sun data and Sr/Ba dark data. The model results better approximated the data for both atoms when ionization originated from populated metastable levels but still fell short of matching experimental results. Speculation is made as to what other processes could have been responsible for the CRRES data. Possibilities include either charge stripping or Alfvén's critical velocity ionization (CIV), neither of which are well understood. A peculiarity of the data in the form of twin peaks in the first maximum of the spectrometer flux counts was also investigated. Either an instrument sensitivity problem or a two process mechanism appears to be responsible. Due to insufficient information concerning experiment conditions, though, a firm determination is not available.

ANALYSIS AND INTERPRETATION OF ION DATA ASSOCIATED WITH NEUTRAL GAS RELEASES IN THE EARTH'S IONOSPHERE

1. INTRODUCTION

1.1 Opening Description

In the summer of 1991, natural and man-made disturbances in the earth's ionosphere were studied utilizing instrumentation on board the Combined Release and Radiation Effects Satellite (CRRES). Neutral particles, consisting of barium doped with strontium in a thermite mixture, were contained in 24 canisters carried by the satellite. These canisters were released at several positions and times over the Caribbean Ocean and subsequently detonated, dispersing the contents. Instruments on board CRRES coupled with ground based and aircraft mounted equipment were used to observe the resulting cloud. Observations centered around noting the effect on the surrounding ionosphere as well as the investigation of space plasma issues (Hunton, 1993). A particular goal was to gather evidence for the "critical ionization velocity" (CIV) effect, an ionization process hypothesized by Hannes Alfvén. The basic idea of the hypothesis is that if neutral particles flow through a plasma with a kinetic energy at least as great as the ionization potential of the atom, very rapid ionization will take place. Injecting neutral gases into the ionosphere at the satellite orbital velocity provided an environment favorable to testing this concept.

1.2 Statement of Problem

The releases and associated experiments conducted with the twenty-four chemical canisters were labeled G-1 through G-14 (some involved the ejection of multiple canisters). Dr. D. E. Hunton of the Air Force Phillips Laboratory on Hanscom AFB, MA had for some time been working with data from an ion mass spectrometer on board the satellite which measured ion counts from the cloud during the release experiments. He had developed a mathematical model to simulate the flow of neutrals and the formation of ions at the spacecraft location. The goal of this thesis was to use this model to mathematically reproduce the ion counts data obtained from the CRRES satellite, specifically during the G-1 and G-11b experiments. Determination of the ionization processes responsible for these ions was the ultimate objective.

The G-1 and G-11b releases and their associated data sets were chosen as the subject of this investigation. They were alike in all but one respect. The relevant data for each of the experiments are listed in Table 1 (Hunton, personal communication and Stenbaek-Nielsen et al., 1993). The releases were conducted at nearly identical altitudes--495 and 478 kilometers (km) respectively. This is just above the F2 region maximum, or the location of maximum plasma density in the ionosphere. This relatively low height represents an advantage to studying ionization in the ambient environment, since relative concentrations of the ionospheric constituents can be specified with greater accuracy at these altitudes than at the much higher levels of other releases. Both releases also involved a neutral gas injection velocity nearly perpendicular to the geomagnetic field lines and the angle between the spin axis and the velocity vector varied by only 3 degrees

between the two situations. Last, the same masses of materials were placed inside each of the canisters. The only major factor that changed between the two experiments was the presence of sunlight. G-1 occurred near the solar terminator (line dividing night and day) on the sunlit side, and G-11b was executed also near the terminator but on the dark side. These circumstances are shown pictorially in Fig. 1.

As stated above, one of the initial reasons for undertaking the chemical release mission of CRRES was to gather evidence for CIV. This process, through a transfer of energy from neutrals released at the satellite orbital speed to electrons, enables the resultant high energy electrons to rapidly ionize the neutrals as well as produce high kinetic temperatures. As part of this thesis, I initially spent a large amount of time researching CIV and analyzing the G-1 and G-11b releases to determine if CIV had occurred. This research is covered in some detail in Appendix A. As is explained there, CIV occurrence would probably have been limited to very early times, before the gases released and ions formed from those gases reached the spectrometer on board the satellite. However, elevated temperatures resulting from this process could have accelerated ionization at later times, in ways which I will address in this paper. The end result of the research discussed in Appendix A was that CIV occurrence is undetermined, although there is more evidence pointing to its absence than its presence. For details on this result and an in-depth explanation of CIV, see the appendix.

Table 1: Conditions for CRRES G-1 and G-11b Releases

	<u>G-1</u>	<u>G-11b</u>
Date	July 13, 1991	July 25, 1991
UT (hh:mm:ss.s)	08:35:25.5	08:37:11.1
UT (s)	30925.5	31031.1
Altitude (km)	495	478
Latitude (degrees)	17.8 N	17.3 N
Longitude (degrees)	62.9 W	69.5 W
Light Conditions	Dawn, sunlit	Dawn, darkness
Titanium Mass (kg)	1.269	1.27
Boron Mass (kg)	0.572	0.573
Barium Mass (kg)	1.468	1.471
Strontium Mass (kg)	0.019	0.019
Total Neutral Density (m⁻³)	6x10 ¹³	5x10 ¹³
Total Electron Density (m⁻³)	5x10 ¹¹	7x10 ¹¹
Spacecraft Velocity (m/s)	9.97x10 ³	9.98x10 ³
Spacecraft Velocity Perpendicular to Magnetic Field (m/s)	9.94x10 ³	9.95x10 ³
Magnetic Field Strength (Tesla)	3.11x10 ⁻⁵	3.19x10 ⁻⁵
Magnetic Field Injection Angle (degrees)	95	95
Angle Between Spin Axis and Velocity Vector (degrees)	29	26

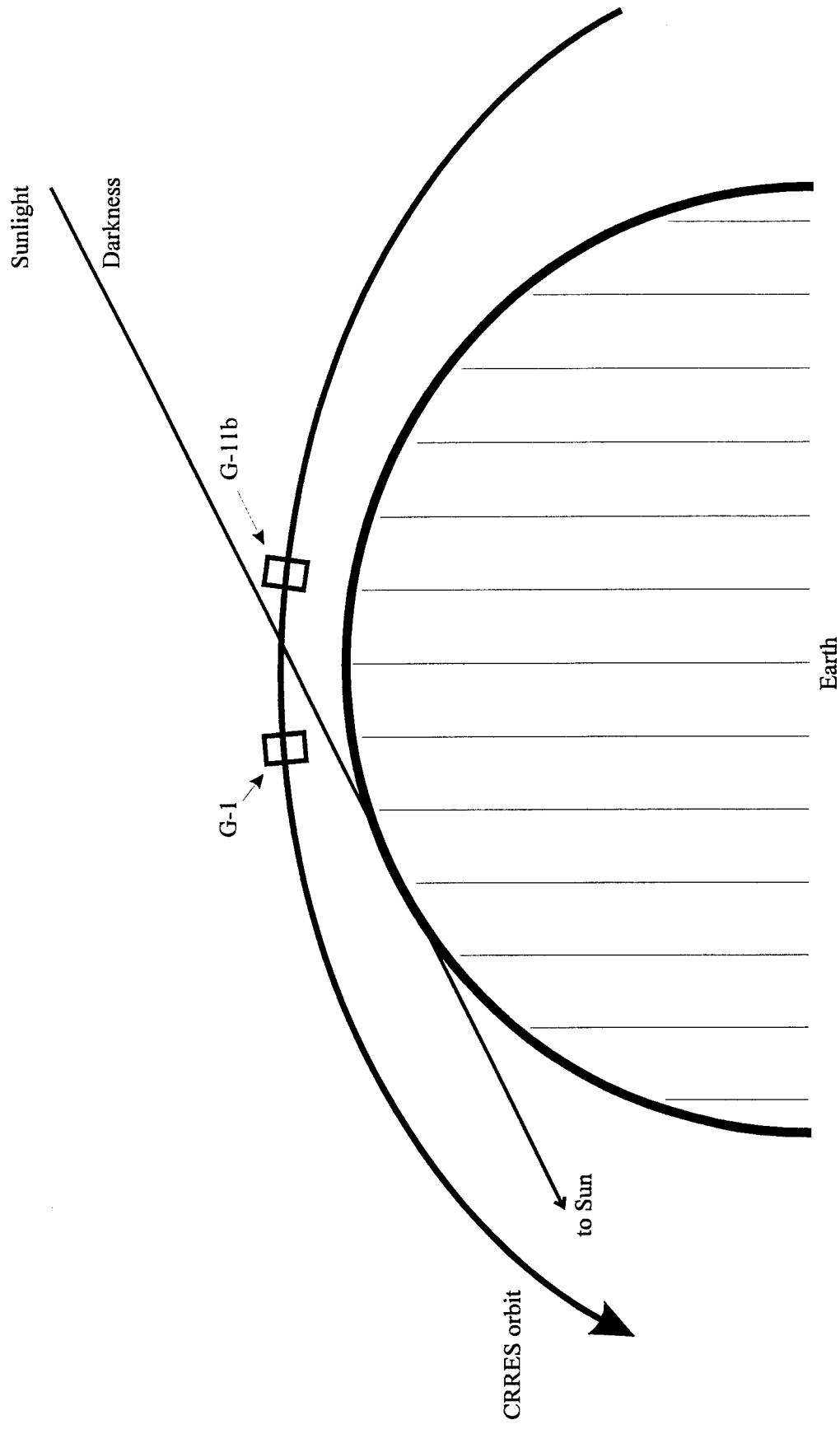


Figure 1. CRRES G-1 and G-11b Release Locations

1.3 History of Experiment

The CRRES program is the unification of three different projects initiated by three organizations. The Air Force space community had an interest in radiation and discharge effects on satellite microelectronics in the ionosphere, while the National Aeronautical and Space Administration (NASA) was concerned with chemical releases in order to understand chemical processes in the upper atmosphere. In addition, scientists at the Air Force's Phillips Laboratory on Hanscom AFB, MA constructed a low altitude satellite study of ionospheric irregularities (LASSII) experiment to investigate both naturally occurring and artificially created perturbations in the ionosphere and their effects on radio signals propagating through the ionosphere (Rodriguez, 1992). These three programs together resulted in the CRRES satellite. This coalescence occurred in 1982, with the Air Force funding the satellite and NASA funding the launch (Vampola, 1992).

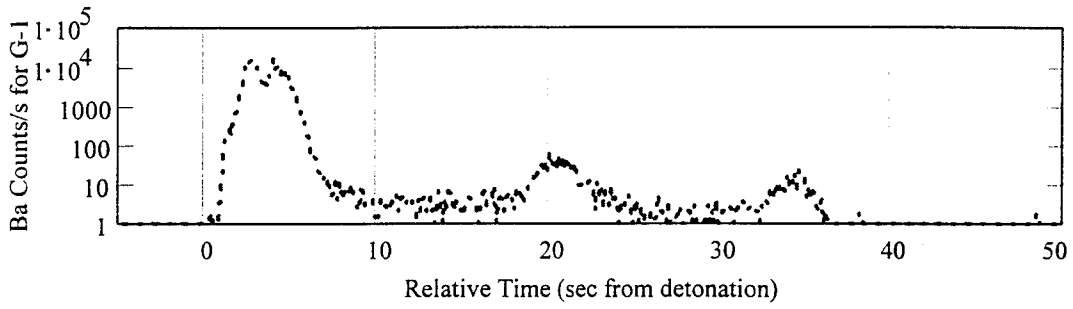
CRRES was originally slated to be launched as a Space Shuttle payload in June 1986, but the Challenger accident earlier that year forced planners to eliminate it from the NASA schedule. The Atlas-Centaur was chosen as the new launch vehicle, and launch finally occurred on July 25, 1990 from Cape Canaveral. The satellite was inserted directly into an elliptical geosynchronous transfer orbit. (Vampola, 1992; Reasoner, 1992)

2. CRRES Chemical Release

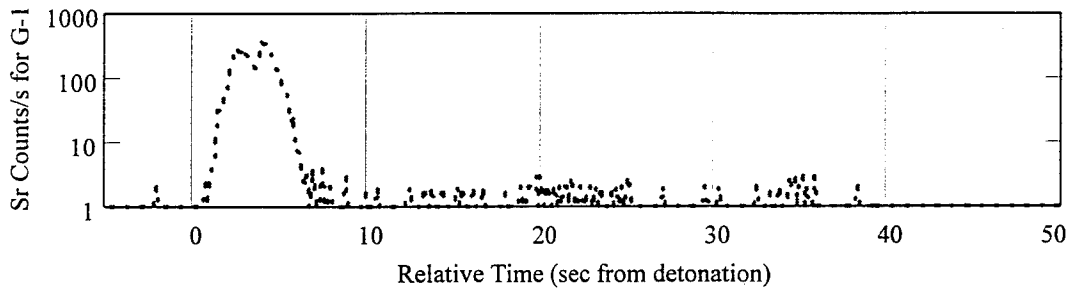
2.1 QIMS Instrument

Relative ion fluxes (counts s^{-1}) measured from the quadrupole ion mass spectrometer (QIMS) are the data that are investigated in this thesis. Ba^+ and Sr^+ counts for G-1 and G-11b are shown in Fig. 2. Here the relative counts (counts per second) measured by the spectrometer can be seen. A steady fall-off in the data represents the decrease in neutral densities as the neutral cloud expanded and rarified. The separation between peaks instead of a steady decrease is due to satellite rotation and will be discussed in the modeling section. The last feature to point out is a split double peak in the first major maximum in each of the data sets. This peak was analyzed in the latter part of the research and this work will be addressed in the discussion of results.

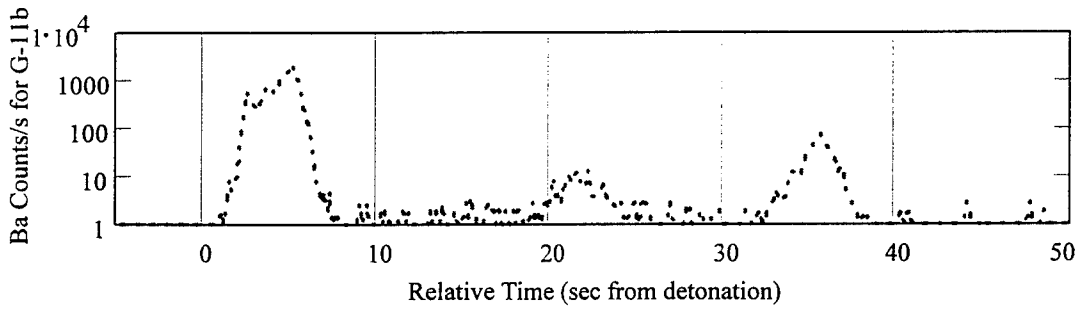
Fig. 3 a - c shows the instrument and its position on the satellite. It was mounted on the top deck of CRRES and pointed radially outward, perpendicular to the spin axis of the spacecraft. QIMS remained turned off at all times except during perigee of the orbit, which is where the chemical release experiments of interest to this thesis occurred. The aperture plate, which was biased at a potential of -10 volts, was uncovered at the beginning of the mission and remained uncovered. The spectrometer is capable of measuring particle masses from 4 to 155 atomic mass units (amu's) with energies from 0 to 100 electron volts (eV). The mass resolution is also more than adequate to differentiate between all ions of significant number density. (Trzcinski et al., 1992)



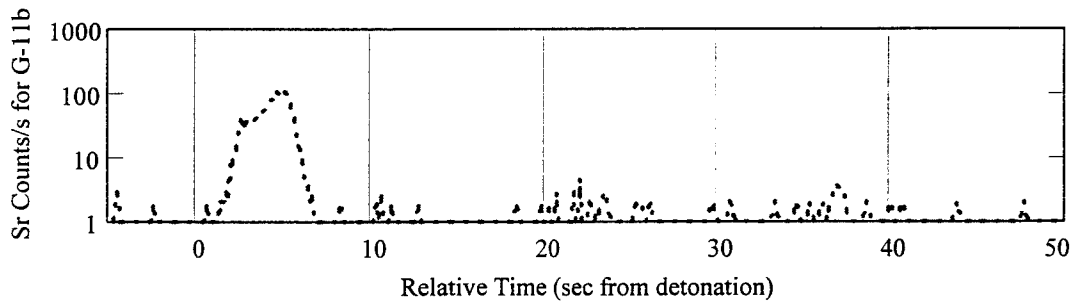
(a) Barium Flux in G-1



(b) Strontium Flux in G-1

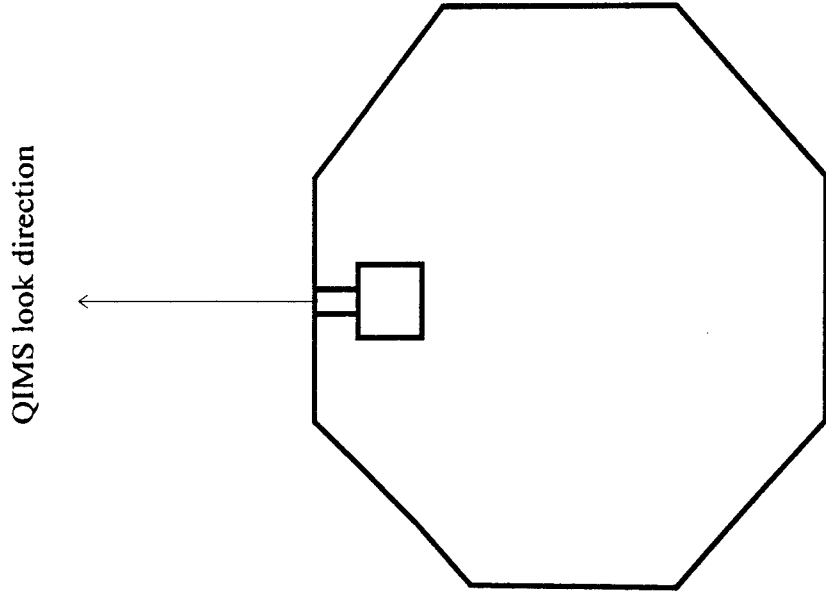


(c) Barium Flux in G-11b

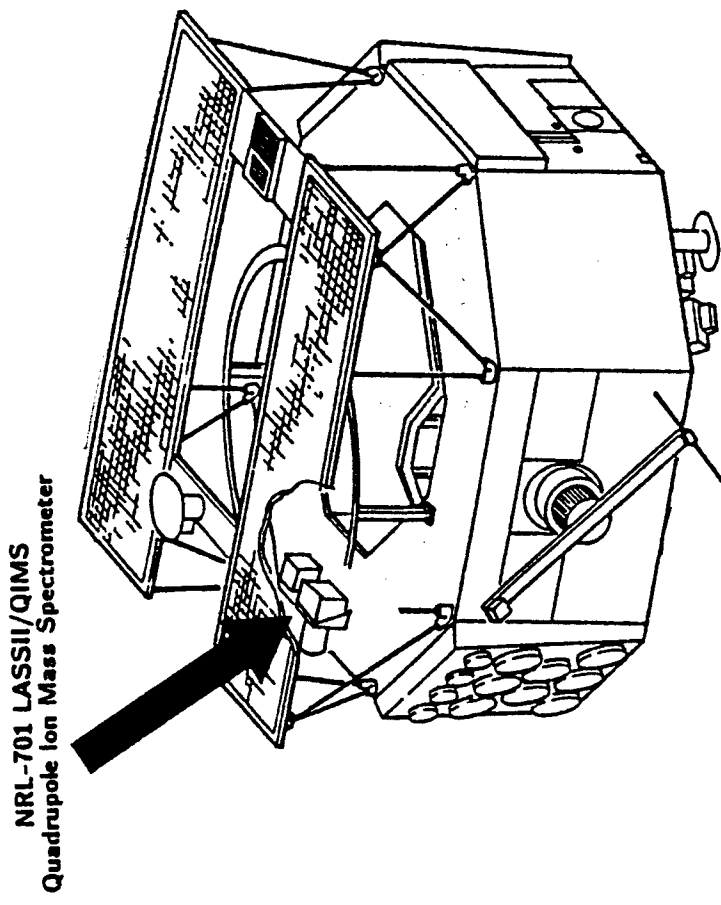


(d) Strontium Flux in G-11b

Figure 2. QIMS Ion Data



(b) Top View



(a) CRRES Cutaway View

Figure 3. QIMS Position on CRRES

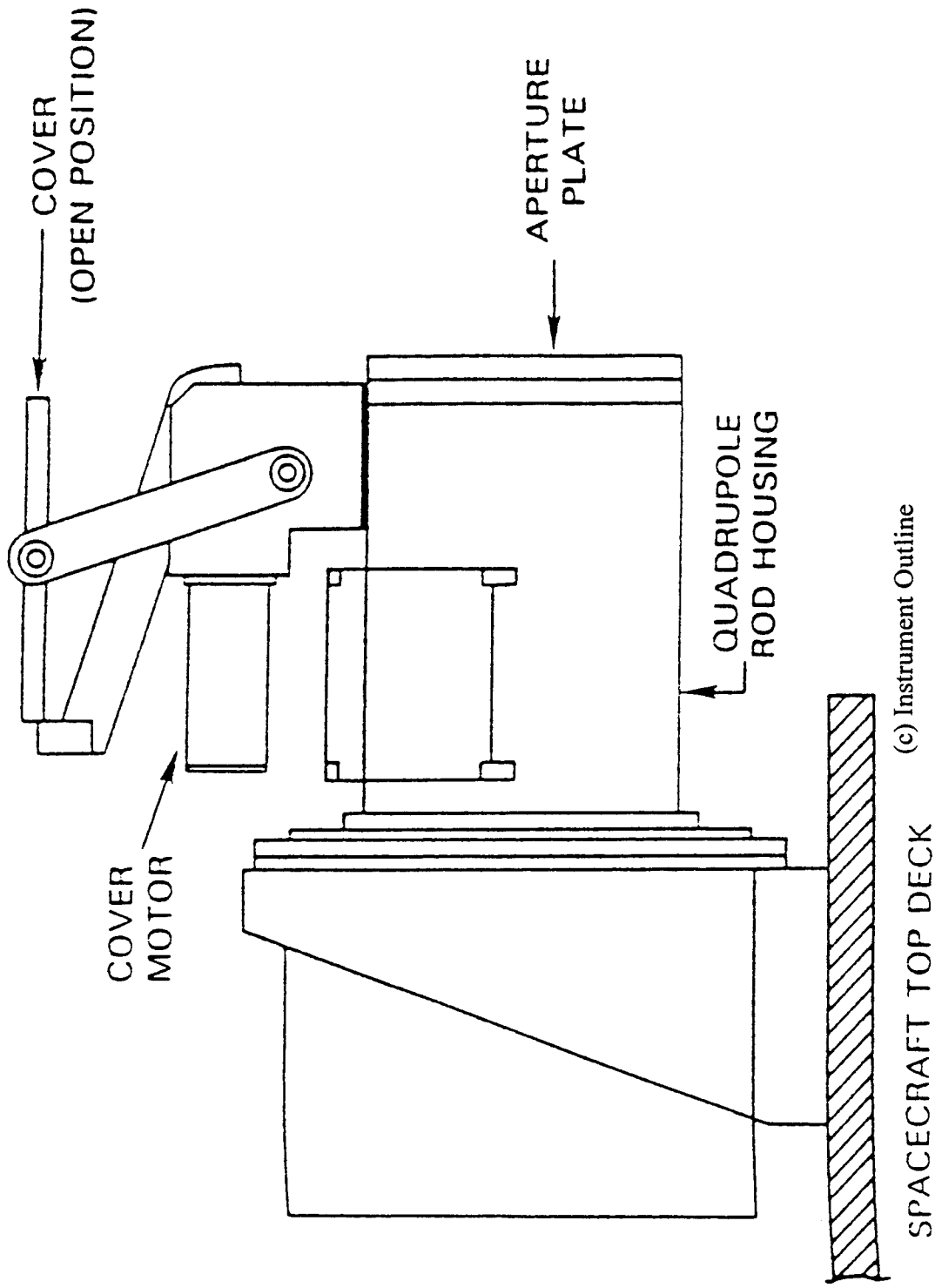


Figure 3. QIMS Position on CRRES

2.2 Satellite Orbital Factors

The CRRES experiments were conducted from a geosynchronous transfer orbit. This elliptical path took the satellite through a perigee of 350 km and an apogee of 33600 km (Bernhardt, 1992). An orbit of this geometry results in a maximum velocity at perigee of around 10 kilometers per second (km/s). This velocity is important, since it is much greater than both the velocity given to the particles upon detonation as well as the speed of the ambient ionospheric particles. The chemical experiments of concern in this thesis were conducted at orbit perigee and thus the neutral gases released were given approximately 3 times the kinetic energy required for the CIV effect.

The placement of the G-1 and G-11b releases on opposite sides of the solar terminator facilitated studying the two experiments with a single variable factor--sunlight. G-11b was positioned near the dawn terminator so as to cross into sunlight a short time after release and allow aircraft and ground observers to record emissions from the neutral cloud and the ionization products. The timing of the cloud's movement into regions illuminated by various portions of the solar spectrum is depicted in Fig. 4. For the release initiated in darkness (G-11b), CRRES crossed the geometric terminator 10 seconds after detonation of the canister. The geometric terminator is the straight-line path drawn from the sun's surface (the photosphere) to the edge of the earth and beyond. Portions of the sun's spectrum are visible to a satellite before reaching the geometric terminator due to diffraction. The exact point where energy from the sun becomes available depends on the particular frequency of light being observed. The ultraviolet (UV) terminator, the line beyond which UV light first becomes visible, was penetrated at 20 seconds. In the model

used in this thesis, the spacecraft and cloud are assumed to be exposed to slight amounts of UV light before crossing the terminator due to reflection of radiation from matter across the terminator. Finally, the spacecraft was in full intensity UV after 30 seconds. (Hunton, personal communication) Since the light which photoionizes barium lies in the UV band, it is not until this radiation is present that photoionization begins. The modeling of this gradual transition to photoionization is included in Appendix B in order to show the effect of the transition on the model and ionization in the cloud.

2.3 Release Description

As mentioned earlier, the gases were released in a thermite mixture. Thermite is a mixture of titanium and boron required to vaporize the barium and strontium since they were in solid form within the canisters. The vaporization and dispersal of the barium and strontium mixture were brought about by the following reaction:



which yields enough heat to produce the metal vapor cloud for the experiment from the solid matter inside the canister (Reasoner, 1992). Vaporization of the cloud in the immediate vicinity of the spectrometer would have been advantageous in that ionization products could be counted when neutral densities were at their highest values. However, certain hazards prevented the canister detonation from being executed close to the satellite. In addition to high energy particle impact effects from the explosion, scientists were concerned about possible coating of the CRRES instruments with neutral and charged particles from the cloud. The canister was ejected from the satellite and a timer

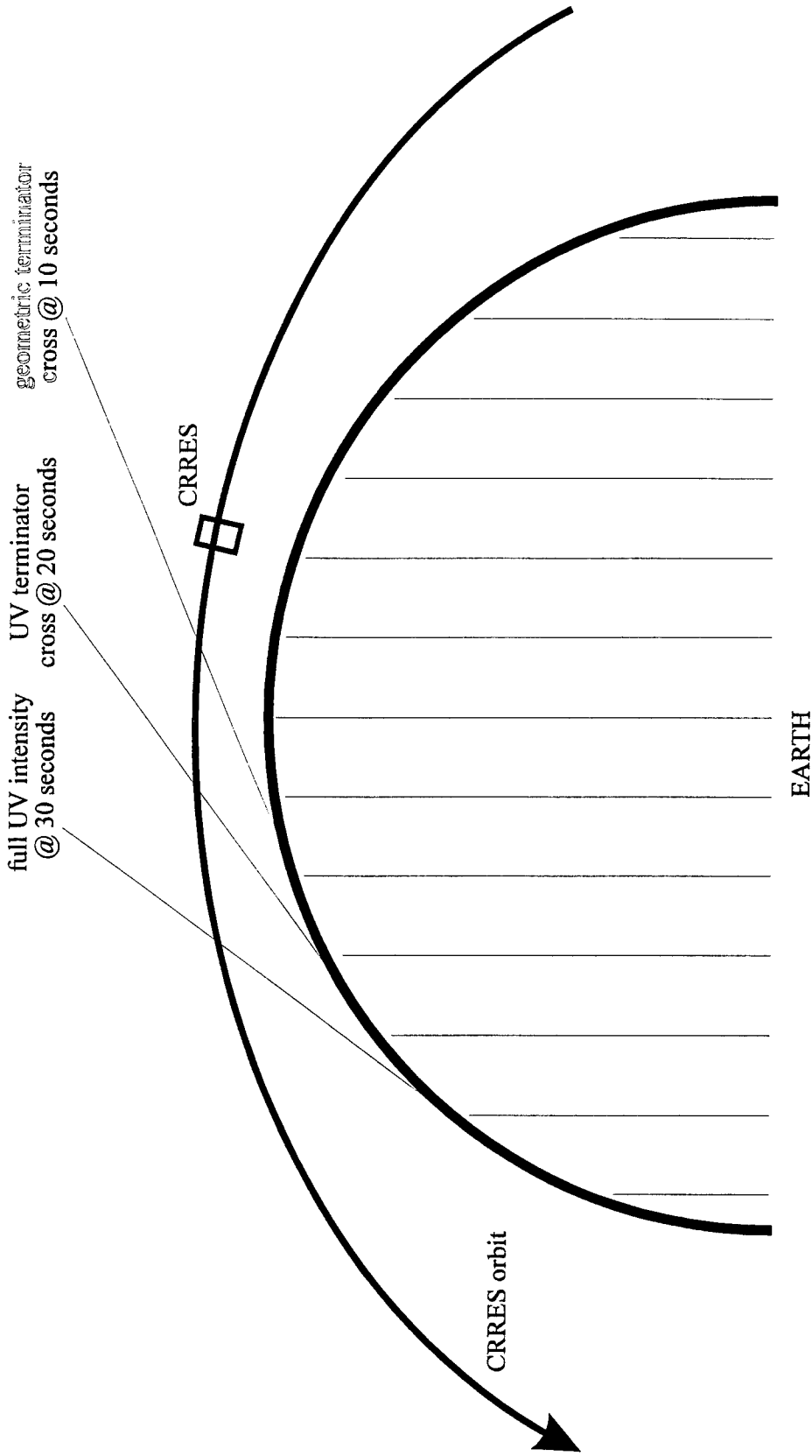
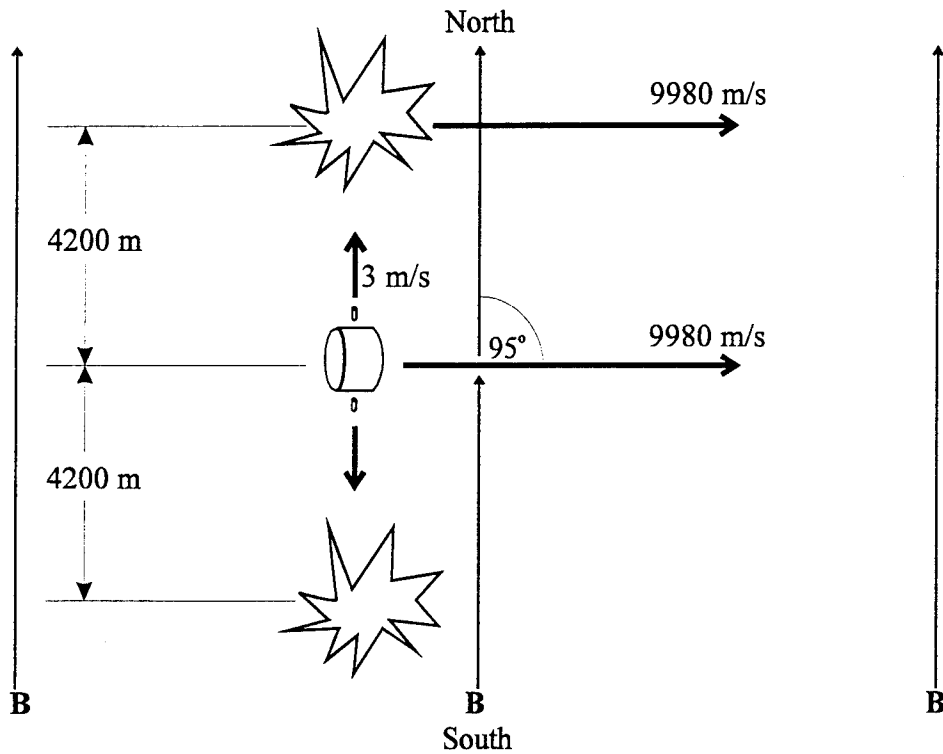


Figure 4: Terminator Crossings

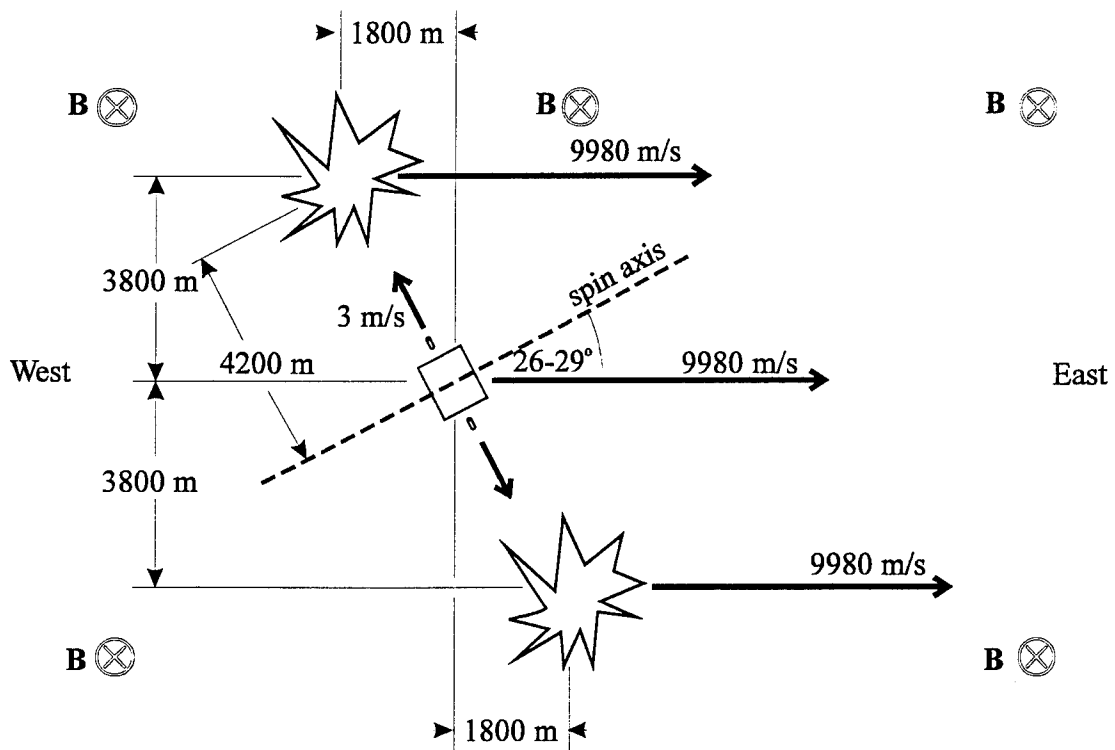
counted down from approximately 1498 seconds before detonation (Johnson and Kierein, 1992). This allowed the canister to reach a distance of 3.8 to 4.2 km from CRRES, depending on the specific geometry (see next paragraph), before the thermite ignited. (Hunton, 1993)

The injection geometry can be seen in Fig. 5. The G-1 and G-11b releases were very similar in this respect and so the same figure will be used to describe both. As is evident, the satellite velocity vector was about 95 degrees off of the magnetic field vector, which points from south to north (Stenbaek-Nielsen et al. 1993). Also, the spin axis was at a 26 degree angle to the velocity vector (Hunton, personal communication). What this means is that both the ejection module and QIMS varied with respect to their orientation to the magnetic field as the satellite rotated. The range of this angle is from 21 to 159 degrees.

This variation with satellite rotation has two implications. First, it is not known exactly which direction the ejection module was pointing when the canister was fired in each release. As indicated in Fig. 5 (a), if the ejection module fired when exactly perpendicular to the satellite velocity vector, then the 1498 second timer allowed the canister to reach a point 4.2 km from the satellite at a point exactly alongside CRRES in its orbit (neither ahead nor behind). The figure shows 2 canisters being ejected in order to represent either of the possible directions of travel in this situation. The other extreme occurred if the canister was at either end of the possible range of angles (21 or 159 degrees). Then it would have ended up 3.8 km over and 1.8 km either ahead of or behind the spacecraft, as depicted in part (b) of the figure. Again, the 2 canisters demonstrate both possible results of this situation--a cloud center of mass ahead of or behind CRRES.



(a) Conditions for Detonation Alongside CRRES



(b) Conditions for Detonation Ahead of or Behind CRRES

Figure 5. Release Geometry

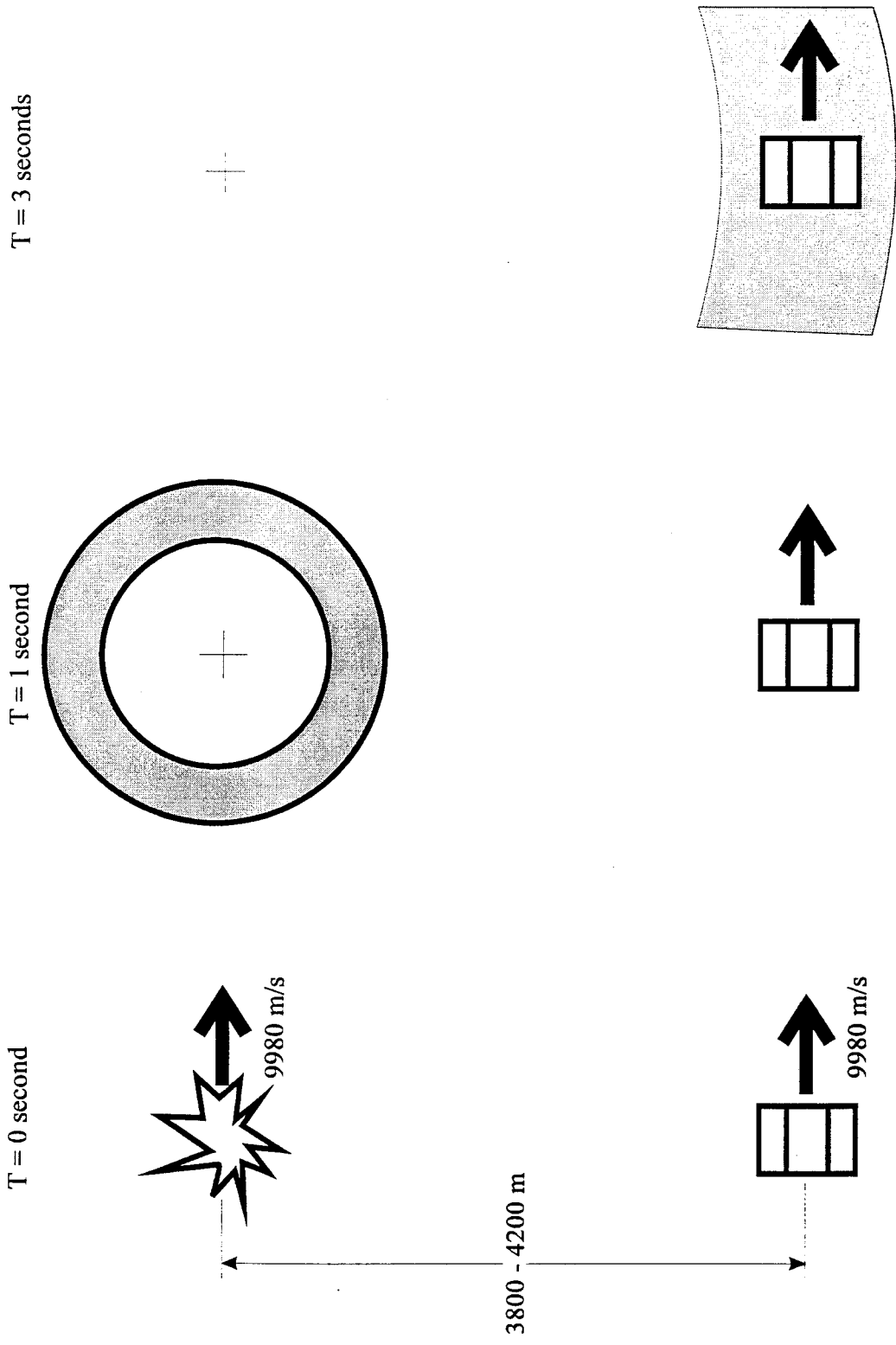
Any injection angle inside this range would yield a geometry between these two limits. This affects the mathematical simulation of the cloud movement used in the ion density model, altering both the timing of when the cloud reaches CRRES as well as the neutral density magnitudes seen at the satellite position. For the studies completed here, the average position was taken, assuming the detonation point to be exactly 4.2 km directly across from where the canister was ejected. The second implication is the fact that the cloud center of mass was in a different orbit than the one in which the canister started. If it was in a higher or lower orbit, its orbital velocity would of course have been different. Since a difference of around 4 km is small compared to the distance from the center of the earth (which is the relevant radius that determines the orbital velocity) and also since the new orbit is unknown, we ignored this factor.

2.4 Cloud Expansion

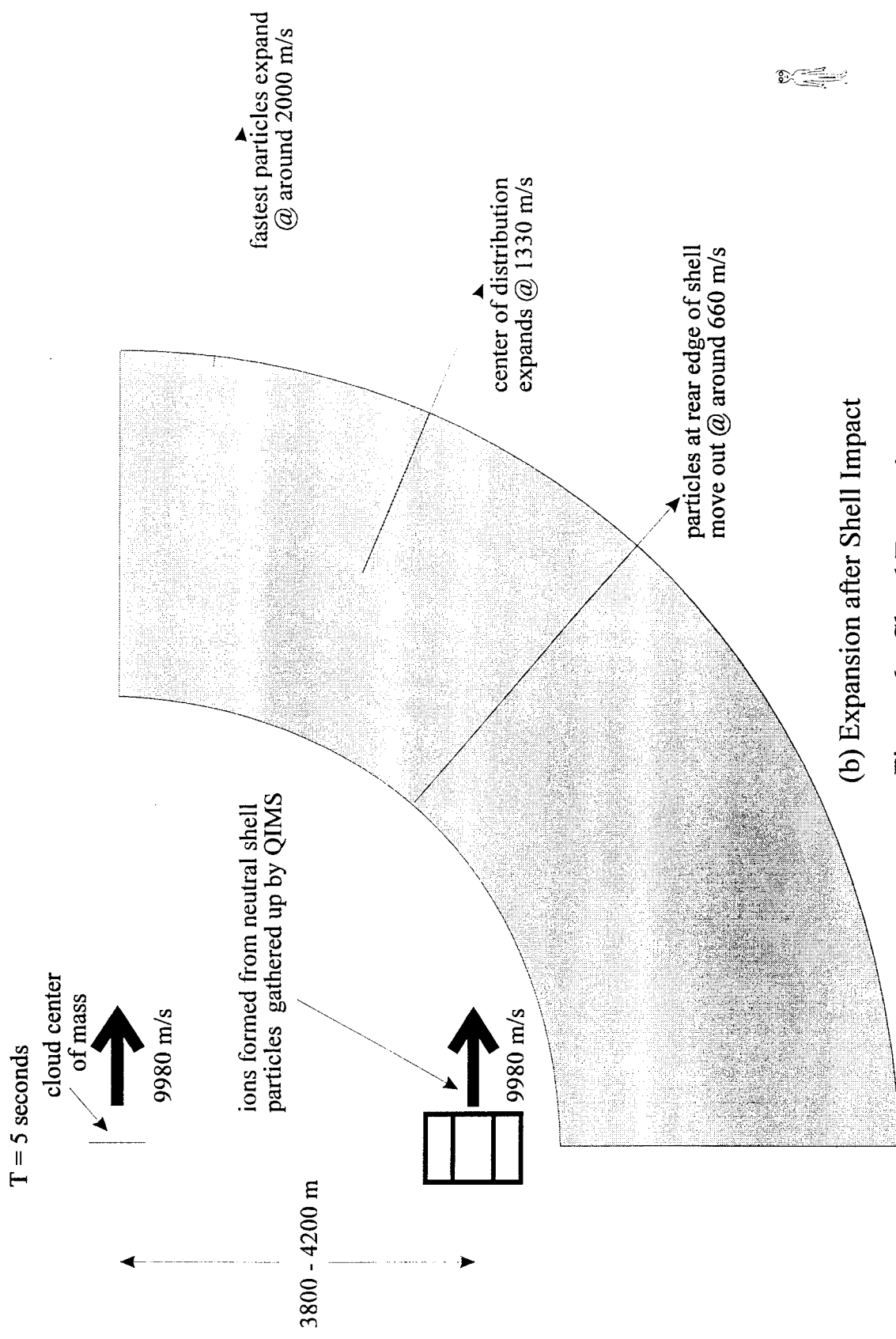
Upon initiation of the thermite reaction, about 40 percent of the metal inside the canister was vaporized (Stenbaek-Nielsen et al., 1993). The gas then proceeded to expand outward in spherical form with a Gaussian velocity distribution. See Fig. 6 (a) and (b) for a pictorial representation of this scenario. Detonation of the canister was marked at zero seconds relative time. We used relative time in the modeling for this thesis and in all the comparisons between model output and experimental data shown in the results section. At around 1 second the cloud was already in the form of a Gaussian shell. Particles that were ionized were subsequently trapped by the geomagnetic field lines (this assumption is discussed later) Thus ions formed at this point in time would stop expanding outward with the cloud and would not reach the satellite. The shell first

impacted CRRES just past 2 seconds after detonation and accordingly this is when QIMS first registers ion counts. By 3 seconds the satellite was enveloped by the shell of neutral particles. Fig. 6 (b) depicts the cloud expansion after the rear edge of the neutral shell passed CRRES' position. After this point the spacecraft no longer encountered neutral cloud particles. However, it did continue to move through regions where the cloud had been and thus "picked up" ions that were formed at some earlier time. Using neutral barium and strontium emissions, optical evidence both immediately after detonation (≈ 1 second) and minutes later show that this form of cloud expansion did occur (Stenbaek-Nielsen et al., 1993 and Wescott et al., 1994). The releases in Stenbaek-Nielsen et al. and Wescott et al. involve larger masses of neutrals than in G-1 and G-11b, but the smaller masses here should behave the same. As support for this argument, Szuszczewicz et al. (1993) report that spherical symmetry in thermite releases in space has consistently been confirmed by optical diagnostics.

Based on optical data analysis, the average thermal expansion speed of barium was calculated to be 1.33 km/s with a Gaussian width of 0.30 km/s (Wescott et al., 1994). As shown in Fig. 6 (b), the slowest particles (at the rear edge of the shell) moved outwards at around 0.6 km/s and the fastest (in front) expanded at around 2 km/s. The strontium included in the canister might be expected to expand at a velocity inversely related to the square root of its mass, or faster than the barium. Its mass-dependent average thermal velocity is 1.67 km/s. Szuszczewicz et al. (1993) found for a mixture of barium and lithium in the CRRES G-9 release that lithium, which like strontium is also lighter than barium, did not move outwards at its thermal velocity. They concluded that mass-



(a) Expansion up to Shell Impact
 Figure 6. Cloud Expansion



(b) Expansion after Shell Impact

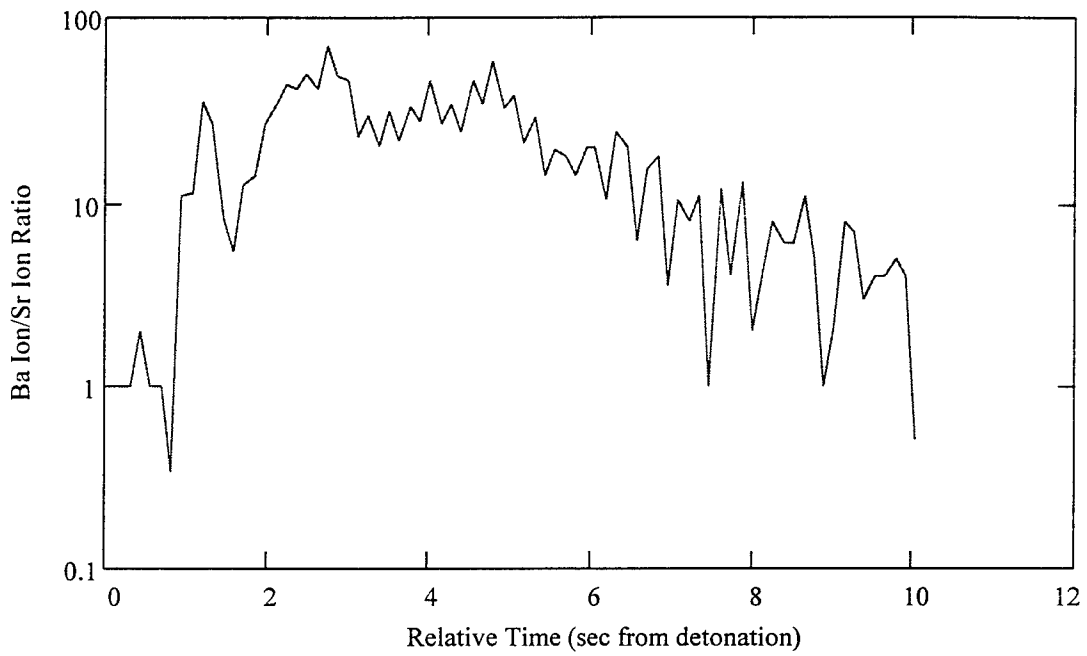
Figure 6: Cloud Expansion

dependency does not play that large of a role in the expansion. We used the data from QIMS to calculate a time-dependent ratio of Ba^+ to Sr^+ . As shown in Fig. 7, these results do not indicate a strong mass dependence of the expansion velocity either. A faster population of strontium should have produced a ratio of Ba^+ to Sr^+ that steadily increased with time. The ratio in the figure does grow stronger over small sections of time, but the appearance of the initial peak and subsequent decrease destroys the ability to make any conclusions of strontium dominating the front edge of the cloud. Thus we assumed that both species had an average expansion velocity of 1.33 km/s.

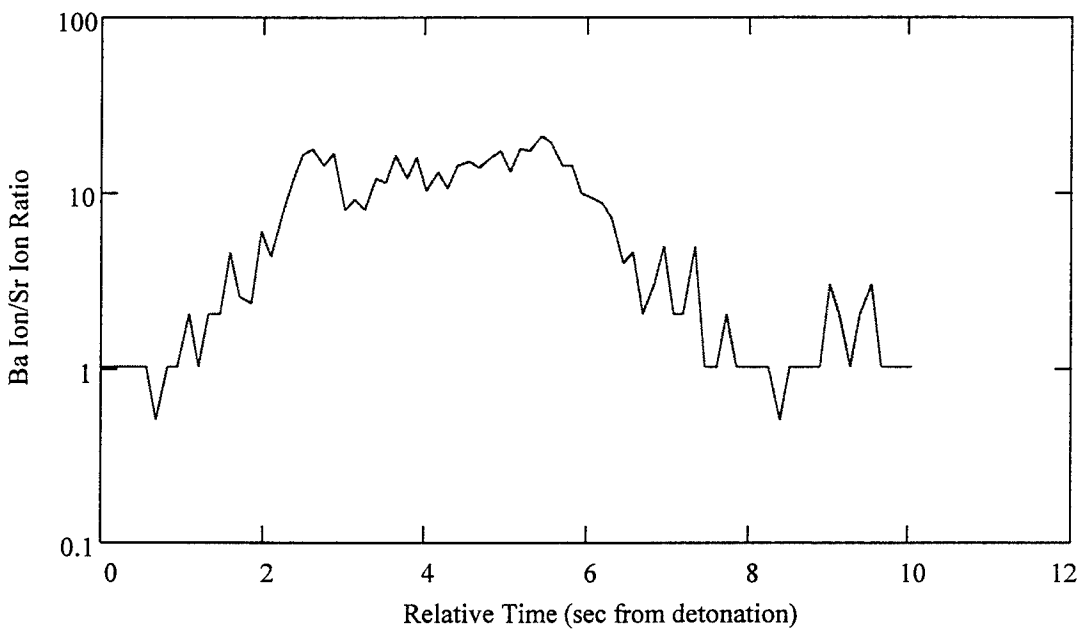
We also assumed that the velocity distribution of the cloud expansion remained constant. The only condition that might have prevented this would have been a high momentum-altering collision frequency with the ambient atmospheric particles that would have slowed the spherical expansion. Given that the mean free path between a single cloud particle and all the ambient population at altitude was more than 100 km (see Appendix C), which was significantly larger than the cloud dimensions during times in which barium and strontium ion counts were measured, this assumption is probably realistic. In addition, photographs of expanding barium clouds in previous experiments have shown the expansion speed to be equal to that of the thermal distribution out to at least several seconds (Wescott et al., 1994).

2.5 Transverse Motion Across Magnetic Field Lines

In order to simplify the study of the cloud expansion, we assumed that newly formed ions would very quickly if not immediately be attached to a line of force of the earth's magnetic field and be forced to gyrate around that line. The gyroscopic frequencies and



(a) G-1 Ratio



(b) G-11b Ratio

Figure 7. Ratio of Ba^+ to Sr^+

radii for all relevant particles are listed in Appendix C. However, some research has been done which indicates that immediate gyroscopic motion is not always the case in space release experiments. When a charge separation occurs, the ion and electron will rotate around the field line in opposite directions, resulting in a finite current density. This leads to a buildup of charge at the cloud edge which in turn leads to a polarization electric field. This field interacting with the geomagnetic field yields an $\mathbf{E} \times \mathbf{B}$ force, allowing the ion cloud to drift transverse to the field lines in the direction of the neutral cloud velocity. (Mitchell et al., 1985) It will maintain form until the ion densities are no longer high enough to create a polarization field able to cause particles to drift. This field usually persists until the ambient ion density is greater than that within the cloud. This effect, in which Ba^+ and Sr^+ continue to follow the neutral cloud movement, was observed in the CRRES releases and is generally referred to as "skidding". It was initiated immediately after detonation, with a finite delay allowing for the polarization field to develop after the first ions form (Huba et al., 1992). As stated above, Delamere et al. (1995) reported transverse motion for 7.5 km, or just under a second after detonation. It is also postulated in their paper that parts of the ion cloud may have skidded for much farther than this. As complete separation of the Ba^+ cloud from the neutral cloud did not occur until around 10 seconds in the larger G-12 release (Stenbaek-Nielsen et al., 1993), it is certainly possible that ions were able to cross field lines for at least 2 or 3 seconds in G-1 and G-11b. There is no hard data, however, that this continued long enough to allow particles created early on in the experiment to reach QIMS. Thus we concluded that only particles formed along the satellite orbit could have been counted and the skidding effect was not

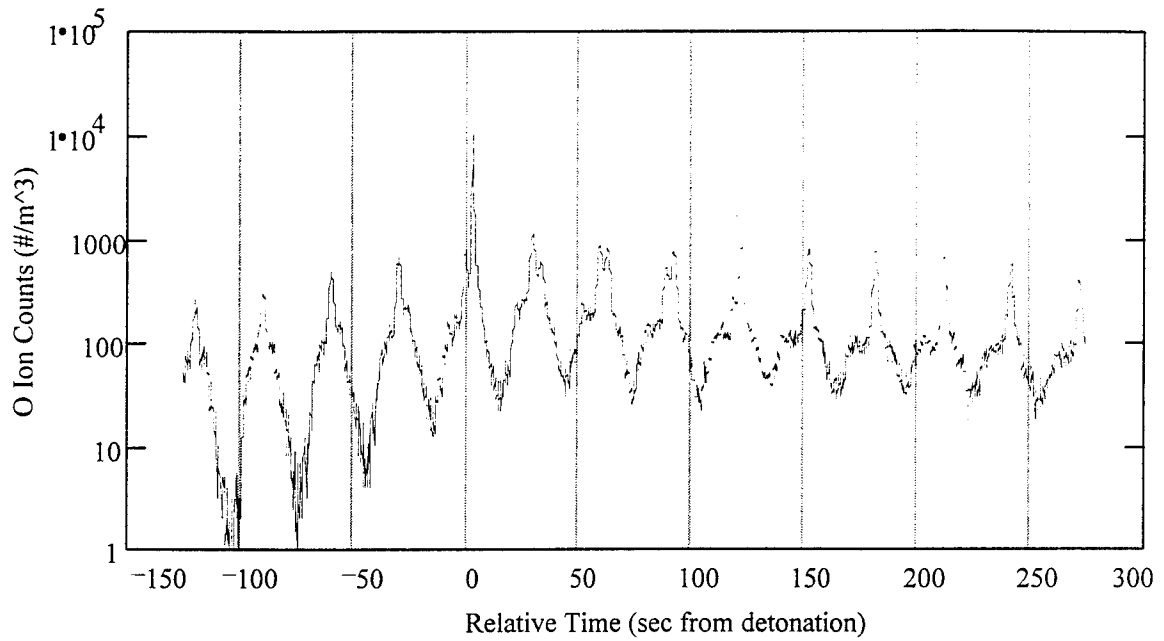
included in the mathematical model for this thesis. However, the polarization field is very important in another phenomenon, the snowplow effect.

2.6 Snowplow Effect

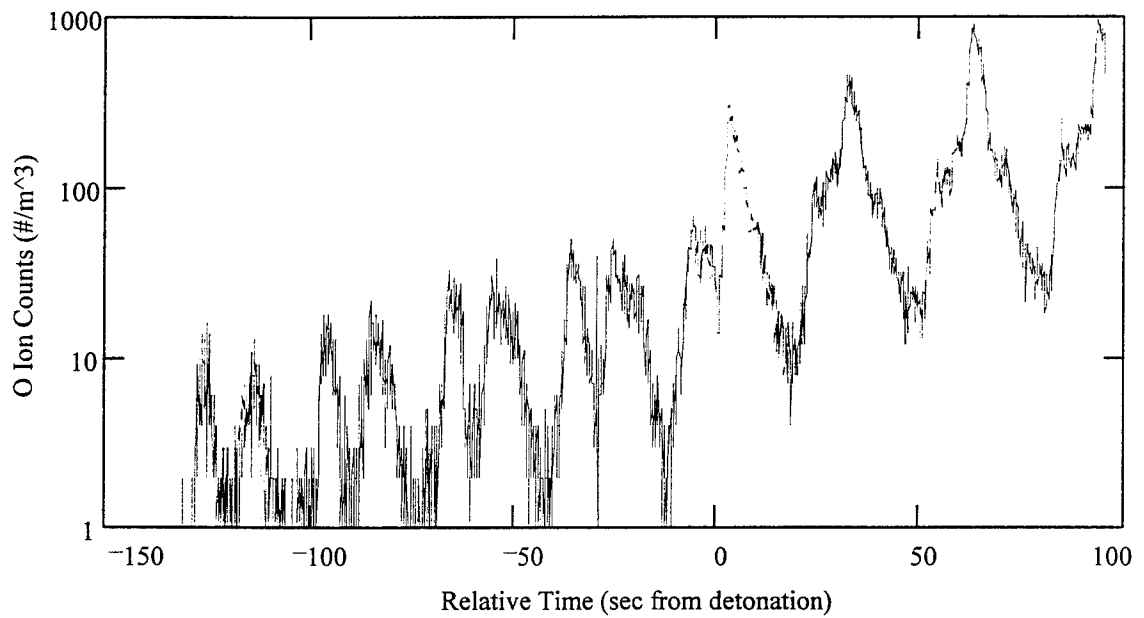
Another factor created by the expanding ion cloud ensues from the fact that it is traversing through a plasma and not a vacuum. The same polarization electric field that results in a drift of Ba^+ particles creates an electrostatic "wall" beyond which it is difficult for ambient ions such as O^+ to penetrate. Only those ambients with enough velocity opposite in direction to that of the expanding cloud can get through. This creates an O^+ density "hole" within the Ba^+ cloud and a density increase in front of the leading edge of the cloud. From these traits comes the name by which this effect is known--the snowplow effect. If this could be shown to have occurred in the G-1 and G-11b releases, it might help explain the double peak in the first maximum seen in the ion measurements.

Another signature of the snowplow effect is an increase in the kinetic electron temperature ahead of the expanding Ba^+ front. This is found in computer simulations to speed up the expansion as well as to increase the strength of the snowplow. (Schunk and Szuszczewicz, 1988) A continuous temperature plot throughout either of the releases was not available and so it is unknown if any temperature increase was experienced as the front wall of the shell passed CRRES' location.

There was an order of magnitude increase in O^+ in the G-1 release and a half an order of magnitude jump in G-11b, as shown in Fig. 8 (a) and (b) respectively. It was not determined whether or not this is actually real. In the G-9 release, a very large surge from 70 to 30,000 at the front edge of the ion cloud was attributed only partially (on the order



(a) G-1 (Sunlit) Release



(b) G-11b (Dark) Release

Figure 8. Oxygen Ion Data

of a few percent) to snowplow. The bulk of it was considered a result of QIMS interrogating the ions at a zero degree incident angle (ram) at the time of the increase. (Szuszczewicz et al., 1993) As will be discussed in the modeling section, the satellite's rotation caused a sinusoidal ram-wake variation relative to the ion motion past the spacecraft.

However, computer simulations, conducted on a smaller scale than space experiments but shown to be realistic in terms of plasma expansion of the cloud, have produced O^+ density increases between 6 and 100 percent, depending on the exact circumstances. The high end of this range appears to occur when a component of the velocity through the plasma is along the magnetic field lines. (Ma and Schunk, 1993; Schunk and Szuszczewicz, 1991) At an angle of 95 degrees to the geomagnetic field, there was not a large parallel component in G-1 and G-11b. However, at the time of the O^+ increase, QIMS was receiving particles with a small additional parallel component due to the spherical expansion. If the density surge was a result mostly of timing of the ram receive direction of QIMS with the front edge of the cloud, then it is a coincidence that both releases show the same timing. However, it may also be unrealistic to consider the apparent O^+ behavior to be a true indication of the cloud expansion. The increase seen is definitely comparable in magnitude to the largest results produced in simulations. Also, the effect occurred at around 2 seconds after detonation, after Delamere et al. (1995) observed large-scale skidding to have disappeared. Additional information such as continuous temperature plots, which was not available, might have proven helpful in making a more certain determination here.

3. Background Theory

3.1 Ionospheric Chemistry

The ionosphere begins where charged particles start to populate the atmosphere and extends upwards. The chemical profile of this atmospheric region changes with height. At the lowest altitudes (60-90 km), atomic and molecular ions are present in both positive and negative form. At around 100 to 200 km, negative molecular ions cease to be present in significant numbers. Finally, above 200 km, the primary charged particles are positive atomic ions. (Hargreaves, 1992) The species present determine the chemical activity of each of these regions. The location of the CIV experiments was in the highest (called the F2) region where the chemistry is the simplest and the highest plasma densities (around 10^{12} ions m^{-3}) reside. This uppermost part of the ionosphere stretches through the F2 density maximum (350-450 km) and upwards. Below a mobile boundary that positions itself anywhere from 1000 to 500 km (depending on the time of day and year, solar cycle, latitude, and geomagnetic conditions), singly ionized oxygen is by far the most numerous ionic constituent. Other ions exist--most notably hydrogen and helium--but at an altitude of 475 km it is oxygen that is the most numerous and the most important to the experiment studied here. The oxygen dominance is reflected in the fact that the mean molecular weight at this altitude is right around 16 atomic mass units (U.S. Standard Atmosphere, 1976). Outside of this sphere and beyond the reach of the CRRES G-1 and G-11b release heights, hydrogen ions become more numerous than oxygen. (Kelley, 1989; Gonzalez et al., 1992) As Tascione (1988) states, this regime is often differentiated

from the ionosphere and referred to as the plasmasphere. The region of oxygen ion dominance, that with which this thesis is concerned, is called the topside ionosphere.

Principal reactions occurring naturally in the F2 region include photoionization, photodetachment, electron-ion recombination, ion-ion recombination, and charge exchange, as listed respectively below,



where X and Y are atomic particles, $h\nu$ represents a photon, and e is an electron. (Rishbeth and Garriott, 1969) At F2-region altitudes, the ionosphere becomes optically thin to ionizing UV radiation, meaning that the atmosphere is rare enough that all particles are equally exposed to solar high energy photons. Due to the abundance of both atomic oxygen and UV radiation, then, the dominant process is the photoionization of oxygen by Lyman-band photons. Recombination involving atom-ion interchanges with molecules occurs also, but since molecular densities are relatively low this high in the atmosphere, the loss rate is not able to empty the upper regions of the ionosphere at night. (Tascione, 1988) Plasma densities simply decrease around a half to an order of magnitude or so while the sun's energy is absent (Kelley, 1989).

One more aspect of the ionosphere was important to this study. In attempting to model ionization processes, it is important to know the relative velocity between the

interacting particles. The speed of the released gas is known; the motion of ambient ionospheric particles is then also required. According to Kelley (1989), the ionosphere to first order corotates with the earth along with resident neutrals. The zonal rotation speed of the earth at the equator is around 464 meters per second and neutral winds at this altitude are usually at most 200-300 meters per second (Hargreaves, 1992). These velocities are very small compared to the orbital speed of the CRRES satellite and cloud and thus ambient particles are considered to be at rest.

3.2 Selection of Barium and Strontium

As shown in Table 1, barium was the primary chemical released in the CRRES experiments. Its weight is 137.33 atomic mass units. Barium has consistently been used in ionospheric release experiments because it is easily ionized, having an ionization potential of 5.21 electron volts. (Bernhardt, 1992) It very rapidly ionizes in sunlight, having a photoionization time constant of 28 seconds (Calrsten, 1975). Another item that benefited ground observers is the fact that barium ions and neutrals have rather strong resonance lines in sunlight and both emit radiation in the visible spectrum (Reasoner, 1992).

Strontium weighs in at 87.62 atomic mass units. Its ionization potential is listed as 5.69 electron volts (Bernhardt, 1992). It is present in barium samples most often as an impurity, but was inserted in additional amounts into some of the CRRES canisters as a tracer. It would then assist in tracking the neutral cloud by way of its visible emission lines. Strontium is estimated to have a photoionization time constant of 1920 seconds

(Wescott et al., 1990), and so was expected to remain part of the neutral cloud. In other words, significant ionization of Sr atoms was not expected.

4. Approach to Modeling Problem

4.1 Initial Basic Model: Description and Analysis

The initial model was based on the expansion characteristics of barium clouds described by D. E. Hunton (1993). This product was used with only slight modification as the basis for all of the modeling completed in this thesis. Several assumptions were utilized here. We assumed that the cloud expansion took on the form of a spherically symmetric gaussian shell. This was also discussed in the section describing the release. It was also necessary that we consider the cloud to be in radiative equilibrium with incoming solar radiation. Finally, we assumed that ions were trapped by the earth's magnetic field immediately after forming and that ion drifts such as that from an $\mathbf{E} \times \mathbf{B}$ force were insignificant. The following text describes the development of the model and addresses the validity of these assumptions.

The number density of neutral barium or strontium can be written:

$$\rho(r, t) = \rho_{\max}(t) \exp\left(-\left(\frac{r - v_0 t}{v_w t}\right)^2\right) \quad (3)$$

where v_0 is the peak of the cloud expansion velocity distribution, $v_w t$ is the width of the distribution, and r is the radial distance from the cloud center. The total number of neutrals at time t can be evaluated by integrating the density over all space:

$$N(t) = \int \rho(r, t) dV = 4\pi \rho_{\max}(t) \int_0^{\infty} r^2 \exp\left(-\left(\frac{r - v_0 t}{v_w t}\right)^2\right) dr \quad (4)$$

and solving for the peak neutral density at time t :

$$\rho_{\max}(t) = \frac{N(t)}{4\pi \int_0^{\infty} r^2 \exp\left(-\left(\frac{r - v_0 t}{v_w t}\right)^2\right)} \quad (5)$$

If an ionization process of time constant τ is assumed to reduce the total number of neutrals, the neutral number density becomes:

$$N(t) = N_0 \exp\left(-\frac{t}{\tau}\right) \quad (6)$$

where N_0 is the initial number of gaseous neutral atoms in the cloud and τ is equal to the inverse of the ionization rate constant, "k". This rate constant is defined as the product of the number density "n" of the ionizing particle, the cross section "σ" of the reaction, and the relative velocity "v" between the 2 particles. Substituting (5) and (6) into (3), an expression for the density as a function of radial position and time is obtained:

$$\rho(r, t) = \frac{N_0 \exp\left(-\frac{t}{\tau}\right) \exp\left(-\left(\frac{r - v_0 t}{v_w t}\right)^2\right)}{4\pi \int r^2 \exp\left(-\left(\frac{r - v_0 t}{v_w t}\right)^2\right) dr} \quad (7)$$

The denominator can be integrated to simplify the expression. This becomes easier if a u -substitution is made.

$$u = \frac{r - v_0 t}{v_w t} = \frac{r}{v_w t} - \frac{v_0}{v_w} \quad (8)$$

This will be substituted into the exponential. However, the r^2 term must also be stated in terms of u . Using (8), r is found in terms of u :

$$r = v_w t u + v_0 t$$

Then:

$$r^2 = v_w^2 t^2 u^2 + 2v_0 v_w t^2 u + v_0^2 t^2 = t^2 (v_w^2 u^2 + 2v_0 v_w u + v_0^2)$$

and:

$$du = \frac{1}{v_w t} dr \implies dr = v_w t du$$

Finally, substitution yields:

$$\int_0^\infty r^2 \cdot e^{-\frac{r-v_0 t}{v_w t}} dr = v_w t^3 \int_0^\infty (v_w^2 u^2 + 2v_0 v_w u + v_0^2) \cdot e^{-u^2} du$$

$$= v_w t^3 \cdot v_w^2 \int_0^\infty u^2 \cdot e^{-u^2} du + 2 \cdot v_0 v_w \int_0^\infty u \cdot e^{-u^2} du + v_0^2 \int_0^\infty e^{-u^2} du$$

Using integral tables (Weast, 1974-1975), this becomes:

$$v_w t^3 \left(\frac{\sqrt{\pi}}{4} v_w^2 + v_0 v_w + \frac{\sqrt{\pi}}{2} v_0^2 \right) \quad (9)$$

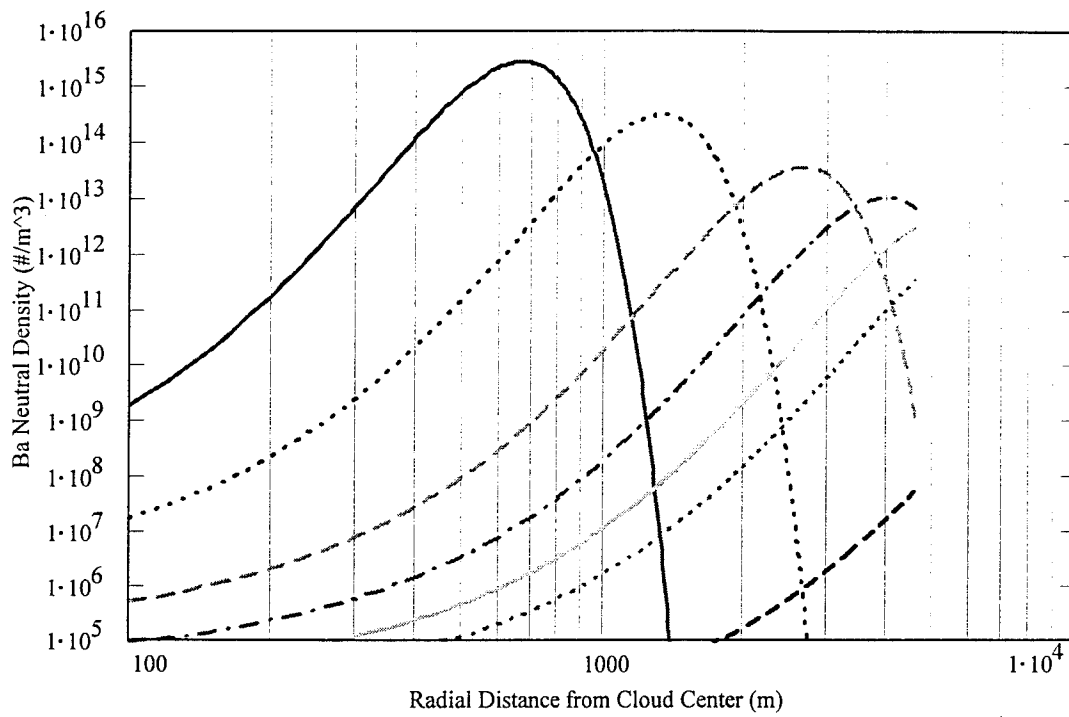
Then using (9), the density expression in (7) is restated:

$$\rho(r,t) = \frac{N_0 \cdot \exp\left[-\frac{t}{\tau}\right] \cdot \exp\left[-\frac{r-v_0 t}{v_w t}\right]}{4 \cdot \pi \cdot v_w t^3 \cdot \left[\frac{\sqrt{\pi}}{4} \cdot v_w^2 + v_0 v_w + \frac{\sqrt{\pi}}{2} \cdot v_0^2 \right]} \quad (10)$$

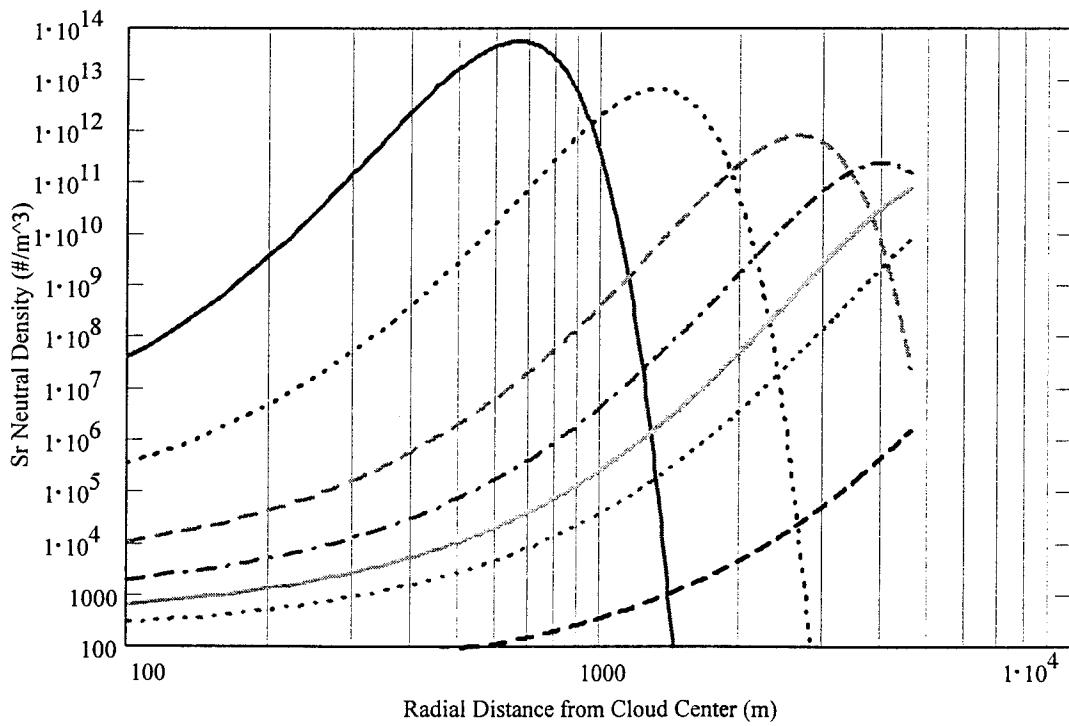
This specifies the evolution of the neutral gas cloud; it states the neutral density as a function of radial distance "r" and time "t". Ground-based optical observations indicate that the neutral cloud was close to spherically symmetric. The center of the expansion in

this case was the detonation point of the canister. Here N_0 is the initial number of vaporized neutral atoms, r is the radial distance from the cloud center, v_0 is the expansion speed of the cloud, t is the time from detonation, and v_w is the velocity width of the Gaussian (or the distance from the average velocity at which the number of particles is $1/e$ the number at the average). In Fig. 9, the neutral density distribution as a function of radial distance from the cloud center is shown for both barium and strontium in releases G-1 and G-11b. The function is graphed, from left to right, at times of 1/2, 1, 2, 3, 4, 5, and 10 seconds. Photoionization is assumed to be the decay factor in these plots. As expected, they indicate that as time increases the maximum neutral density moves farther away from the cloud center and decreases as the shell spreads out and rarifies.

What is desired now is an expression for the ions detected at the spacecraft location. Remember that the while the cloud was expanding and ions were being created, the spacecraft and cloud system was moving through space at the orbital speed v_s . After the shell moved past the satellite, CRRES no longer saw any neutrals, as indicated in Fig. 6(b). However, it continued to pick up ions formed and trapped on the field lines at some earlier time when the cloud passed. The assumption that after being formed ions were immediately trapped by the geomagnetic field lines makes this possible. A supplementary assumption to this is that if particles had parallel velocity and moved away from the point at which they were formed (along the field line), there were just as many that advected in from another point on the same field line and therefore ion density at a



(a) Barium



(b) Strontium

Figure 9. Neutral Density Plot

particular point on CRRES' path remained relatively constant. The ion density is then:

$$\rho_{ion}(t) = \frac{k}{v_s} \int_0^{1.5v_s t} \rho(r, t) dz \quad (11)$$

where k/v_s is multiplied by the integral to yield units of ion density. This quantity is k , the ionization rate constant (s^{-1}), divided by the orbital speed (m/s).

A final modification will now be added to the model. Since it is from onboard the spacecraft that the ions are being counted, it is that frame of reference in which the model should be located. Thus:

$$\rho_{ion}(t) = \frac{k}{v_s} \int_0^{1.5v_s t} \rho(r', t') dz \quad (12)$$

where $r' = \sqrt{R^2 + z^2}$ and $t' = t - \frac{z}{v_s}$. R is the displacement of the spacecraft from the cloud center of mass (around 4 km) and z is the distance along the satellite path. The new radius definition is depicted in Fig. 10 on the next page.

The first ions counted by QIMS will be formed right at the instrument when the shell initially contacts the satellite; after this it will be encountering charged particles which were formed at some earlier time when neutrals passed through that point. The factor $t - \frac{z}{v_s}$ introduces this time retardation--as larger z 's are encountered, ions are being picked up from earlier times. The integral accounts for the gathering action and the ion density is calculated as a function of time. At a particular point in time, an integration is made from zero out to the distance the cloud shell has moved out ahead of the spacecraft.

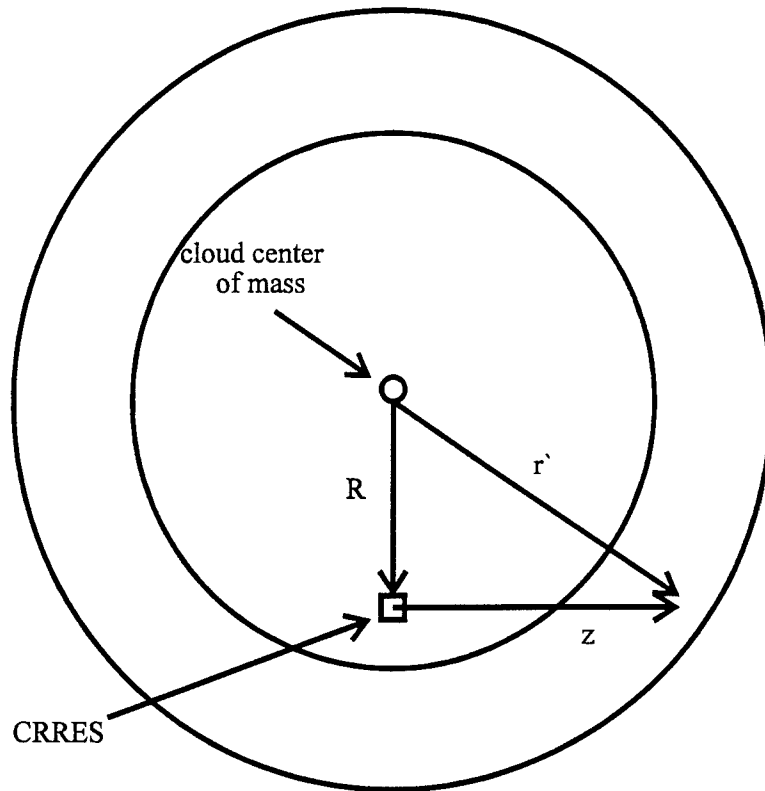


Figure 10. Radius in Spacecraft Reference Frame

The upper limit of the integral determines how far ahead of CRRES to count. The cloud's position on the path dz is becoming farther away from the satellite at roughly the expansion velocity v_0 . So why is the upper integration limit one and a half times v_0 ? This has to do with the width of the Gaussian velocity distribution. Remember that, v_0 --1.33 km/s--is the average speed of the shell and there are particles populating velocities all the way up to 2 km/s. Thus an upper limit of one and a half times 1.33 ensures that the limits on the integral reach out far enough to account for the fastest neutrals in the expanding shell. In actuality, instead of narrowing it down to a precise number that would account for all ionization, an upper limit much larger than $1.5v_0$ could have been used without having to do any calculation and the same ion number densities would be

returned. Since there are no fast neutrals to ionize at distances beyond the cloud edge along the satellite path, the integral would be evaluated as zero there. However, to keep from doing unnecessary work every time the density function is evaluated, integration limits as narrow as possible are used.

The number density calculation has been explained in terms of an integration along a particular path. If this is unclear, another perspective might be useful. Picture counting the number of ions in existence at a particular point along the spacecraft orbit. This population consists of relatively new ions, created when the trailing edge of the shell passed the point, "old" ions, generated when the leading edge of the shell made contact here, and everything in between. Thus we count ionizations through a period of time at this particular point from detonation to when CRRES finally gets here. The first few seconds and the last few seconds of this period may yield zero ion counts, especially at a point very far from the detonation, but the time interval in which fast neutrals were transiting will yield the charged particles that formed and then were trapped by the magnetic field.

4.2 Consideration of Assumptions

Several assumptions were utilized to apply the model previously described to the CRRES experiments, some of which were mentioned above. One assumption was that the ions are trapped immediately after being formed. Obviously charged particles will be trapped by magnetic field lines. According to Schunk and Szuszczewicz (1991), ions may have as long as a gyroperiod of freedom after formation before actually being trapped by the field lines. The length of time that an ion could travel across field lines

would depend on the strength of the geomagnetic field and the momentum of the particle. For barium, the gyroperiod, or maximum duration of freedom, amounts to about 0.28 seconds (calculation in Appendix C). Freedom to cross field lines translates to ions formed on the satellite orbital path "sliding" off of the path before being constrained in gyroscopic motion. This could be significant, but for purpose of simplicity we considered it valid to assume that just as many ions "slid" into the path of CRRES as "slid" off of the path.

Above in the model discussion a supplementary assumption (to ions being trapped) was made that once particles were trapped by the field lines, any velocity along the lines would translate to just as many ions advecting in as advecting out. The parallel velocity component rapidly decreases, as shown in Fig. 11. Here the cloud's expansion can be seen as it changed with time. The time at which the center of the velocity distribution reaches each radial distance is on the left side and the average radius of the shell at each time is listed on the bottom of the page. The lower left corner of the figure is the cloud center of mass and the tail of the satellite path arrow is the satellite location. The parallel velocity component along CRRES' path is then listed at each point in the expansion. After about 6 seconds, the spacecraft was gathering ions whose momentum is almost entirely perpendicular to the field lines. Earlier than 6 seconds, when parallel velocities were significant, the ions did not have enough time to move far along the lines before they were counted by QIMS, since CRRES approached at the 10 km/s orbital velocity. Thus we neglected the parallel velocity components in the model. In other words, we assumed that ions formed on the satellite path remained there.

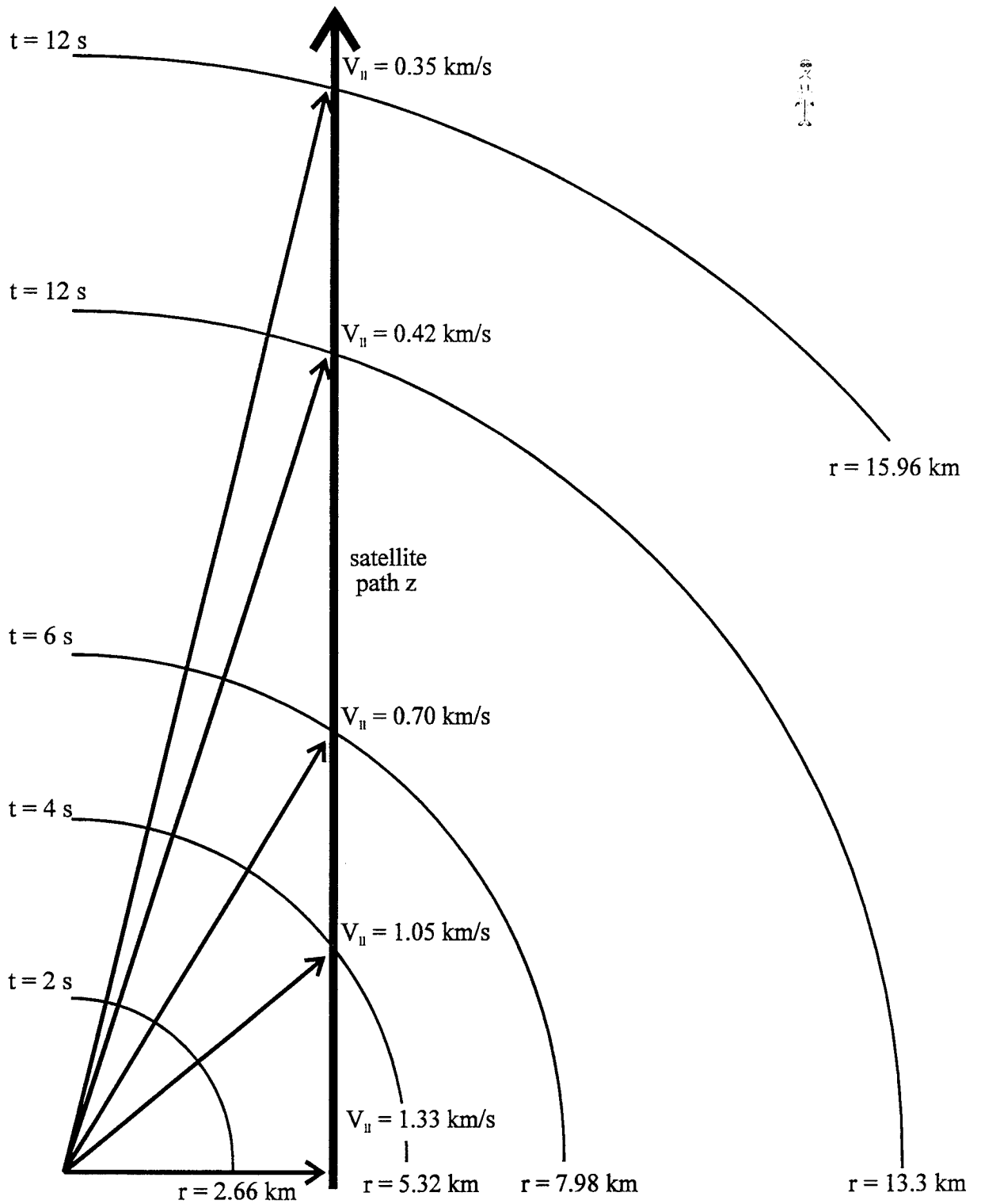


Figure 11. Parallel Velocity Component

If an electric field developed, it would have caused the particles to \mathbf{ExB} -drift and not remain stationary at a location in space. This was covered in the snowplow section. In the CRRES releases G-1 and G-11b, it was determined that this effect probably lasted no more than 7.5 km of travel for much of the cloud (Delamere et al., 1995). Since the system--satellite and cloud--was moving at the orbital speed, this translates to less than a second. The cloud edge did not reach the satellite until more than 2 seconds, so we neglected this effect.

For all ionization processes, we considered all neutral particles in the cloud to be equally exposed to ionizing particles (ambient neutrals and ions) and energy (sunlight). For photoionization this condition corresponds to radiative equilibrium with incoming solar radiation, which is covered later in the photoionization section. Based on information in that section, radiative equilibrium was considered a valid assumption. For collisional processes, the above condition implies that all ambient particles were able to penetrate the expanding cloud. Based on the fact that the cloud expansion was nearly collisionless and that the polarization electric field associated with the snowplow effect lasted less than a second, we considered the barium cloud to have been nearly transparent to all particles in the ambient ionosphere.

4.3 Validation of Initial Model and Normalization

Once the ion density integral was defined, it was necessary to compare it to the data to see if the form matched. Data taken by QIMS is in units of counts per time, a relative measure of flux, while output from the model is in counts per volume, an absolute measure. In order to compare the two, a normalization was accomplished. We chose the

data set from the CRRES releases about which the most was known and normalized the model to that. The obvious choice was the barium sunlit data (G-1), since it is almost unquestioned that photoionization dominates all other processes in sunlight. Thus UV radiation was assumed to be the only ionization source. Then the initial peaks in both the data and the model were compared. The number that when multiplied by the model made the maximum intensities of the two peaks (G-1 experimental data and model output) exactly match became the normalization factor. The normalized model and G-1 barium data are shown together in Fig. 12. Here the solid line is the model and the dotted plot is the data. The less-than-perfect fit for the second and third peaks in the data is probably due to either recombination or ions moving off of the satellite path at times where the cloud has expanded out to long distances in front of CRRES.

4.4 Rotation of Spacecraft

Another obvious trait displayed by the data is the periodic nature of the number of counts instead of a steady decay as produced by the model. This is due to rotation of the spacecraft. As pictured in Fig. 3 in the section describing QIMS, the spectrometer is pointed radially outward perpendicular to the satellite spin axis. Thus the strength of the flux into the instrument varied sinusoidally as the aperture plate moved into and out of the ion flow. The satellite rotated at approximately 2.02 revolutions per minute (rpm). This was calculated from time-dependent data including the angles between the QIMS pointing direction and the velocity and magnetic field vectors. This may not be exact, as the angle data was not of high time resolution, and there were some indications that the

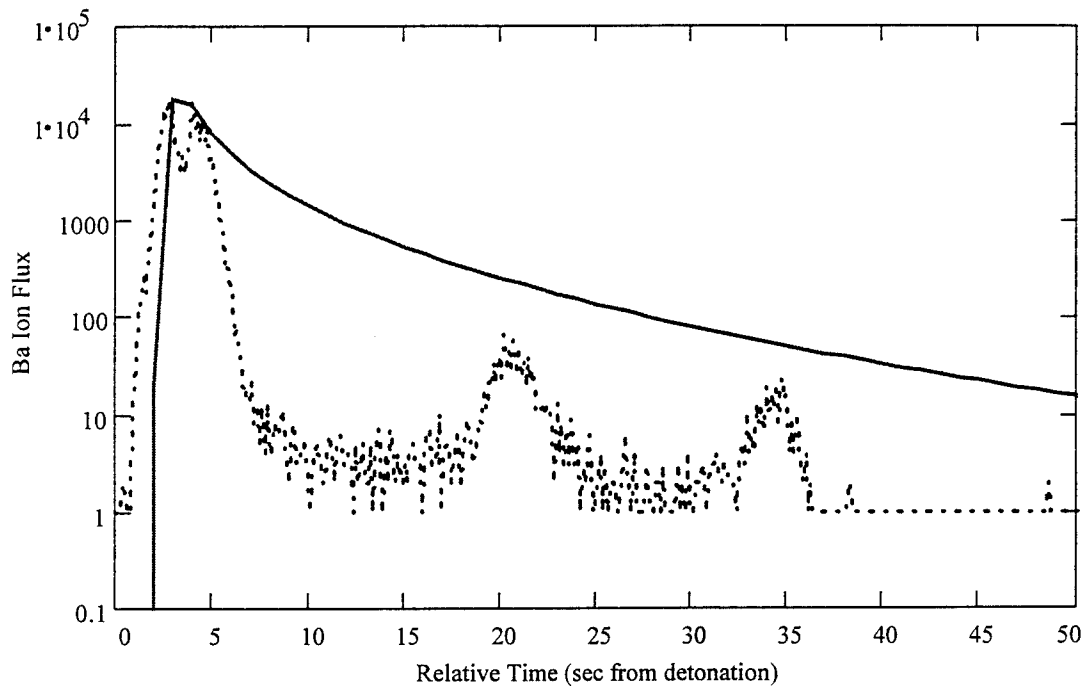


Figure 12. Normalization of Barium Model to G-1 (sunlit) Data

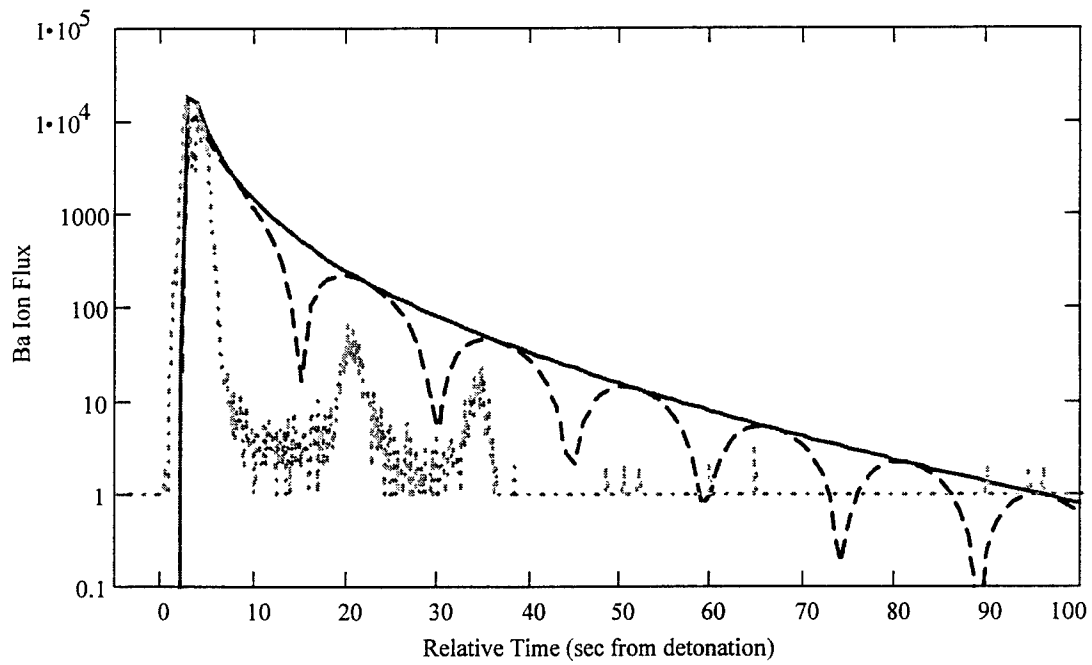


Figure 13. Barium Model with Rotation Compared to Data and Basic Model

rotation period may have grown slightly longer as time went on. Publications list the spin rate as 2.0 rpm (Johnson and Kierein, 1992), so our calculation was considered close enough. As was discussed above, the ions gyrated around the field lines after they were formed and thus were doing so when counted by the spectrometer. Since the bulk of the charged particles have very little parallel velocity, the maximum sensitivity of the instrument was when it was pointing perpendicular to the geomagnetic field. At this point the ions, whose instantaneous velocity was constantly perpendicular to the field lines, would have entered QIMS at the highest rate. This situation existed twice per rotation period, or about every 15 seconds. The behavior of the data can then be imitated by including in the model a sine factor accounting for the rotation. This is shown in Fig. 13. Here the three plots include from top to bottom the pure model results without rotation considered, the model with rotation, and the QIMS barium ion counts from the G-1 release. Once this behavior of the QIMS data was properly modeled with satellite rotation, it was set aside and no longer included in the model. Thus it will no longer be used in this paper.

5. Discussion of Results

5.1 Research into Ionization Processes

Given the conditions in the ionosphere surrounding the CRRES releases, 6 sources of ionization were considered as possible processes responsible for the ion fluxes measured. They are photoionization, charge exchange, electron impact, associative ionization, charge stripping, and thermal ionization from the thermite burn. Each of these are discussed here. A determination is also made as to the likelihood of the process' involvement in the chemical releases. Following this discussion, the likely reactions are modeled and compared to the experimental data in the next section.

5.1.1 Photoionization

Of all the ionization processes considered in this study, solar UV photoionization is probably the best understood. It takes the following form:



Before the chemical release experiments were installed into the CRRES platform, the decision was made to include barium and strontium in the G-1 and G-11b canisters. As was stated earlier, barium was known to photoionize easily and earlier time constant calculations for strontium had only resulted in very high values. Thus high ion fluxes were expected for barium in sunlight while ionization of strontium was not expected. However, the data only partially agreed with this prediction. There was certainly a large amount of barium ion production in the sunlight, but there was an even higher rate of

ionization for strontium under the same conditions. Therefore photoionization and its properties were reconsidered.

Before any of the time constants were evaluated, we had to make a determination of the cloud's exposure to UV radiation. Could the cloud be considered optically thin? By optically thin, we mean that each neutral particle in the cloud had to be equally exposed to sunlight. Light which ionizes barium is shorter than 326.5 nanometers (Drapatz, 1972). Radiation of those wavelengths has enough energy to surpass the ionization potential. Using a solar flux below this cutoff of 4×10^{19} photons per m^2 per second, the barium time constant of 28 seconds corresponds to a cross section of $10^{-21} m^2$. Thus the column density within the neutral shell must fall below 10^{21} per m^2 before the cloud can be considered optically thin. (Delamere et al., 1995) Obtaining the maximum neutral density from Fig. 9 and dividing by the cloud's diameter, I concluded that this condition must have been present within a small fraction of a second. For the G-9 release, which involved three times more mass than G-1 and G-11b, Delamere et al. calculated a time of 20 milliseconds at which the column density requirement is met. Therefore we considered the barium cloud to have been optically thin. Strontium was also considered to be optically thin as its number density is much lower than barium. However, this should not be important, as its photoionization rate is insignificant in comparison to the other process(es) that must have occurred.

Next, since the model was normalized to the barium sun data assuming solar radiation as the dominant source of ionization, I reviewed the calculation of the 28 second time constant. Drapatz (1972) found from experimental work that solar flux at the frequencies

necessary to ionize barium directly from the ground state was not adequate to explain the rates of ion formation in artificial clouds in the ionosphere. However, flux densities at frequencies required to ionize the atoms from some metastable states, particularly the 1D and 3D levels, are much higher. Metastable states are elevated atomic energy levels in which transition directly to the ground state is electric dipole forbidden. Thus the lifetime of these excited states is typically on the order of milliseconds or longer. He also noticed that in an optically thin cloud these metastable states were rapidly populated. The basic conclusion was that photoionization in barium atoms is primarily from the metastable states. Carlsten (1975) completed a detailed determination of the time constant by calculating the equilibrium populations of the metastable levels and using spectroscopic data from atomic transitions. He found that barium is most readily ionized from the triplet D level and that the composite photoionization time constant from the ground state is 28 ± 6 seconds. This number then was used with confidence throughout this thesis.

There is less certainty in the time constant for strontium in many of the publications. Already referenced was the study that seems to have the best argument for its finding. Wescott et al. (1990) find a time constant of 1920 ($\pm 30\%$) seconds. Earlier calculations had placed the value at even longer times. From calculations by Wolf (1995b), solar radiation is not adequate to significantly populate the long-lived metastable levels. Thus strontium cannot take advantage of elevated energy states as a "stepping stone" to shorten the time to charge loss. A higher frequency photon is required for ionization than would be for an excited atom. When the lack of metastable state population to increase the rate of photoionization is combined with the fact that strontium has a higher ionization

potential than barium and the solar flux density is even lower at these higher frequencies, it makes sense that strontium has a much longer time constant. We then used a photoionization constant of 1920 seconds for strontium.

5.1.2 Charge Exchange

Charge exchange (CE) is another reaction that has been researched. It takes the form:



or:



(14) and (15) describe, respectively, resonant and nonresonant charge exchange. Resonant CE in this case would involve barium neutrals transferring an electron to barium ions and would not change the ion density. This type of charge transfer was not considered here. Nonresonant charge exchange between fast neutrals (Ba and Sr atoms traveling at 10 km/s as opposed to ambient neutral particles traveling at only 400-500 m/s) and ambient ions may produce high numbers of barium ions. This reaction has an advantage in that it generally requires no minimum velocity (exothermic) and utilizes ions already present in the environment surrounding the CRRES experiments. As stated in the ionospheric chemistry section, atomic oxygen is the dominant charged particle at around 500 km. It then would be the primary species interacting with barium as in (15). Liou and Torbert (1995) conducted detailed calculations of charge exchange cross sections which produced good results. Wolf (1995a) used a similar method and for the

ground states of barium and O^+ , estimated the cross section at $7 \times 10^{-20} \text{ m}^2$. The cross section of strontium and oxygen ion ground states obtained was $8 \times 10^{-21} \text{ m}^2$.

The O^+ data from QIMS indicated that densities were more than an order of magnitude higher in sunlight than in the dark. Electron densities indicated the reverse trend. As the CRRES summary at the beginning of this paper shows, the Langmuir probe measured 5×10^{11} electrons per m^3 in G-1 and 7×10^{11} electrons per m^3 in G-11b. The O^+ data seems more credible, since it makes more sense that the ionosphere would exhibit higher plasma densities on the dayside than on the nightside. It is possible that QIMS was more sensitive in one release than the other due to differences in the angle at which the particles were interrogated. Also, it is not known when the electron densities were measured for each release. Thus we ignored the reverse density trend in the Langmuir probe data. Since the O^+ concentration at 500 km is an order of magnitude greater than that of any other ion, we assumed it to be identical to the electron density. It also was assumed to increase by a half an order of magnitude from dark to light. The densities used were 5×10^{11} and 1×10^{12} ions per m^3 , respectively.

Another way to gauge the likelihood of an interaction between two particles in a confined area is to calculate the mean free path, which is shown in Appendix C. For charge exchange between barium or strontium and O^+ , the distance one of these fast neutrals is likely to travel before encountering an ambient ion (definition of mean free path) is on the order of 10^4 km. This is quite a long distance compared to the dimensions of the neutral cloud. The calculation here agrees with that found by Wescott et al. (1994), who find a mean free path of 42,000 km. In contrast, Delamere et al. (1995) calculate a

distance of a few km between collisions and Swenson et al. (1991) find that the correct value at an altitude of 400 km is approximately 15 km. It is not known how these numbers were obtained, although that it is possible that they calculated instead the distance an O^+ particle would travel before impacting Ba or Sr. Due to the reasonable certainty in the calculations completed in the appendix, the resulting much larger number was used. Such a large mean free path and low collision frequency implies that CE might not have been important in the CRRES releases, although early on in the experiment when neutral densities were high, there still might have been a significant number of collisions between barium or strontium and O^+ when considering the entire cloud population. In other words, a very small percentage of a very large number of neutral atoms experiencing ionizing collisions could still have produced a significant number of ions.

Finally, available studies of optical results were researched. Emission rates from both the G-1 and G-11b releases were analyzed in a paper by Stenbaek-Nielsen et al. (1993). The barium ion resulting from charge exchange with ground states O^+ is in an excited state and should lead to emissions at 4957 and 5013 Angstroms. These lines are completely missing from the data. The light from the thermite burst would probably have covered up this evidence during detonation, but the emissions do not appear after any amount of time. This suggests that either charge exchange did not occur except in minimal amounts, or if it did, it was limited to the first few seconds when the photo burst from the titanium-boron reaction flooded optical sensors.

The second option might be conceivable if a detail of the QIMS O^+ data is considered to be real. These results show over an order of magnitude jump in the oxygen ion density at the leading edge of the expanding neutral cloud in both releases. This occurred at a time and stage of the expansion when neutral densities were high enough that even with a very low collision frequency, enough interactions might have taken place to produce significant charge exchange products compared to the experimental results. However, if it is real, it is not certain from where this density increase could have emanated. The snowplow effect (discussed above) is a possible source, but there is debate as to how much of an ambient increase can be caused by this phenomenon. If charge exchange were to occur at the very front edge of the cloud, it would also take advantage of higher neutral velocities, which would result in a higher reaction cross section. Until the O^+ density “spike” can be physically explained, however, this proposed situation cannot be taken as a fact in the CRRES experiments.

5.1.3 Electron Impact

Electron impact ionization (EI) is the process by which CIV is primarily rendered (Mobius et al., 1987). It involves high energy electrons colliding with the fast neutrals and yielding an ion:



This reaction is self-sustaining only as long as Townsend’s condition is met. Basically, this criterion requires that electrons within a cloud and with high enough energy to ionize barium or strontium must ionize at least one atom before escaping the cloud. This is

further explained in Appendix A. If Townsend's condition ceases to be met, some other ionization process has to supply seed ions in order for electron impact to be perpetuated.

Two papers were sources of cross sections for EI: McFarland (1967) and Vainshtein et al. (1972). These took different approaches to calculating probabilities for several different species and compared them to experimental data. Values used for the purposes of this study resulted from taking an average of the two papers for both barium and strontium. The results were $1.2 \times 10^{-19} \text{ m}^2$ for barium and $8 \times 10^{-20} \text{ m}^2$ for strontium. These are based on electron energies of 10 eV, requiring very high velocities. Thus a mechanism such as CIV would be required to heat the electron population in order for EI to be very efficient. At lower electron kinetic temperatures, the cross sections significantly decrease.

5.1.4 Associative Ionization

Associative ionization (AI) has only recently been considered as a possible ion source in neutral gas releases in space. Lai et al. (1992a) investigated AI as both an independent ion production mechanism as well as an accelerant to the CIV process adding hot electrons to the cloud in the CRIT II case. Lai and Murad (1989b) looked back at early CIV experiments that reported enhanced ionization--Porcupine and Bubble Machine--and demonstrated that it was possible that AI had accounted for the fast ion production. There is still not much known about it, though. Cross section determinations have primarily been educated speculations. However, this process was still investigated given the limited information available.

To start with, associative ionization for barium and strontium is:



Both of these reactions are endothermic. The threshold energy for barium in the center of mass frame is 0.68 ± 0.07 electron volts (eV) or 6.5 eV in the laboratory frame. The difference between the energy requirement for laboratory and center of mass reference frames is due to the requirement that momentum be conserved throughout the reaction. A velocity of around 3 km/s in the laboratory frame (same as earth reference frame) is then required, which is easily met in both releases. (Lai et al., 1992a) The energy requirement for strontium to participate here might be assumed to be similar, since its ionizing potential is so close (6.60 ± 0.05 eV to barium's 6.46 ± 0.07 eV) (Dyke et al., 1987). In order for AI to contribute to the ion counts seen in the experiments, the barium and strontium oxide ions would need somehow to be converted to Ba^+ and Sr^+ . According to Lai et al. (1992a), the primary mechanism for this is Lyman-alpha (UV) radiation, through either of the following schemes:

Scheme I



Scheme 2



Either (18) or (19) would enable AI to produce atomic barium ions indistinguishable from ions yielded by any of the other processes.

Immediately there is one noticeable advantage to this ionization method. At 500 km altitude the most numerous ionospheric particle, neutral or ion, is atomic oxygen. Densities are around 10^{14} per m^3 (U.S. Standard Atmosphere, 1976). With guesses for cross sections of 10^{-20} m^2 from Lai and Murad (1989b) and between 10^{-19} and 10^{-21} m^2 from Lai et al. (1992a), ion production could be quite significant.

Evidence for AI occurrence in the CRRES releases was then sought out. The results were negative. Wescott et al. (1994) looked for increased 4554 Angstrom emissions that should be present if BaO^+ is dissociating on a large scale. These were not observed. Another possibility for signs of AI could have been found in the QIMS data. Since the spectrometer was supposed to be sensitive up to 155 amu's, BaO^+ at 153 and SrO^+ at 103 amu's should have registered. However, since planners did not anticipate AI occurrence, the instrument was not directed to look for particles of those masses. Any such counts would not have been recorded. (Hunton, personal communication) The final consideration was that in accordance with known processes, AI would require sunlight to produce Ba^+ . This was simply not present in the G-11b release until approximately 20 seconds after detonation. Most of the barium ion counts had already been taken. Thus associative ionization was not investigated any further and was determined to not have played a part in the CRRES chemical release experiments. It is possible that there are other methods by which BaO^+ could dissociate, such as collisions with ambient particles, but the cross sections of these processes are unknown at this time.

5.1.5 Charge Stripping

Charge stripping is the last ionization process that was investigated in the interpretation of the CRRES data. It is also endothermic and according to Stenbaek-Nielsen et al. (1990) has a threshold energy of 5.21 eV for barium in the center of mass frame. This requires the neutrals to be moving at a rapid 8.4 km/s, assuming the ambients are at rest. For strontium the threshold energy would be 5.69 eV (the ionization potential), necessitating a velocity of around 8.8 km/s. These basic requirements were met in both the G-1 and G-11b releases and so the research continued. The basic form is:



As is evident, this is another reaction that takes advantage of the naturally high concentrations of atomic oxygen. It has an advantage over AI in that it converts neutral barium and strontium directly to Ba^+ and Sr^+ . The disadvantage is that even less is known about stripping cross sections. There have been several theoretical studies done, but no laboratory tests were found with which these estimates could be compared. According to Stenbaek-Nielsen et al. (1990), cross sections produced by these studies have ranged from 10^{-22} up to 10^{-20} m^2 for barium interacting with the ambient oxygen. Similar cross section estimates for strontium have not been found. The action taken upon acquiring this information was to test the range of cross sections for Ba against the experimental data, given the standard oxygen densities at the resident height in the atmosphere. The results of this action are shown in the next section.

5.1.6 Thermal Ionization and Population of Metastable States from Thermite Burn

The titanium-boron reaction required to vaporize the barium and strontium was stated earlier. Stenbaek-Nielsen et al. (1993) state that the temperature brought about by this detonation in each release was 2750 Kelvins. This is about twice the usual ambient temperature at this altitude (Kelley, 1989), so the possibility of ionization due to initial thermal effects was investigated. As reported by Hunton (1994), this does not even present enough energy to significantly populate the metastable states of barium and strontium. Stenbaek-Nielsen et al. (1990) found that the same reaction in the CRIT I release could not have much consequence. The small amount of ionization that would occur must do so in the first few tens of microseconds after detonation. These ions would never reach the spacecraft, of course. Also, CRIT I was a shaped charge release, which would concentrate the thermal energy more and allow a slower temperature fall-off with time than in a spherical expansion. A CRRES-type cloud would thermally produce even fewer ions. This source was then ignored.

5.2 Comparison of Modeled Processes to Experimental Data

We then had 4 reactions for which conditions were favorable and which were possible sources of ionization in the CRRES releases. For each of these processes, the model was compared to the appropriate data set, using the ionization time constant and rate constant as shown in the model section. It is important to remember that the speed or efficiency of each reaction depends on 3 factors, the number density of the ionizing particle, the cross section or probability of occurrence of the reaction, and the relative velocity between the species involved. The relative velocity is the same no matter what the reaction, so the

relative dominance of any process depends on the number density and cross section. If in the comparison of 2 reactions “a” and “b”, we find that the cross section of “a” is 100 times greater than that of “b”, but the number density in “b” is 100 times greater than that in “a”, the yields in ion density will be equal. This is important to keep in mind as the comparisons are made.

The time constants required for the model to match each of the data sets were calculated in Appendix C. The value of τ needed to match the barium G-1 ion flux would simply be the photoionization time constant, 28 seconds, since the model was normalized to that data. The time constants required to match the G-1 strontium and G-11b barium and strontium data sets are 26, 260, and 90 seconds respectively. Thus the strontium neutrals were apparently ionized at about the same rate as the barium atoms in G-1 (sunlit release) and at a much faster rate in G-11b (darkness release). This section will basically be comparing the time constants for each of the 4 processes to those required to match the data. For all the comparisons, the model curve is displayed as a solid line and the data as a dotted line. In addition, where the model output falls below the baseline of the experimental data represents an ion flux below the sensitivity of the spectrometer.

5.2.1 Photoionization

The model was normalized to the barium sunlit release (G-1) assuming photoionization, so the 2 curves exactly match and there is no need for further comparison. However, in the strontium G-1 data, we found a surprising result. As shown in Fig. 2, there was a significant ion flux measured. In Fig. 14, strontium photoionization

is compared to the G-1 data. Our model falls almost 2 orders of magnitude short of matching the data. Another process must be producing the strontium ions in sunlight.

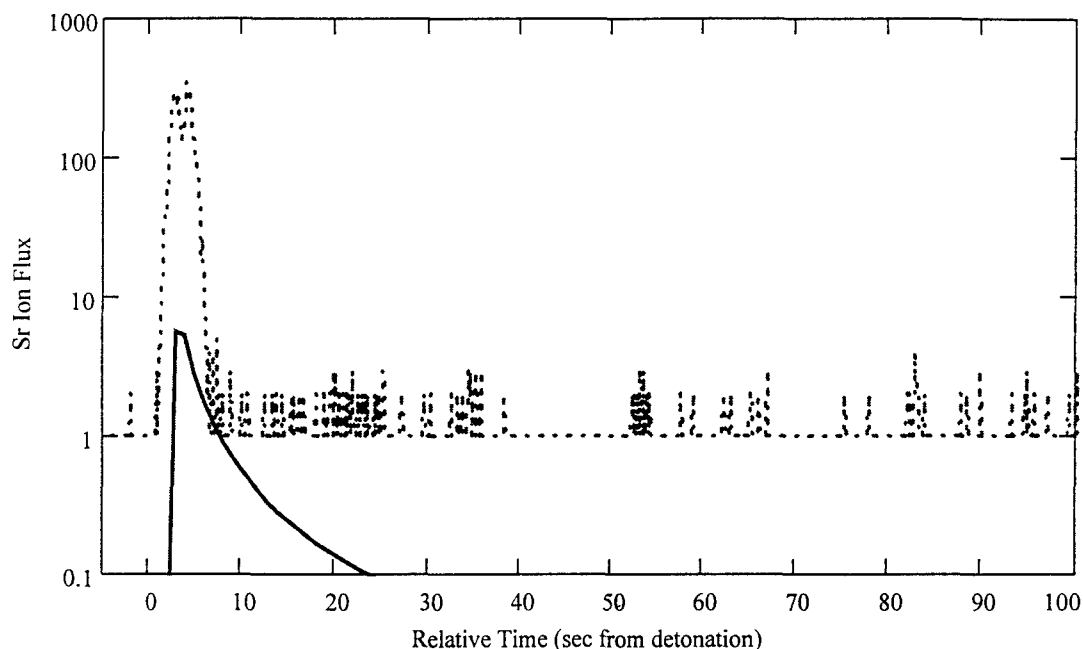
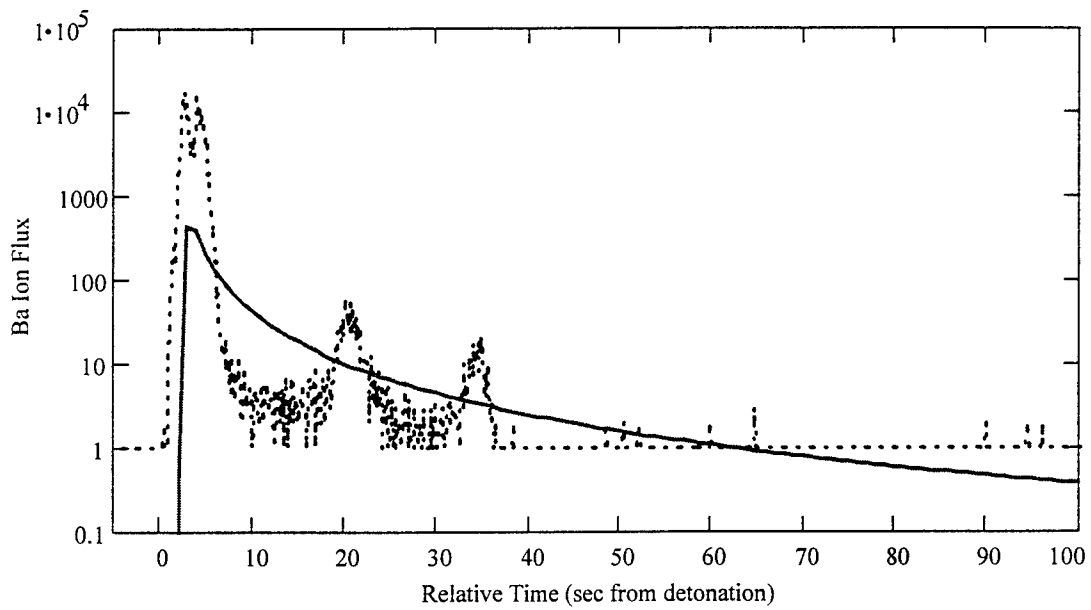


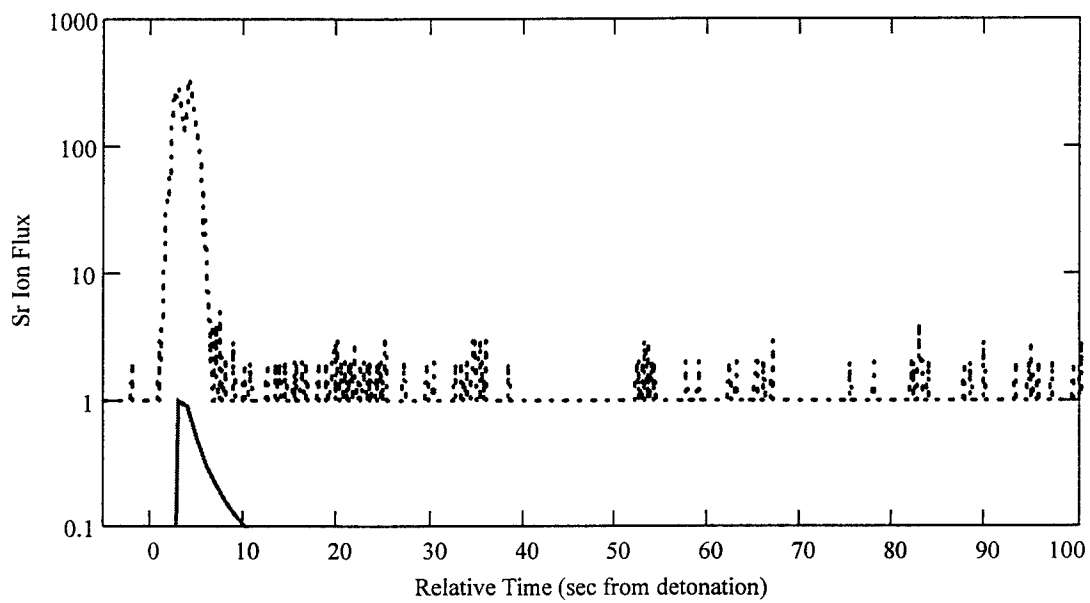
Figure 14. Comparison of Photoionization Model with Data

5.2.2 Charge Exchange

Conditions favorable to charge exchange were present in both sunlight and darkness. Thus the model is compared to the measured ion fluxes for both releases. The only change is that, as stated above, we assumed the O^+ density to be half an order of magnitude higher on the day side of the terminator. In Fig. 15 (a) and (b), the nighttime CE model is shown with the G-1 data for both barium and strontium, and in (c) and (d), CE in sunlight is compared to the G-11b data. For barium in sunlight, we find that the model produces a first maximum about one and a half orders of magnitude smaller than the maximum flux measured in the experiment. This was expected, since the model was

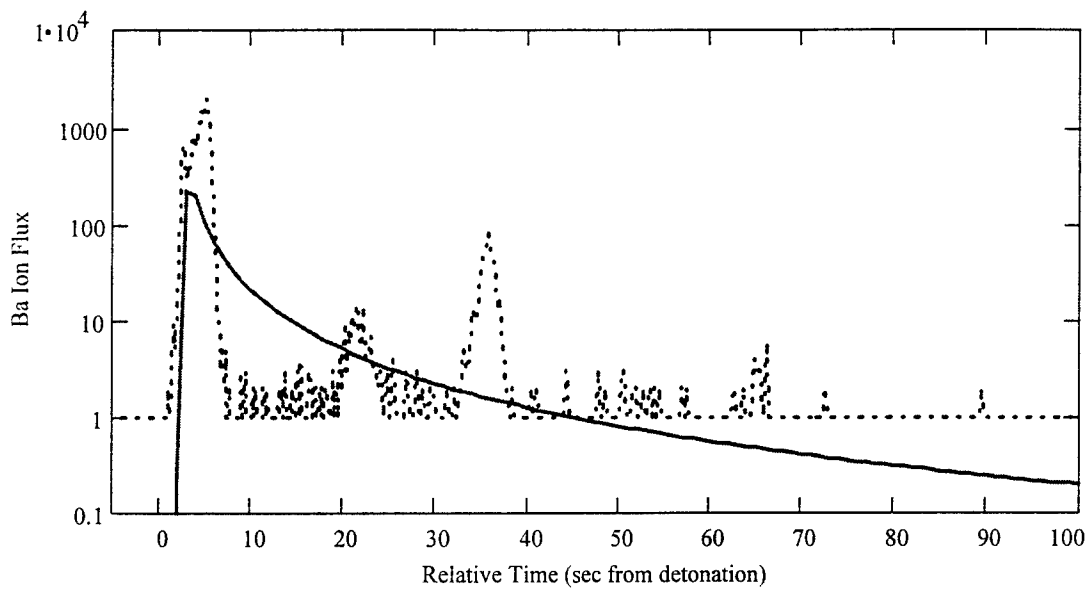


(a) Ba CE against G-1 (Sunlit) Data

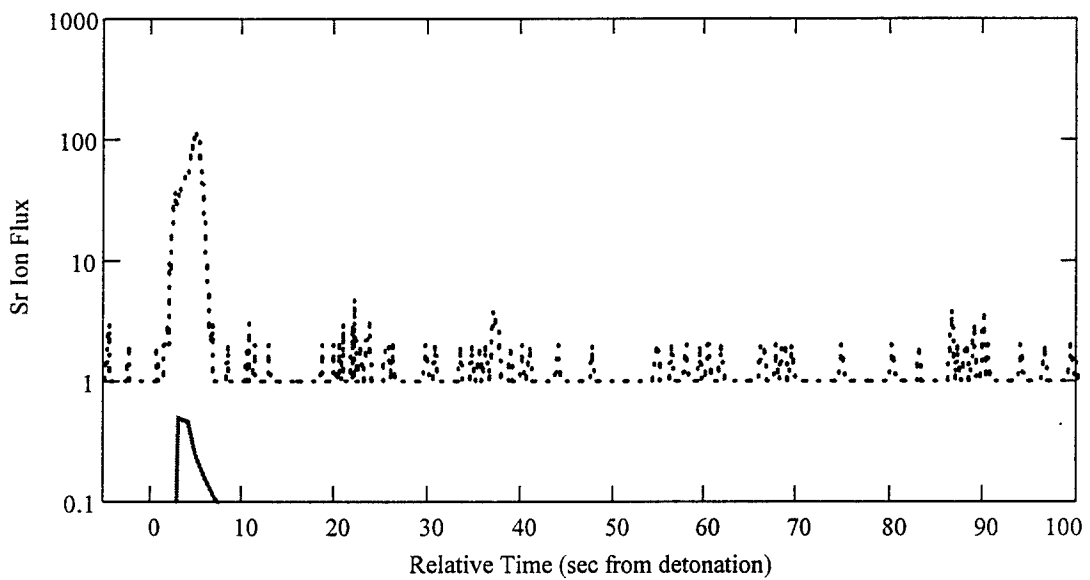


(b) Sr CE against G-1 (Sunlit) Data

Figure 15. Comparison of Charge Exchange Model with Data



(c) Ba CE against G-11b (Dark) Data



(d) Sr CE against G-11b (Dark) Data

Figure 15. Comparison of Charge Exchange Model with Data

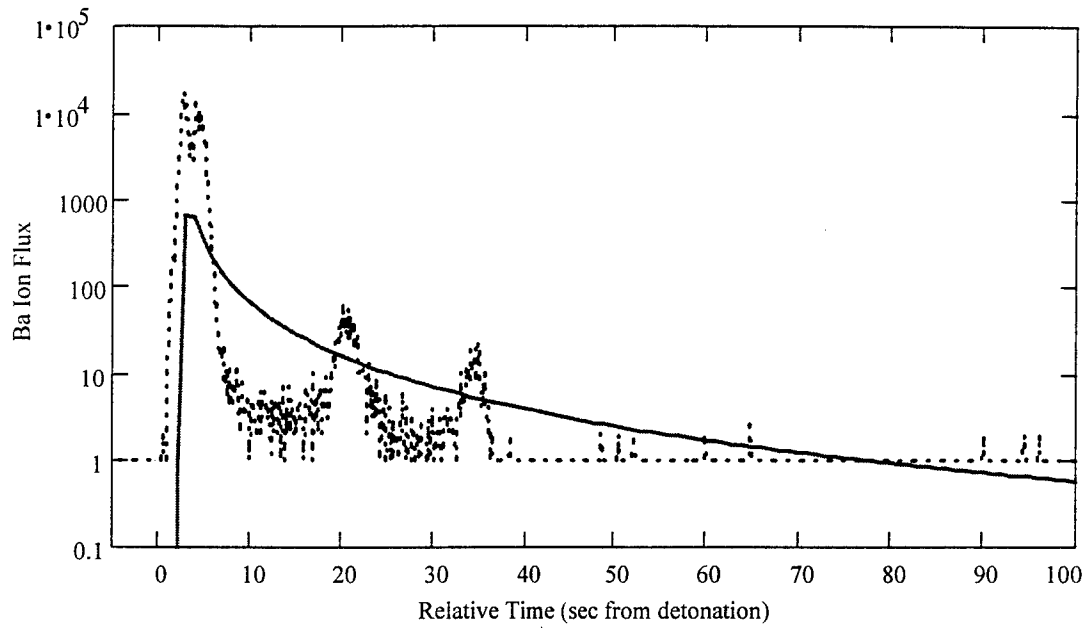
normalized using photoionization and charge exchange is a much slower reaction than photoionization for barium. Initially, we thought that CE would be dominant in the G-11b release, where sunlight was absent. However, we also found a one and a half order of magnitude difference between the CE model output and the barium data in darkness. Analyzing the strontium comparisons, we see that CE can account for neither the G-1 data, in which the model output is a half an order of magnitude less than the measured flux, nor the G-11b case, in which there is a whole order of magnitude shortfall.

What has not been considered in the modeling of charge exchange is the possible role of metastable states. Generally speaking, the cross sections for charge transfer between barium and strontium metastables and O^+ are higher than those for the ground states (Wolf, 1995b). These have been ignored here. It is unknown whether or not a large portion of the neutral cloud was elevated to metastable states. In the release without sunlight, this would have required a mechanism to energize the particles, most likely kinetic heating. Hunton (1994) calculated the population of these levels for different temperatures and found that there was not a significant number of atoms in metastable states until around 10,000 Kelvins. At this temperature, 15 percent of the barium and 12 percent of the strontium atoms would be in the forbidden energy levels. This obviously would require that a highly efficient energy transfer, such as in CIV, was taking place to energize the particles and produce such high temperatures. However, since even 15 percent of the population in metastable states could not produce a model output comparable in magnitude to the data and there is no way of knowing the temperature reached in the early-time cloud, the metastable states were ignored. Charge exchange as

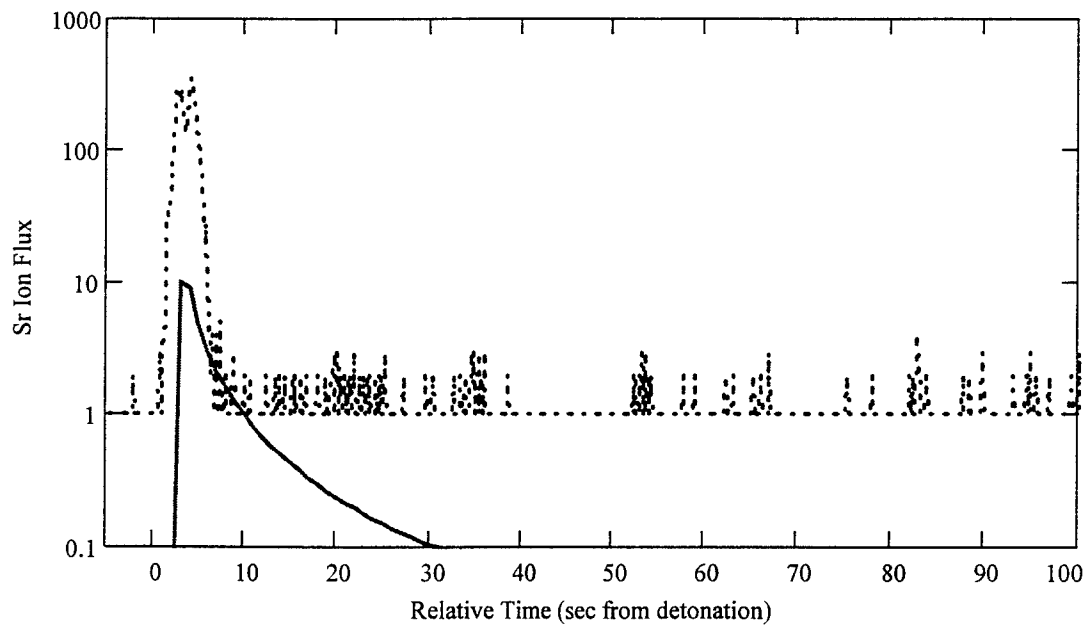
modeled in this study cannot reproduce the magnitude of ion fluxes measured in G-1 and G-11b.

5.2.3 Electron Impact

Recall that the EI cross sections used are for 10 eV (“hot”) electrons. Since the daytime and nighttime electron densities in the reaction are defined as 1×10^{12} and 5×10^{11} electrons per m^3 respectively, we are assuming the number of hot electrons to be equal to the normal ionospheric plasma density. The EI model output is compared to both barium and strontium ion fluxes for first the G-1 release in Fig. 17 (a) and (b) and then for G-11b in (c) and (d). We found that the EI model produced an ion flux one order of magnitude less than that in the barium G-1 experiment and one and a half orders of magnitude less in all the other data sets. Assuming that the cross sections are not any higher, the energetic electron densities would have to be higher than that used for these calculations in order to match the experimental results. The electron number densities required to match the intensities of the experimental results can be found using the cross sections from McFarland and Vainshtein and the ionization time constants of the experimental data mentioned in section 5.2. For G-11b the electron density needed is approximately 3×10^{12} m^{-3} for Ba and 1×10^{13} m^{-3} for Sr. For the strontium sunlit release, the required electron density would be about 4×10^{13} m^{-3} . These are on the order of or higher than normal daytime ionospheric densities. Given that only 10 percent of the electron population is typically in the hot tail of the energy distribution, as discussed in the CIV theory section in Appendix A (Lai et al., 1989b), it is obvious that Alfvén’s process (CIV or self-sustaining EI) would have been limited to very early times in the experiment when

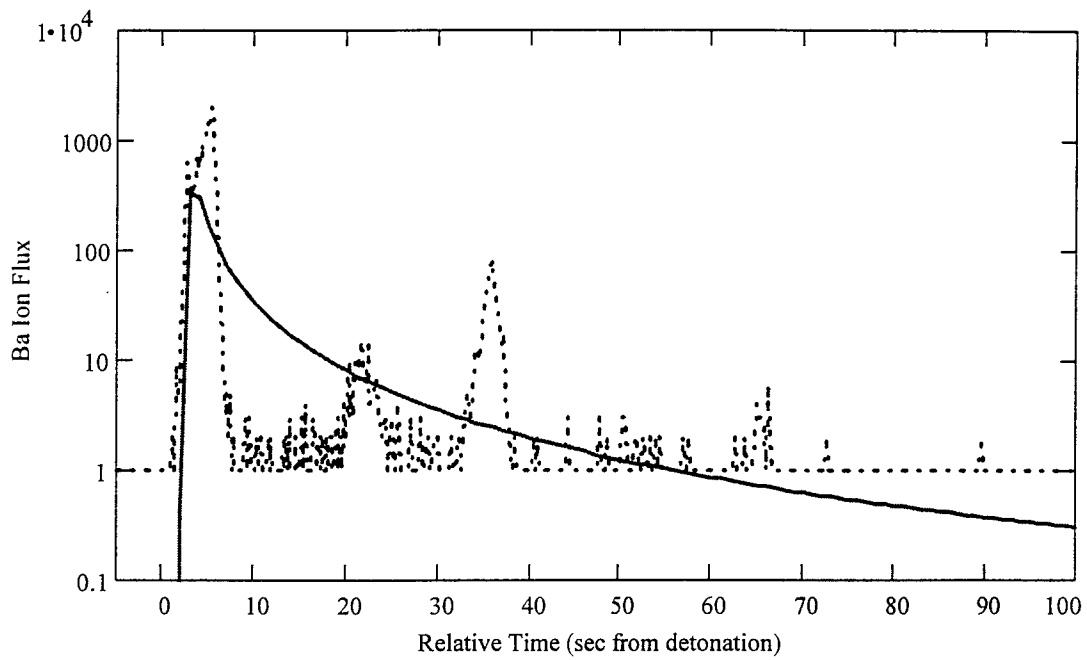


(a) Ba EI against G-1 (Sunlit) Data

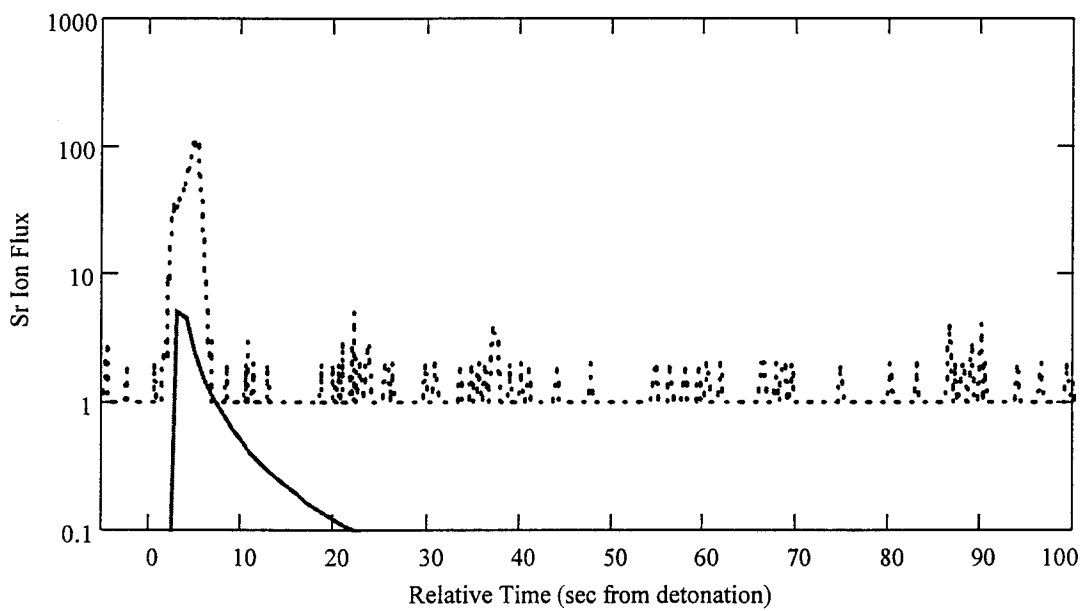


(b) Sr EI against G-1 (Sunlit) Data

Figure 16. Comparison of Electron Impact Model with Data



(c) Ba EI against G-11b (Dark) Data



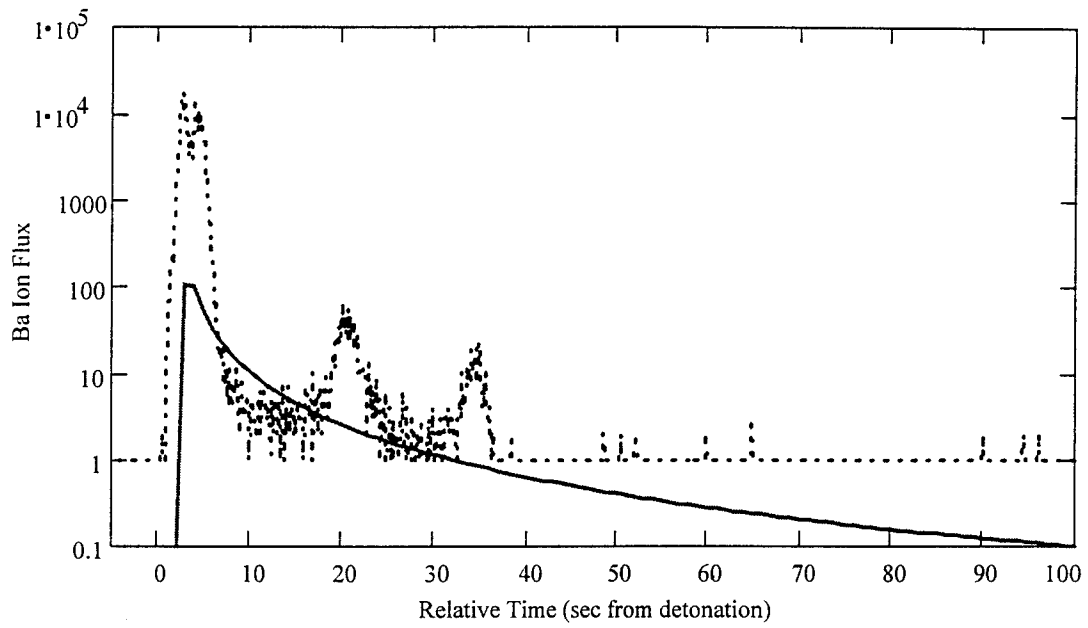
(d) Sr EI against G-11b (Dark) Data

Figure 16. Comparison of Electron Impact Model with Data

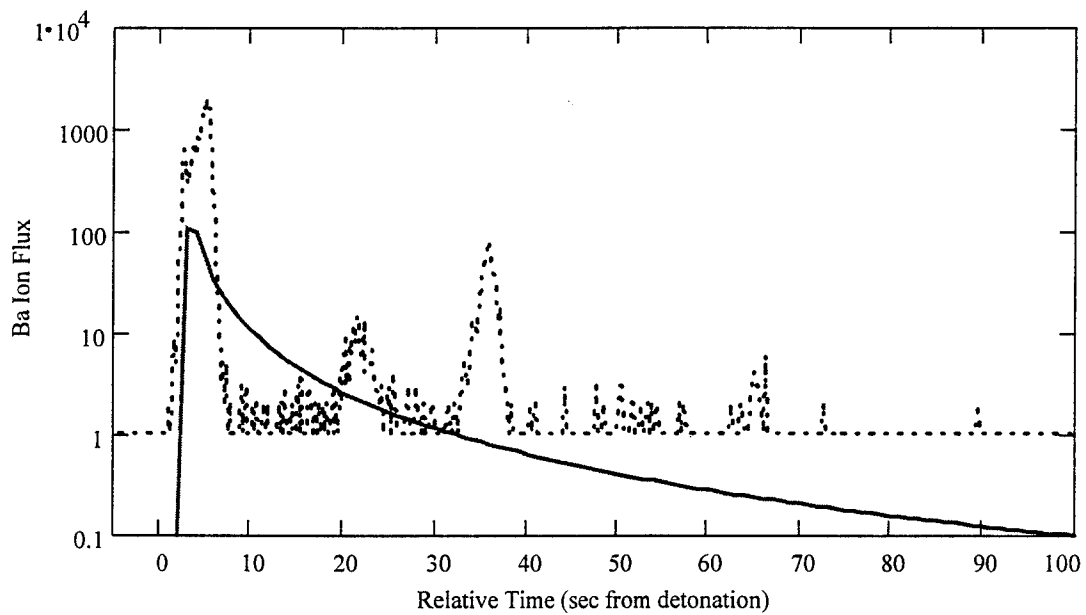
densities were high. As for conclusions on whether or not CIV took place via electron impact, that is uncertain. What does seem to be certain is that EI by itself could not have accounted for the ion fluxes measured by QIMS.

5.2.4 Charge Stripping

Since the only available estimates for cross sections of charge stripping by atomic oxygen were for barium, there is no model comparison with the strontium data. For the case of Ba, the stripping model using the conservative end of the cross section range is compared to the G-1 and G-11b data in Fig. 18 (a) and (b). Here, the result is similar to that of charge exchange and electron impact. The ion flux measured in sunlight is more than 2 orders of magnitude greater than the model output and the ion flux in darkness displays one and a half orders of magnitude greater intensity than the model. In Fig. 18 (c) and (d), the stripping model is again compared to the experimental data, this time using the high estimate for the cross section. In this case we found that the charge stripping model yielded an ion flux comparable in magnitude to that measured in the sunlit release and an order of magnitude greater than the quantity measured in darkness. In this hypothetical situation, the output of the model and speed of the reaction are comparable to those of photoionization. Thus the range of available cross section estimates encompasses the experimental results.

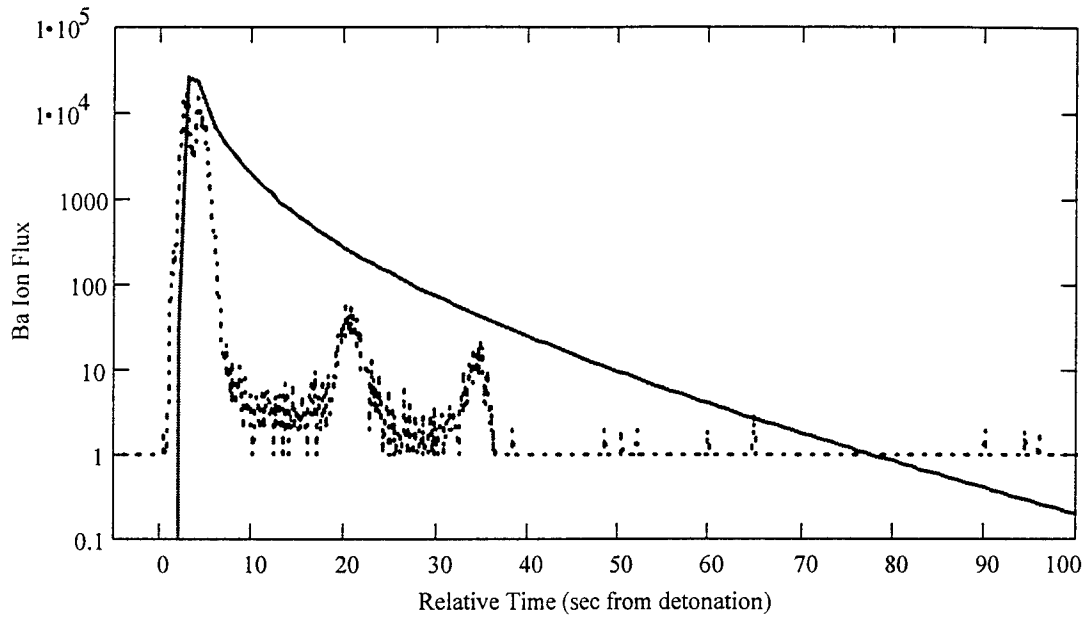


(a) Ba Stripping vs G-1 (Sunlit) Data Using Low Estimate of σ

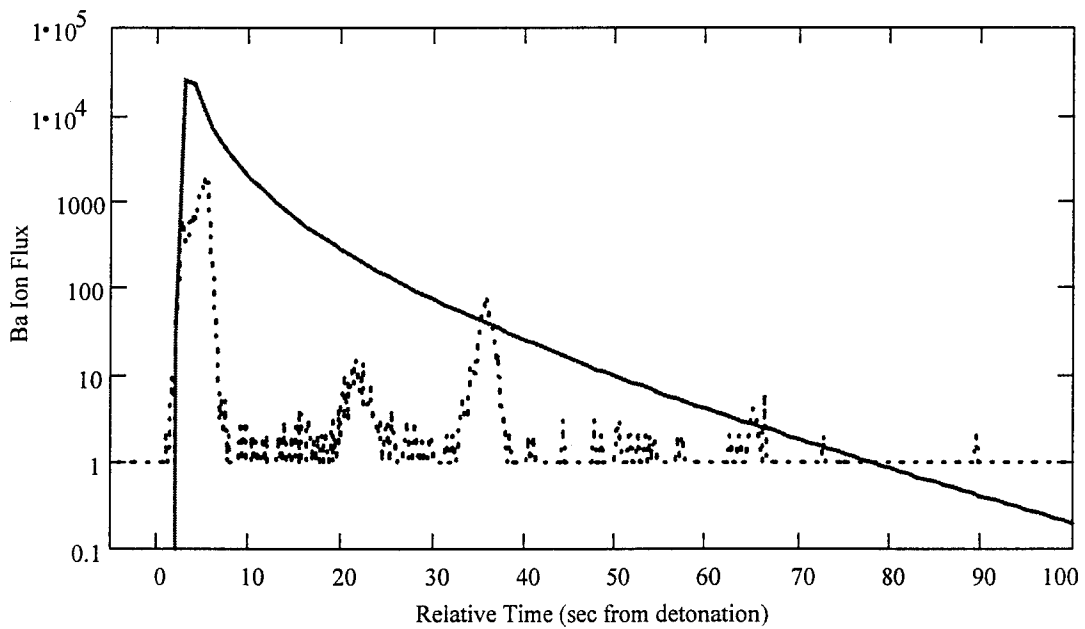


(b) Ba Stripping vs G-11b (Dark) Data Using Low Estimate of σ

Figure 17. Comparison of Charge Stripping Model with Data



(c) Ba Stripping vs G-1 (Sunlit) Data Using High Estimate of σ



(d) Ba Stripping vs G-11b (Dark) Data Using High Estimate of σ

Figure 17. Comparison of Charge Stripping Model with Data

Using the time constants required to match each set of data (discussed in section 5.2) and an atomic oxygen density of 10^{14} atoms m^{-3} , the charge stripping cross sections required to exactly match the experimental data were calculated. These values are summarized as follows in Table 2:

Table 2. Required Cross Sections for Charge Stripping to Match Data

Ba Dark:	$7 \times 10^{-22} m^2$
Sr Light:	$7 \times 10^{-21} m^2$
Sr Dark:	$2 \times 10^{-21} m^2$

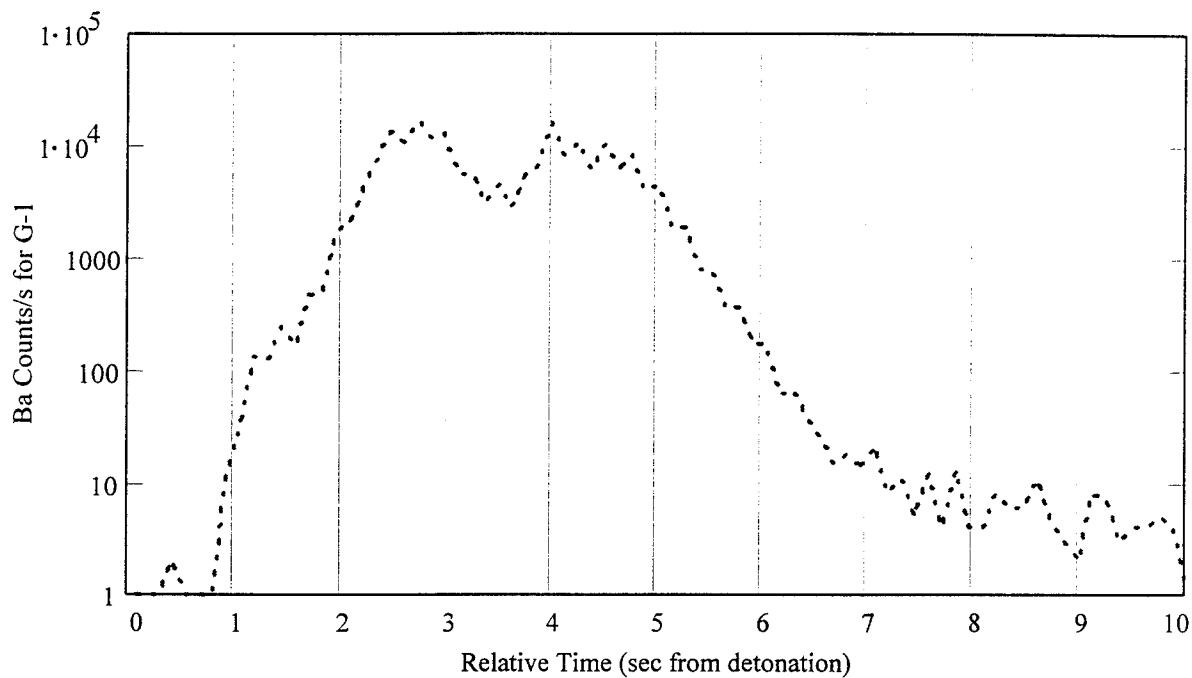
These fall within the latitude of values for barium that were listed above. The reason that charge stripping works better than charge exchange or electron impact is because of what was discussed at the beginning of 5.2. The ionization rate constant is directly related to the product of "n" and "σ", and even if the stripping cross section is an order of magnitude or so less than that for CE or EI, the atomic oxygen density is at least 2 orders of magnitude greater than that of O^+ or electrons. Assuming Sr reacts similarly with atomic oxygen, this reaction is also a possible source of ions in the CRRES experiments. In fact, stripping very well poses a possibility as being the dominant collisional process in these releases. The positive results of this comparison must of course be tempered with the fact that, as we mentioned before, the cross sections listed are only estimates and have not been experimentally tested as far as we know. Further research would have to be accomplished in order to extend this charge stripping solution beyond a hypothesis.

5.3 Investigation of Twin Peaks at First Maximum

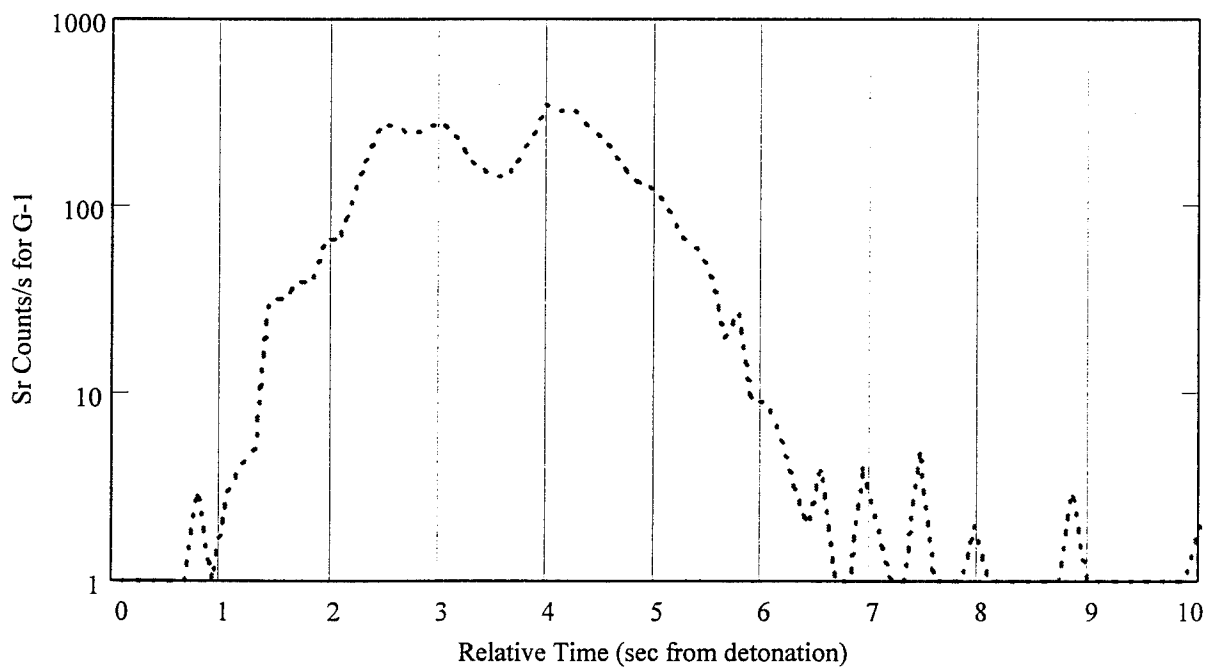
A peculiarity evident in both barium and strontium data sets in both releases is the appearance of two miniature peaks forming the first flux maximum encountered at QIMS. In sunlight this appears as two equally intense peaks, while in G-11b the initial sub-vertex is of less strength than the one following. This behavior in G-1 barium and strontium and G-11b barium and strontium is shown in Fig. 19 (a) - (d) respectively.

We investigated several mechanisms to see if they could explain this phenomenon. A physical explanation is required to properly account for what is seen in the data. It was noticed early on that the charge exchange reaction, especially utilizing the higher O^+ densities "seen" at the cloud leading edge, could easily account for the magnitude of the first and smaller minor peak in G-11b. The timing of this first peak corresponds to the fastest barium and strontium neutrals at the front edge of the expanding shell. As calculated in Wolf (1995a), the charge exchange cross sections for Ba and Sr increases with increasing energy. These faster particles could have been interacting with the ambient ions in the O^+ density "bump" mentioned earlier in the snowplow section, which also occurred at the same time as the first miniature Ba^+ and Sr^+ peak. This situation represented the best conditions for charge exchange available throughout the experiment.

If this is the case then what faster Ba^+ -producing reaction could have created the second larger maximum? As seen above, the charge stripping reaction is a potential candidate. This mechanism requires neutral atomic oxygen to produce ionize Ba/Sr. One idea was briefly considered in which these particles would be temporarily evacuated by the shock wave of detonation, effectively giving stripping a "late start." However, an

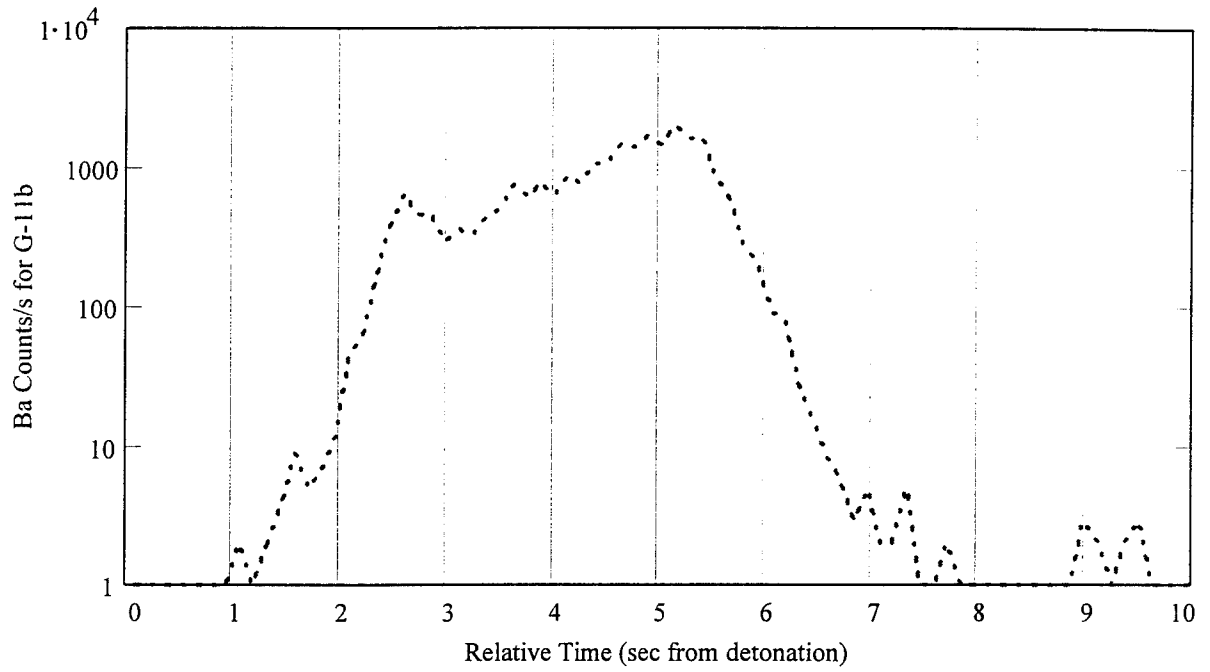


(a) Ba G-1

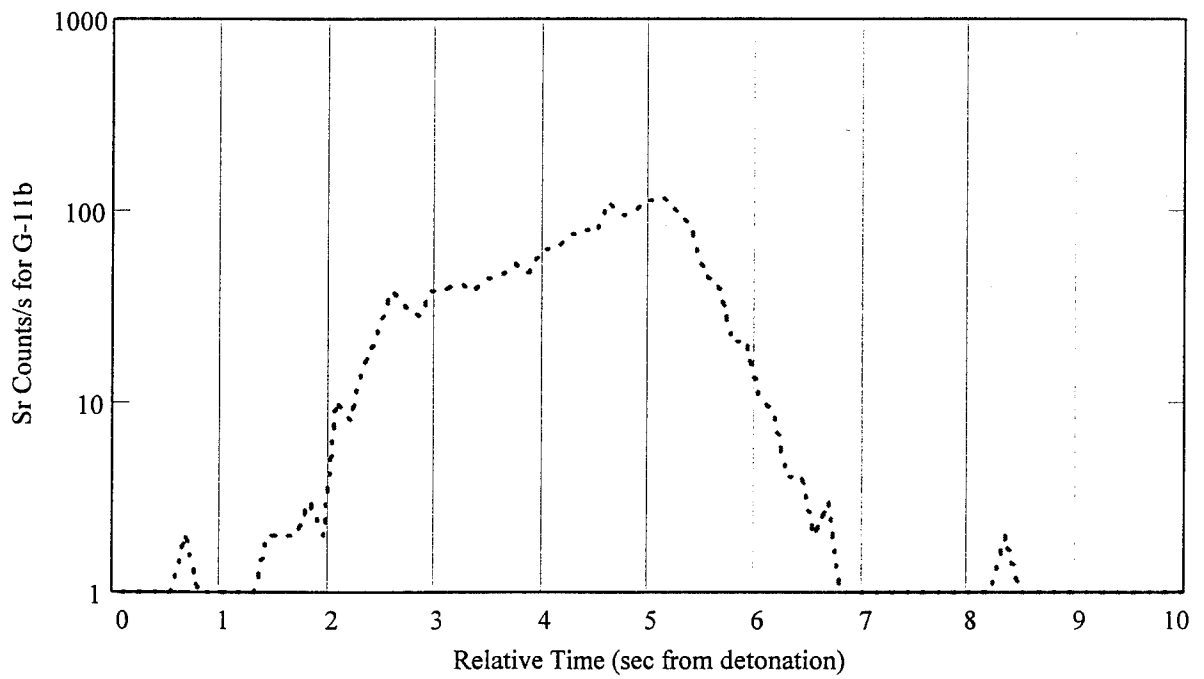


(b) Sr G-1

Figure 18. Twin Peaks at First Maximum



(c) Ba G-11b



(d) Sr G-11b

Figure 18. Twin Peaks at First Maximum

order of magnitude decrease in the O density would be required to provide an adequate delay. This is unrealistic, since the environment is considered at least nearly collisionless and pushing 90 percent of the particles outwards would imply a highly collisional environment. This idea was then abandoned.

We also considered the possibility that the stripping cross section is highly velocity dependent. For most reactions, the cross section increases with velocity (kinetic energy) up to a maximum value and then falls off with larger velocities. Nothing is really known about the behavior or velocity dependence of the stripping probability, but we hypothesized here that the velocities in G-1 and G-11b (10 - 12 km/s) were in the region of the stripping cross section curve in which the reaction probability decreases with kinetic energy. The cross section would then have increased at CRRES as the spacecraft encountered the fastest expanding particles first, followed gradually by the slower individuals. For the change to be significant enough to allow for the delay in the second flux maximum, an order and a half change in the magnitude is required within a time of around 4 seconds. In addition, a linear change of velocity with time is not fast enough to allow the ion production to decrease from charge exchange before stripping begins. The behavior must display quadratic or even exponential growth over time. This hypothesis then depends on very rapid cross section growth as well as on a relatively unknown ionization process (stripping).

A third possibility that we only briefly considered is related to a finding by Delamere et al. (1995). What was observed here was a backjet and expanding neutral disk traveling in the reverse direction of the cloud center of mass and formed about two or three seconds

after detonation. They theorized that this neutral disk formed and propagated due to resonant charge exchange between Ba and Ba⁺. We investigated whether or not these neutrals could have yielded a second Ba population reaching the spacecraft and producing ions, causing the early miniature peak in both releases. Due to the fact that the disk was traveling opposite to the orbit direction at 10 km/s (20 km/s relative to the cloud and CRRES) it would have had to be large enough to already be out at the position of QIMS when it was first observed. However, the radius is not stated in the paper and it is difficult if not impossible to explain how the neutrals making up the disk could reach the satellite in advance of the main neutral cloud. Due to the high velocity of the disk in the opposite direction of CRRES and the unlikelihood of these particles reaching its position, we determined that this option could not have been a source of additional ions.

The timing of the peaks in the 4 data sets divulges some additional information which may be relevant to the explanation of the double peak. In both G-1 and G-11b, the first miniature crest occurs outside of the normal rotation period. The second minor crest is just under 15 seconds from the next major peak, and this maximum is just over 15 seconds from the third major peak. Thus these are separated roughly by half the period of the spacecraft rotation as expected. The first miniature crest is between 2 to 3 seconds out of phase with this cycle. It occurs at the same time as the O⁺ density increase. What this means is that either the ionization of the cloud was characterized by some process occurring primarily at the very far front of the cloud or that the double peak is not due to physical processes occurring in the cloud but is simply a phenomenon of QIMS, perhaps related to the manner in which the spectrometer rotated through the ion cloud. If the first

option is true, it might be an indication of an increased rate of charge exchange in the dark release due to both the O^+ density bump and the higher velocity particles at the leading edge exhibiting a higher cross section. In the sunlit release it could represent the elevated charge exchange effect plus photoionization ionizing the neutrals out on the front fringes of the expanding shell. However, this option still requires a mechanism to explain a delay in an additional process creating the second minor peak. The split nature of the first peak in the experimental data was also modeled assuming that a double process was responsible. Since there is not yet a physical justification for such a process, the comparison between this model and the data is not discussed here but is included in Appendix B.

6. Synopsis

6.1 Summary of Results

We have not been able to match the CRRES data using known processes with fairly certain cross sections. We have, however, established that photoionization is not able to account for the Sr^+ flux in sunlight and the ground state charge exchange model is not able to reproduce either the Ba^+ or Sr^+ flux in darkness or sunlight. The model output was anywhere from a half to two orders of magnitude less than the maximum fluxes measured by QIMS. Summations of the tested processes, such as strontium photoionization plus charge exchange, were not able to account for the experimental ion counts either. Stripping ionization, about which there is not much known, presents the best possible explanation of the CRRES data, even though it remains speculation without experimentally proven cross sections. While CIV is also capable of producing large ion number densities, if it did occur it probably would only have been able to maintain the required temperatures and densities through the first second or two of the releases. CIV may have been able to increase the cross sections of other processes such as charge exchange through population of the metastable states, but kinetic temperatures would have had to rise to at least 10,000 Kelvins in order to significantly do so. At this point in time there is no way of knowing if such plasma heating took place. The optical evidence from these releases certainly do not seem to indicate such high temperatures. It is much easier to envision that a process such as stripping was accountable for the higher than expected ion counts. This takes advantage of the plentiful neutral atomic oxygen present at these altitudes. Table 3 summarizes these findings by listing each ionization process

considered and whether or not the modeled process was able to match the appropriate data set.

Table 3. Summary of CRRES Modeling Results

Ionization Process	CRRES G-1 Release		CRRES G-11b Release	
	Barium	Strontium	Barium	Strontium
Photoionization	Yes	No	NA	NA
Charge Exchange	No	No	No	No
Electron Impact	No	No	No	No
Associative Ionization	No	No	No	No
Charge Stripping	Yes	Yes	Yes	Yes
Thermal Ionization	No	No	No	No

The findings from the modeling of the split peak in the first ion flux maximum of the QIMS data are also somewhat vague. There appears to be signs that 2 processes might have been responsible. The problem resides in explaining the delay in a second process. A rapid increase in the stripping cross section from near zero to a much larger value would be adequate to do so, but nothing is known of this parameter to suggest that this is justifiable.

6.2 Conclusions

The ion data from the CRRES experiments of 1991 has presented some interesting and difficult problems to solve. As this thesis progressed further and further, the objective became more and more complex. The unknowns in the experiment also continued to

increase throughout the investigation, or at least awareness of them continuously expanded. Additional and more detailed research is needed to properly understand the results of these releases. In particular, effort would be valuably spent in three major areas. The first would be to gather more data from the onboard instruments and ground-based diagnostics that were active during the releases to determine the exact direction the canisters were ejected and their precise location at the time of detonation. Next, further literature searches into the nature of charge stripping reactions as well as experimental work on determining exact cross sections between the species involved in chemical releases in space is necessary to understanding the relative importance of each ionization process. Since instruments are generally not placed right at the detonation point and do not travel outwards with the expanding neutrals, CIV can probably never be directly detected. However, indirect determination of CIV occurrence in space can never be accomplished either if reaction rates of all other processes producing identical ion products are not known. Last, additional investigation into how QIMS sampled the newly formed ions and how its sensitivity varies with angle of incidence would help to model the experiment even closer and might possibly explain the double peak in the data sets instead of a delayed process mechanism.

If further work with the model used in this study is conducted in the future, it is strongly recommended that the unknown release configuration and exact location of the cloud center of mass be determined. There exist three avenues which could possibly provide this data. The first option would probably be the easiest but is also the least reliable. The angles between QIMS and both the geomagnetic field and the velocity

vector are known at the time of detonation. The angle between QIMS and the particular ejection hole holding the G-1 and G-11b canisters should be available from the satellite platform manufacturer. From a diagram of the spacecraft in Trzcinski et al. (1992) it appears to be 45 degrees. Since the transit time from ejection to detonation as well as rotation rate of the satellite are also known, the pointing direction of the ejection module could be calculated 1498 seconds before detonation at the time of ejection. Then assuming a straight line path, the location at the time of the thermite burn could be found.

The second option is an extension of the first. It could be taken if data is available 1498 seconds before detonation. Here the angle data could be acquired from archives and the pointing direction at that particular point in time be used to locate the cloud center of mass position.

The last option involves another feature measured by on board instrumentation. The geomagnetic field at CRRES was continuously measured throughout the release. Apparently there was a fluctuation in the field measurement when a signal was sent to the module and the canister was ejected (Hunton, personal communication). Using the angle data at this point in time, the cloud could then be placed in its proper location.

The exploration into these matters is not simply a foray into remote processes in the earth's ionosphere that will only benefit theoretical science. On the contrary, if enhanced ionization or any other processes that are not fully understood reside in the upper atmosphere, it is important to know as much as possible about them. CIV may have implications in the space shuttle environment, causing glow and possibly harming instrumentation (Lai and Murad, 1989b). This danger exists similarly for all other

spacecraft that are sensitive in any respect to higher than average levels of ionization in the near vicinity. In addition, understanding the processes which create ions in the earth's atmosphere has long been important to reentry vehicles, which lose communication for varying amounts of time due to a high density plasma sheath that forms around the spacecraft. The ability to negate or even counteract the ionization processes by chemical injection or other means would eliminate another hazard in the arena of space travel. In conclusion, this thesis has determined that well known ionization processes cannot account for the ion fluxes measured in the CRRES experiments, directions for further research have been isolated, and much has been learned by the student.

Appendix A: Investigation into CIV

A.1 Critical Ionization Velocity

In the 1950's H. Alfvén described a process that he postulated could be responsible for the formation of solar systems from gas and dust orbiting a new star. He postulated that if a neutral gas moves through a plasma with high enough velocity (the critical velocity), rapid ionization rates will occur. (1954) This enhanced ionization phenomenon has come to be known as critical ionization velocity, or simply CIV. At the present time it is not firmly established in the realm of space physics. While it has been observed with a fairly high degree of certainty in the laboratory, atmospheric experiments have produced at best mixed results. Previous studies have not determined with complete confidence if Alfvén's hypothesis occurred in the CRRES experiments either.

The enhanced ionization of fast neutrals flowing through a plasma requires a very high cloud density, for reasons that will be explained below. Since the G-1 and G-11b clouds rapidly expanded and rarified, this process remained in a favorable environment for no more than a second (before the cloud reached the spacecraft) and thus these ions were never counted by QIMS. However, there are several "rulers" by which the amenity of the CRRES circumstances to CIV occurrence can be measured. A highly exothermic reaction occurring immediately after detonation and exciting a significant percentage of the neutrals to higher energy states might have been effective in increasing ionization rates later in the expansion. Thus it was essential to understand CIV and try to make a rough appraisal of whether or not it occurred in the CRRES releases. This exploration was conducted to ascertain if the CRRES planners goal of finding evidence for CIV had

been met as well as whether or not CIV might have played a part at later times in the experiment (> 2 sec). The following section presents a somewhat detailed explanation of this process in order to be able to evaluate its importance to this research.

CIV is unique in that the neutral particles' own kinetic energy is used to provide ionization energy. Direct translation of the energy into ionization via ion-neutral collisions is not possible since the energy in the center of mass frame is not adequate (Lai et al., 1989a). An indirect process is proposed as the means of effecting CIV. The neutral particles transfer their kinetic energy to ambient electrons in the plasma, which then in turn will ionize the neutrals. Only the fast electrons (those receiving enough energy from the collisions) will ionize the released particles. The velocity at which the gas must move is called the critical ionization velocity. The required velocity is:

$$V_c = \sqrt{2e\phi / m} \quad (\text{A.1})$$

where e is the charge of an electron, ϕ is the ionization potential, and m is the neutral mass. (Liou et al., 1995) The critical velocities for barium and strontium are respectively, 2.71 km/s and 3.55 km/s. It will be seen below that this is not the only requirement for such rapid ionization to occur.

In taking a deeper, more complex look at CIV, the method by which the energy is transferred from the neutral particles to electrons and back to ion production is revealed. Initial conditions for the CRRES-type experiment involve an expanding neutral cloud moving at the spacecraft orbital speed through the ambient plasma field. Typically there is not enough energy for rapid ionization of the neutrals to occur due to direct collision with the ambient ions, which are at rest. First, a seed ionization process must occur to

produce a starter population of high energy ions. Any reaction, including photoionization, charge transfer, etc., will suffice, but Person et al. (1990) report that charge exchange with ambient ions (primarily oxygen) is the dominant process providing these seed ions. Following this process, energy must be transferred from the ions to electrons. Initially this exchange takes the form of classical (collisional) heating. When the plasma increases to sufficient density to efficiently convey oscillations between particles, the method of heating the electrons switches to a plasma (wave) interchange. Specifically, the ions induce electrostatic waves which heat the electrons which themselves excite electrostatic waves and so on. This energy transfer via electrostatic means is usually explained and modeled in terms of a two stream instability in which plasma waves develop and allow energy to flow between the ions and electrons. (Lai et al., 1989a; Lai and Murad, 1989b; McNeil et al., 1990; Person et al., 1990) Using ion spectra of a CIV experiment at different stages, Torbert and Newell (1986) have demonstrated that this collective plasma process actually occurs.

There are a few different outcomes of the resulting hot electron population. As the ions transfer energy, the electron energy distribution will extend to higher and higher temperatures. While this is occurring, electrons will be colliding with other particles or escaping the plasma cloud. If significant numbers of hot electrons are able to escape without an ionizing collision, then of course ionization will stand no chance of being enhanced. This condition will be further addressed below. Another undesired outcome are collisions that do not ionize the fast neutral beam. Energy transferred by electron collisions with ions will also be lost. Either of these non-ionizing interactions represents

a sink to the CIV interaction. Those electrons that actually ionize neutrals will do so through electron impact ionization. It is the electron impact ionization of fast neutrals (as opposed to stationary ambient neutrals) which will be the reaction of primary interest. In order for this mechanism to occur, electrons must have enough kinetic energy to overcome the ionization potential of the neutral atoms. Electrons which do not meet this requirement and collide will simply excite neutrals to a higher state. Collisions which produce excitation to an allowed atomic state will most likely result in radiative de-excitation. This process, referred to as line excitation, occurs because the lifetimes of these states are so short (10^{-8} seconds). Further collisions that might take advantage of the higher energy state and ionize the atom are not very probable before emission of a photon. Such energy is lost and also represents a sink to CIV. (Biasca et al., 1993; Newell and Torbert, 1985; Person et al., 1990) Newell and Torbert (1985) investigated line excitation effects on barium and strontium injection experiments and found that about 60 percent of the electron energy is usually lost therein.

Lai et al. (1989b) have discovered that some nonionizing collisions between electrons and neutrals may aid CIV. They point out that only 10 percent of the electron population in a typical injection experiment populate the hot tail of the electron distribution. These are the only electrons which have adequate energy to ionize the neutrals, and yet CIV is supposed to be very efficient. In an earlier paper, Lai et al. (1988) postulated the use of metastable states to "pool" energy and allow for removal of electrons with energies below the ionization potential. In this proposal, a significant percentage of the excitations that result from nonionizing collisions with electrons will elevate the atom to a "forbidden,"

or metastable state. Dipole transition into such a state from the ground level is not "allowed". In other words the probability that a transition of this sort will occur is very low compared to an allowed transition. Transfer directly down to the ground energy level is also not electric dipole allowed and therefore the electron resides in this energy level for a period of time called the lifetime, which is typically on the order of milliseconds or longer. In this situation, there will be adequate time for a second or third collision with a lower energy electron before emission of a photon occurs and the atom returns to the ground state. Energy is stored in the metastable states until the atoms are ionized and consequently, electrons other than those in the hot tail can contribute to CIV. There are 2 of these metastable states for barium, 1D_2 and $^3D_{1,2,3}$, and 2 for strontium, 1D_2 and $^3P_{0,1,2}$.

Does this pose a possible boost to the rate of ionization in the CRRES releases with which were dealt in this investigation? According to Lai et al. (1989b), it was found that for higher beam velocities, simulations with and without the consideration of this aid show similar results. In other words, metastable states are very important when the energy budget for CIV is very tight, but as the velocity and kinetic energy rise, they have less and less effect. This is evident for velocities as low as two and a half times the critical speed. For releases at a height near 500 km, the neutral beam velocity is around 10 km/s, or 3.7 times the required value. This would seem to indicate that energy pooling in the form of metastable states will have little if any effect on the occurrence or non-occurrence of CIV in the CRRES experiments. Where it might have consequence is in other ionization processes as a boost to the ground state cross section. This possibility will be covered later.

Now that ionization occurs, what characteristics are good indicators that efficient critical velocity interaction will be present? There are several factors of importance. First, it has already been mentioned that the relative velocity between the neutrals and plasma in the center of mass frame must be at least 2.71 km/s for barium and 3.55 km/s for strontium. However, this may not be exact for all species, particularly the ones which are involved in the CRRES experiment. McNeil et al. (1990) has reported that, when including the effects of line excitation, barium is very slowly ionized until the velocity of the neutral gas moving through the plasma reaches twice Alfven's critical value. This means that the barium atoms must be moving at 5.42 km/s through the plasma instead of the normal expected 2.71 km/s. That requirement is more than met by experimental conditions in CRRES.

There is also a maximum velocity above which electron heating becomes inefficient and CIV shuts off. Brenning (1985) points out that in order for the plasma two stream instability to propagate and efficiently transfer energy, the neutral beam velocity must be below a value very close to the Alfven velocity, which is a characteristic speed of the plasma medium (Parks, 1991). It is expressed by:

$$V < V_A * \sqrt{1 + \beta_e} \quad (A.2)$$

where V_A is the Alfven speed

$$V_A = \frac{B}{\sqrt{\rho * \mu_0}} \quad (A.3)$$

(B is the magnetic field strength, ρ is the mass density) and β_e is the beta of the plasma:

$$\beta_e = \frac{p}{B^2 / 2\mu_0} \approx \frac{nkT}{B^2 / 2\mu_0} \quad (\text{A.4})$$

(Parks, 1991). Goertz et al. (1990) go into greater detail and provide numerical simulations indicating that CIV falls off if the neutral flow is much above the Alfvén speed. Since this value is above 17 km/s for both releases, this velocity dependent fall-off in CIV efficiency does not occur for the CRRES releases.

Earlier it was stated that electrons must not escape en masse before ionizing neutrals if CIV is to occur. The next requirement ensures that this will not happen. It is referred to as Townsend's criterion. Mathematically speaking, the neutral gas density integrated along the path of an electron through the gas must be high enough that the electron will impact and ionize a neutral before exiting the cloud. In other words, for every electron escaping there must be at least one ionization producing another hot electron. Thus the process will be self-sustaining. (Brenning, 1992a) Lai et al. (1992a) report that the Townsend condition in a CRRES-like release is satisfied out to about 8 km in the spherical expansion. However, in their calculations, the initial number of neutrals used is an order of magnitude greater than barium (three orders of magnitude greater for strontium) in G-1 and G-11b and the expansion velocity is slower. Thus Townsend's condition is most likely met until the cloud radius is at most 1 km, or less than a second after detonation.

It also appears that the magnetic field strength, neutral particle density, and plasma density all have an effect on CIV occurrence. The influence of each of these parameters is measured in terms of one of 2 ratios investigated in Axnas and Brenning (1990). The

magnetic field strength is gauged in terms of the ratio between the Alfvén velocity and the velocity of the neutrals through the plasma. This appears as:

$$\frac{V_A}{V_0} = \frac{B / \sqrt{\rho\mu_0}}{V_0} \quad (\text{A.5})$$

where B is the magnetic field strength (in tesla), and ρ is the mass density. The dependence upon the other two parameters is expressed in terms of the ratio between the ionization frequency (which is a function of the neutral density and affects the plasma frequency) and the ion gyroscopic frequency.

$$\frac{\nu_i}{\omega_i} = \frac{\nu_i}{(eB / m_i)} \quad (\text{A.6})$$

where e is the Coulomb unit charge (using gyro frequency for singly ionized atoms) and m_i is the ion mass, which would be that for barium or strontium in this case. Axnas and Brenning's two experiments (1990; 1991) and Brenning's summary of CIV experimentation (1992b) seem to agree that the lower limit for the Alfvén velocity/plasma stream velocity ratio is around unity. As this value approaches unity, the interaction gradually shuts off, and for flow velocities above the Alfvénic speed of the plasma, there is no CIV whatsoever no matter the value of the (C.6). With this number--the ionization frequency/ion gyroscopic frequency ratio--there is debate to some extent. When the magnetic field is strong and the velocity ratio is in the regime of 3-4, results have varied. Some have indicated efficient heating for a frequency ratio as low as 0.10, while other tests have required a value above unity for CIV to occur. Conditions for the CRRES G-1 and G-11b releases yield a velocity ratio around 1.7. It is then in the region of

questionable efficiency. The ionization frequency is not known and so the analysis of these requirements cannot be completed for the situation of interest here.

However, an earlier study made conclusions about the electron heating efficiency using the electron gyroscopic frequency and the plasma frequency. If the magnetic field is weak, the quantity:

$$\frac{\omega_{ge}}{\omega_{pe}} = \frac{eB / m_e}{8980\sqrt{n_e}} \quad (\text{A.7})$$

is very small. Here m_e is the electron mass and n_e is the electron (plasma) density. A general value of (A.7) used to represent a weak field strength is around 0.05, which yields very inefficient electron heating and no CIV. Apparently the two stream instability along the field lines is not able to efficiently transfer energy between fast ions and electrons. (Brenning, 1981) That is not to say that this is the inevitable conclusion to any CIV experiment in a weak magnetic field. It is possible that there could be another mechanism to act as the bridge under slightly different conditions. The releases of concern in this thesis operate under a ratio of around 0.001. Thus the magnetic field is very weak by these guidelines and the rules resultant from Brenning's study would declare conditions unfavorable to CIV. Also remember that the study producing these guidelines was conducted in a laboratory and not in space.

When testing CIV in the ionospheric experiments like Porcupine and CRIT I and II (Lai et al., 1991), as well as CRRES, altitude will undoubtedly play a part as the plasma properties change with height. Many different factors, which all depend on altitude, will have varying effects on the interaction. Ingredients which favor lower altitudes (around

the F-region maximum: 400-500 km) are items like electron heating, plasma density, and probability of charge exchange occurrence. Rising above this height means encountering lower electron densities and lower numbers of ambient ions. Fewer electrons translates to fewer particles to receive energy from the fast ions. Indeed, the apparent success of the Porcupine and CRIT II experiments in terms of rapid ion production has been attributed to the higher ambient electron densities, which were above 10^5 cm^{-3} , much higher than any of the other atmospheric experiments conducted. These two experiments have also been the only two in which CIV has been potentially identified. (Stenbaek-Nielsen et al., 1990) CIV apparently seems to favor higher plasma densities. Also, charge exchange, which provides the seed ions to initiate the process, will be more dominant at the F-region maximum where the population of oxygen ions is the highest. (Lai et al., 1991)

Discovering components which favor higher altitudes stems partially from the initial discussion of the critical velocity phenomenon above. Recall that excitation of ambient neutrals results in loss of electron energy. Ionization of ambient neutrals will also produce an energy loss as these ions are too slow and will not form a fast ion beam. Newell and Torbert (1985) found that collisions between suprathermal electrons and ambient neutrals such as atomic oxygen definitely drain energy away and thus apply a minimum requirement on the neutral cloud density for which critical velocity effects can be expected. As ambient neutrals drop off rapidly with altitude, it is obvious why such factors would favor higher regions. Last, Lai et al. (1991) calculate a ratio indicative of the competition between other ionization processes such as associative ionization and stripping. It shows that such processes dominate CIV below about 600 km, while the

critical velocity interaction is dominant above this height. This implies that the reactions responsible for the ion production in the CRRES releases could be those dominant at around 500 km. It is undetermined which of these factors are more important and at what altitudes Alfvén's enhanced ionization would be most at home. Remember also that altitude dependence is only a small part in understanding the complex nature of the ionospheric environment and how CIV fits into it.

A.2 Summary of CIV Importance to CRRES Releases

Critical velocity ionization, if it occurred, most likely did so very early on in the expansion (less than one second). Even so, this process with its efficient electron heating, could have raised the kinetic temperature high enough to populate barium and strontium metastable states and thus accelerate ionization rates later in the experiments. From the above research, a somewhat educated guess can be made as to the probability of CIV occurrence in G-1 and G-11b. A summary of all of the factors listed above and their implication for Ba and Sr ("Yes" for CIV likely, "No" for CIV unlikely) is provided in Table A-1. The conditions for the two releases are similar enough that the factors yield the same conclusion for each. From all of these considerations, it seems that there is a low probability that CIV actually occurred at any point during the CRRES experiments studied here.

Table A-1: Summary of CRRES CIV Determining Factors

	Ba	Sr
Neutral speed > critical velocity	Yes	Yes
Neutral speed < maximum velocity	Yes	Yes
Townsend condition met	< 1 second	< 1 second
Magnetic field strong enough	No	No
Altitude factors		
Electron/plasma density	Yes	Yes
Collisional damping w/ambients	No	No
Competition w/other collisional processes	No	No

Appendix B: Mathcad Model and Output

This is the notepad from which all of the graphics displayed in the thesis were obtained. It represents all of the modeling work which I accomplished throughout the research period. This notepad is included here as a reference to demonstrate how all of the modeling was accomplished using Mathcad 5.0 Plus. Remarks are also included to explain what is being done at each point in the calculations. The first step is to import the ASCII data from 4 files obtained from Hunton.

$$n_1(523\text{-K}) = 2.779 \cdot 10^{17} \cdot \text{cm}^{-3}$$

Ingestion of CRRES Data

ORIGIN = 1 This determines that all matrices will start with row and column 1 instead the default value 0.

BADARK = READPRN(badrkdat)
i := 1..1181

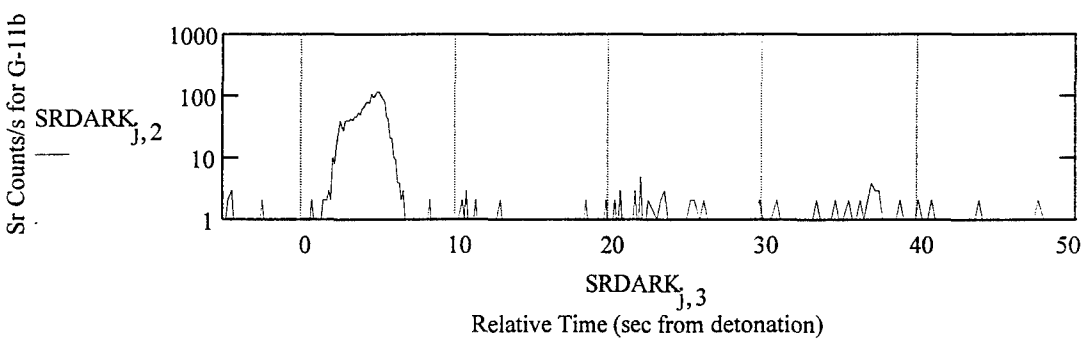
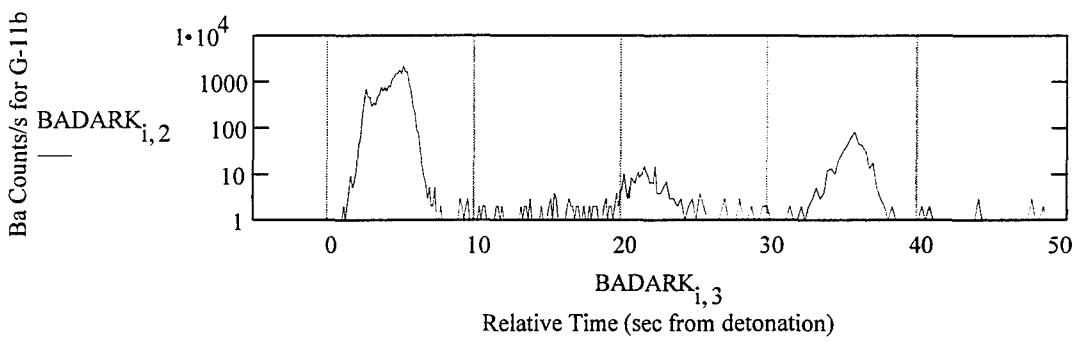
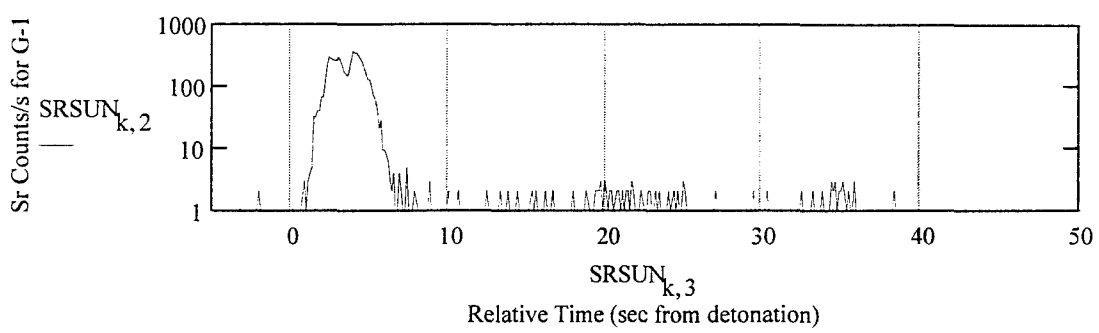
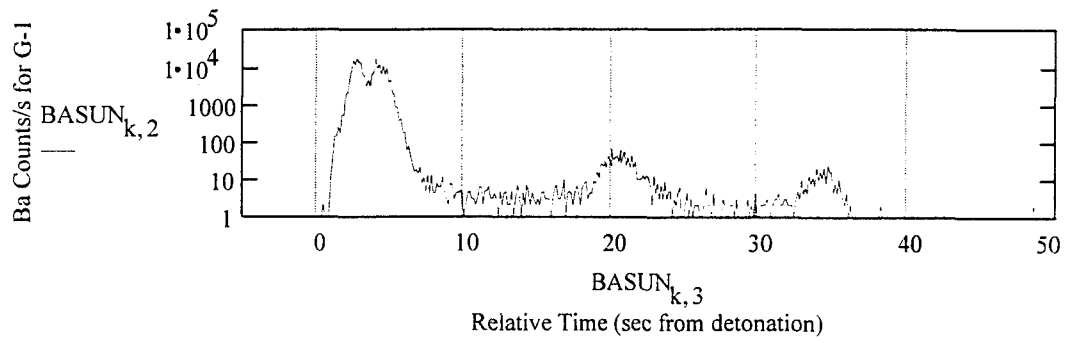
SRDARK = READPRN(srdrkdat)
j := 1..1155

BASUN = READPRN(basundat)
SRSUN = READPRN(srsundat)
k := 1..1563

NOTE: The READPRN command is used here to read the CRRES data into 4 matrices that are 4 columns wide and have as many rows as the index beneath each one. The columns are GMT, normalized counts, relative time, and counts. The argument of each statement is the filename holding the data in ASCII format and the extension of each file is ".prn". Also, the command will read as many rows and columns as exist in the data file. Elements of the matrix can be retrieved by placing a subscript (using the "[" (left bracket) key) of the row # and the column #, separated by a comma. For example, the value in the 27th row and 3rd column of sunlit barium matrix is obtained with:

$$\text{BASUN}_{27,3}$$

To obtain an entire column, replace the 3 with the appropriate range variable (i, j, or k). Finally, BASUN and SRSUN are from release G-1; BADARK and SRDARK are from release G-11b.



Graphing the Neutral Number Density

Several constants must first be defined/calculated.

$$v_0 = 1330 \quad v_w = 300 \quad \text{peak gaussian expansion \& distribution width velocities}$$

$$\tau_{\text{Ba photo}} = 28 \quad \tau_{\text{Sr photo}} = 1920 \quad \text{photoionization time constants (sec)}$$

The #'s of Ba and Sr neutrals in gaseous form are found by dividing the mass of each by the atomic mass (to get # moles), multiplying by Avagadro's constant, and finally multiplying by the % vaporization.

$$N_{\text{Ba } 0} = \frac{1471}{137.34} \cdot 6.02 \cdot 10^{23} \cdot 0.40 \quad N_{\text{Sr } 0} = \frac{19}{87.62} \cdot 6.02 \cdot 10^{23} \cdot 0.40$$

$$N_{\text{Ba } 0} = 2.57912334 \cdot 10^{24} \quad N_{\text{Sr } 0} = 5.2216389 \cdot 10^{22}$$

All constants that are part of the density integral are pulled out and lumped into one constant for each species. This saves time when Mathcad is calculating the integrals many times over the width of the range variable.

$$C_{\text{Ba}} = \frac{N_{\text{Ba } 0}}{4 \cdot \pi \cdot v_w \cdot \frac{\sqrt{\pi}}{4} \cdot v_w^2 + v_0 \cdot v_w + \frac{\sqrt{\pi}}{2} \cdot v_0^2} \quad C_{\text{Sr}} = \frac{N_{\text{Sr } 0}}{4 \cdot \pi \cdot v_w \cdot \frac{\sqrt{\pi}}{4} \cdot v_w^2 + v_0 \cdot v_w + \frac{\sqrt{\pi}}{2} \cdot v_0^2}$$

Barium Neutral Density Plot

$r = 100, 110 \dots 4600$ For values of r much greater than 4600, density values within the Mathcad zero tolerance result and cannot be plotted on a log sca

Neutral densities will be calculated at each of the following times (which are in seconds

$$t_{\text{half}} = 0.5 \quad t_1 := 1 \quad t_2 := 2 \quad t_3 := 3 \quad t_4 := 4 \quad t_5 := 5 \quad t_{10} := 10$$

The subscript on each density indicates the time (in seconds) at which it is computed.

$$\rho_{\text{Ba half}}(r) = \frac{\text{CBa} \cdot \exp\left[-\frac{t_{\text{half}}}{\tau_{\text{Ba photo}}}\right] \cdot \exp\left[-\frac{r - v_0 \cdot t_{\text{half}}}{v_w \cdot t_{\text{half}}}\right]^2}{t_{\text{half}}^3}$$

$$\rho_{\text{Ba 1}}(r) = \frac{\text{CBa} \cdot \exp\left[-\frac{t_1}{\tau_{\text{Ba photo}}}\right] \cdot \exp\left[-\frac{r - v_0 \cdot t_1}{v_w \cdot t_1}\right]^2}{t_1^3}$$

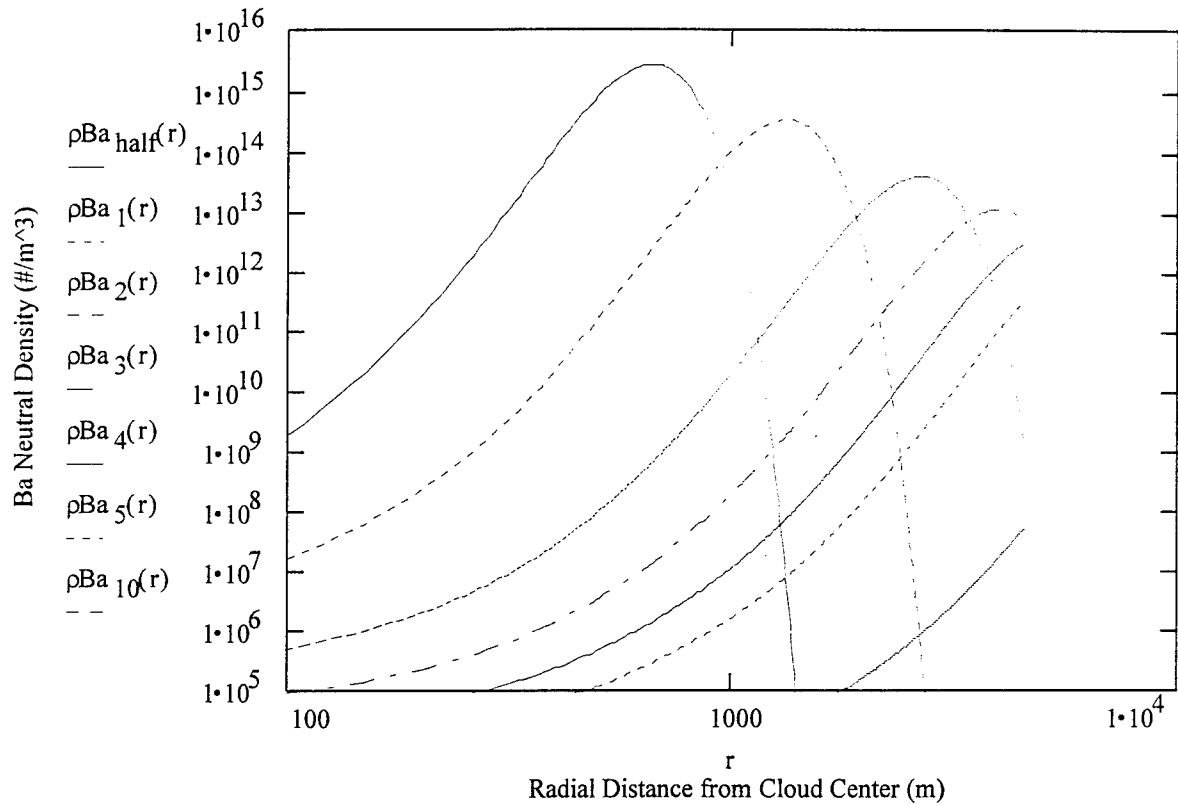
$$\rho_{\text{Ba 2}}(r) = \frac{\text{CBa} \cdot \exp\left[-\frac{t_2}{\tau_{\text{Ba photo}}}\right] \cdot \exp\left[-\frac{r - v_0 \cdot t_2}{v_w \cdot t_2}\right]^2}{t_2^3}$$

$$\rho_{\text{Ba 3}}(r) = \frac{\text{CBa} \cdot \exp\left[-\frac{t_3}{\tau_{\text{Ba photo}}}\right] \cdot \exp\left[-\frac{r - v_0 \cdot t_3}{v_w \cdot t_3}\right]^2}{t_3^3}$$

$$\rho_{\text{Ba 4}}(r) = \frac{\text{CBa} \cdot \exp\left[-\frac{t_4}{\tau_{\text{Ba photo}}}\right] \cdot \exp\left[-\frac{r - v_0 \cdot t_4}{v_w \cdot t_4}\right]^2}{t_4^3}$$

$$\rho_{\text{Ba 5}}(r) = \frac{\text{CBa} \cdot \exp\left[-\frac{t_5}{\tau_{\text{Ba photo}}}\right] \cdot \exp\left[-\frac{r - v_0 \cdot t_5}{v_w \cdot t_5}\right]^2}{t_5^3}$$

$$\rho_{\text{Ba 10}}(r) = \frac{\text{CBa} \cdot \exp\left[-\frac{t_{10}}{\tau_{\text{Ba photo}}}\right] \cdot \exp\left[-\frac{r - v_0 \cdot t_{10}}{v_w \cdot t_{10}}\right]^2}{t_{10}^3}$$



As time increases, the maximum neutral density decreases and moves farther away from the center of the cloud.

Strontium Neutral Density Plot

The same calculations are now completed for strontium

$$\rho_{\text{Sr}_{\text{half}}}(r) = \frac{\text{CSr} \cdot \left[\exp \left[-\frac{t_{\text{half}}}{\tau_{\text{Sr}_{\text{photo}}}} \right] \cdot \exp \left[-\frac{r - v_0 \cdot t_{\text{half}}}{v_w \cdot t_{\text{half}}} \right]^2 \right]}{t_{\text{half}}^3}$$

$$\rho_{\text{Sr}_1}(r) = \frac{\text{CSr} \cdot \left[\exp \left[-\frac{t_1}{\tau_{\text{Sr}_{\text{photo}}}} \right] \cdot \exp \left[-\frac{r - v_0 \cdot t_1}{v_w \cdot t_1} \right]^2 \right]}{t_1^3}$$

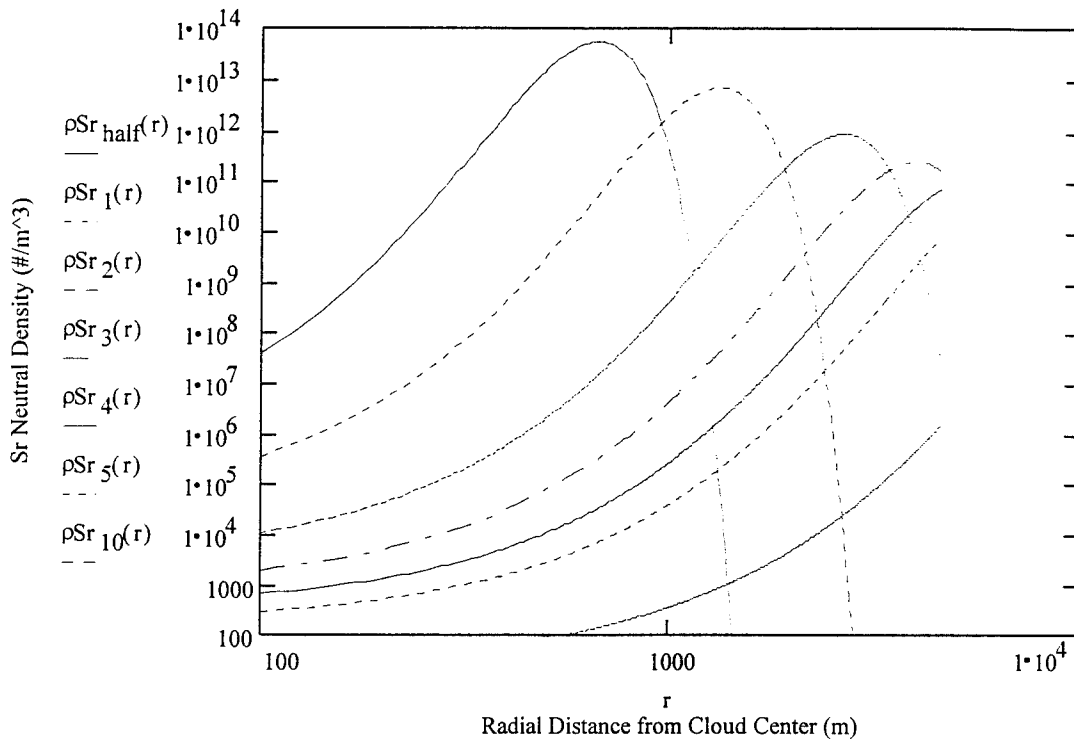
$$\rho_{Sr_2}(r) = \frac{CSr \cdot \left[\exp \left[-\frac{t_2}{\tau_{Sr_{photo}}} \right] \cdot \exp \left[-\frac{r - v_0 \cdot t_2}{v_w \cdot t_2} \right]^2 \right]}{t_2^3}$$

$$\rho_{Sr_3}(r) = \frac{CSr \cdot \left[\exp \left[-\frac{t_3}{\tau_{Sr_{photo}}} \right] \cdot \exp \left[-\frac{r - v_0 \cdot t_3}{v_w \cdot t_3} \right]^2 \right]}{t_3^3}$$

$$\rho_{Sr_4}(r) = \frac{CSr \cdot \left[\exp \left[-\frac{t_4}{\tau_{Sr_{photo}}} \right] \cdot \exp \left[-\frac{r - v_0 \cdot t_4}{v_w \cdot t_4} \right]^2 \right]}{t_4^3}$$

$$\rho_{Sr_5}(r) = \frac{CSr \cdot \left[\exp \left[-\frac{t_5}{\tau_{Sr_{photo}}} \right] \cdot \exp \left[-\frac{r - v_0 \cdot t_5}{v_w \cdot t_5} \right]^2 \right]}{t_5^3}$$

$$\rho_{Sr_{10}}(r) = \frac{CSr \cdot \left[\exp \left[-\frac{t_{10}}{\tau_{Sr_{photo}}} \right] \cdot \exp \left[-\frac{r - v_0 \cdot t_{10}}{v_w \cdot t_{10}} \right]^2 \right]}{t_{10}^3}$$



Again, as time increases, the maximum neutral density decreases and moves farther away from the center of the cloud.

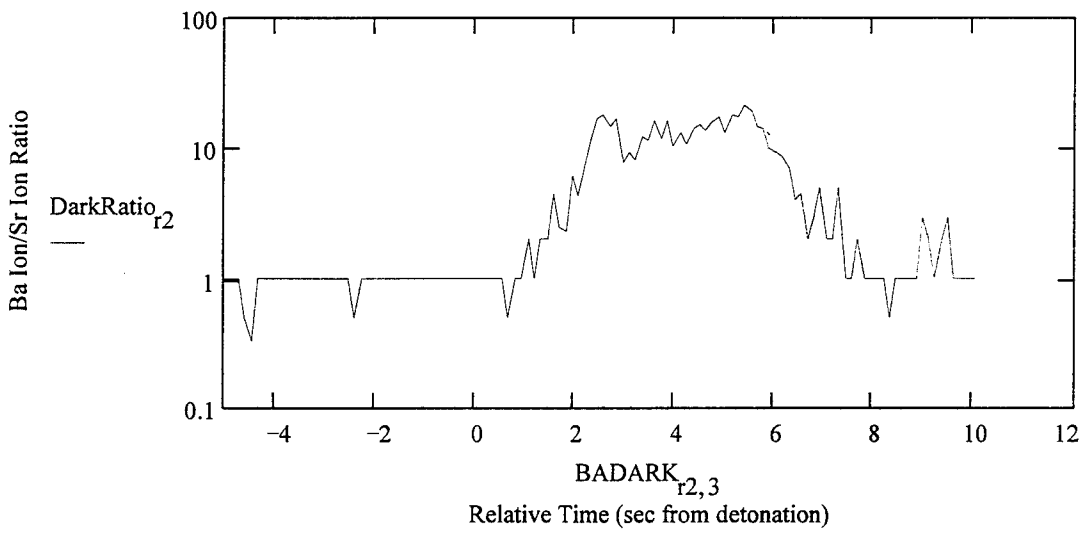
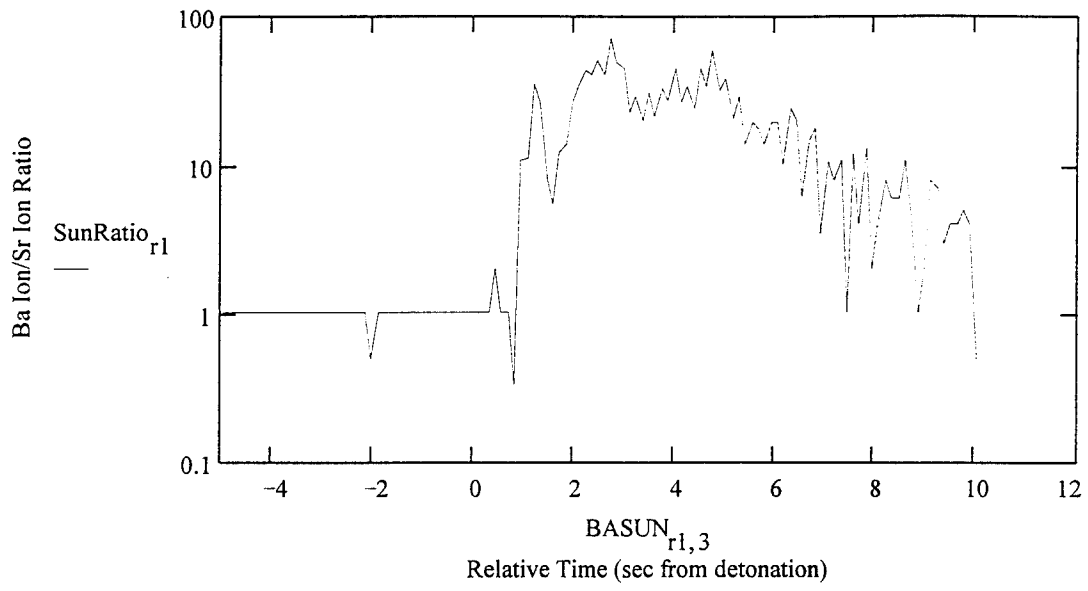
Barium Ions to Strontium Ion Ratio

Sunlight (G-1) Release:

$r1 := 1..278$ $r2 := 1..322$ indices for the G-1 and G-11b data sets, respective

$$\text{SunRatio}_{r1} := \frac{\text{BASUN}_{r1,2}}{\text{SRSUN}_{r1,2}} \quad \text{ratio of Ba ions to Sr ions in sunlit release}$$

$$\text{DarkRatio}_{r2} := \frac{\text{BADARK}_{r2,2}}{\text{SRDARK}_{r2,2}} \quad \text{ratio of Ba ions to Sr ions in darkness release}$$



Normalization of CRRES data

We'll use the barium sunlit release (G-1) and assume the major source of ions is photoionization.

Using the satellite velocity at the G-11b release: $v_s = 9.98 \cdot 10^3$

The photoionization rate constant is the inverse of the photoionization time constant:

$$k_{Ba_photo} = \frac{1}{\tau_{Ba_photo}}$$

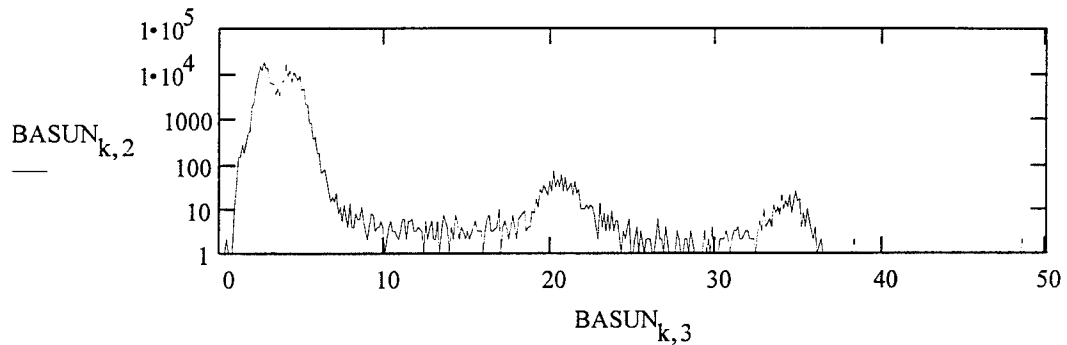
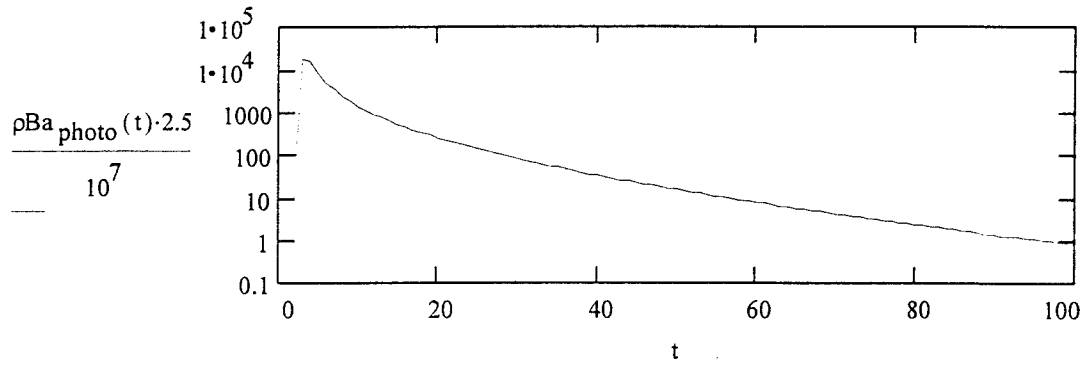
$t = 1 .. 100$ t ranges from 1 out to 100 seconds and R is the
 $R = 4200$ distance between CRRES and canister detonation.

The constant defined above is modified to include the factor which makes the integral give units of ion density.

$$C_{Ba_photo} := \frac{k_{Ba_photo}}{v_s} \cdot C_{Ba}$$

$$\rho_{Ba_photo}(t) := C_{Ba_photo} \int_0^{1.5 \cdot v_0 \cdot t} e^{-\left[\frac{t - \frac{z}{v_s}}{\tau_{Ba_photo}} \right]} \cdot e^{-\left[\frac{\left[R^2 - z^2 - v_0 \cdot t - \frac{z}{v_s} \right]^2}{v_w \cdot t - \frac{z}{v_s}} \right]} dt$$

Now we'll graph the photoionization model and the G-1 data next to each other. The multiplication factor that allows the model to peak at the same value as the data will be the normalization constant.



Using the Crosshair on Mathcad to match the first peaks, it was found that multiplying the model by $2.5/10^7$ results in the model being normalized to the data. Now previous calculation of the constants will be redone.

$$CBa := \frac{CBa}{10^7} \cdot 2.5 \quad CSr := \frac{CSr}{10^7} \cdot 2.5$$

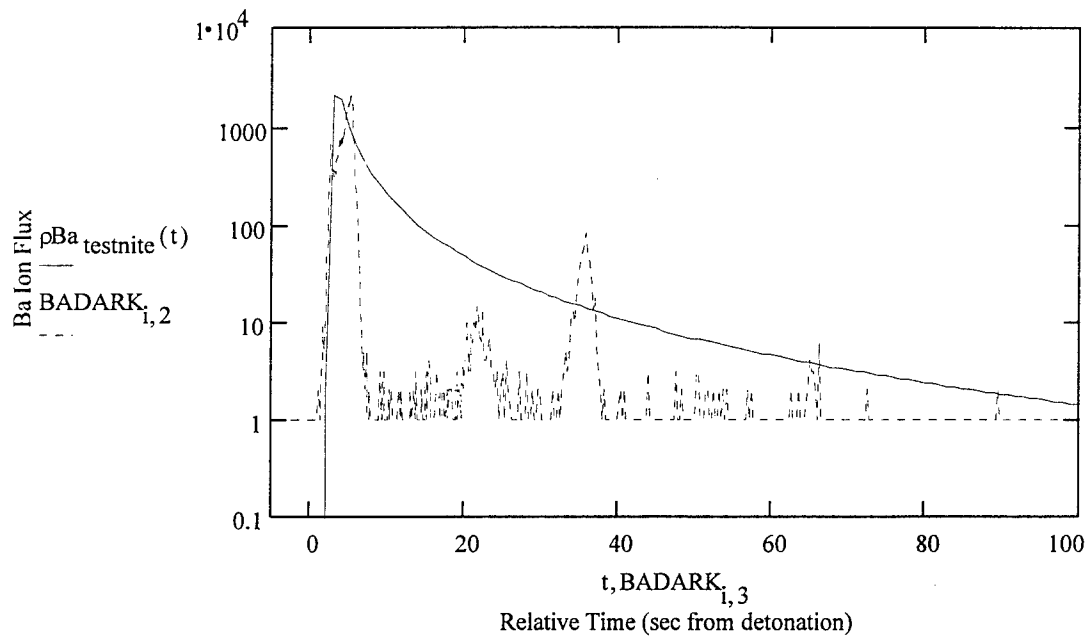
Search for Time Constants

For each set of data, the time constant required to match the QIMS counts to the normal model will be found. This will be done by simply matching the height of the first peaks.

Barium Dark (G-11b)

$$\tau_{Ba\ testnite} := 260 \quad k_{Ba\ testnite} := \frac{1}{\tau_{Ba\ testnite}} \quad CBa_{testnite} := \frac{k_{Ba\ testnite}}{v_s} \cdot CB$$

$$\rho_{\text{Ba testnité}}(t) = C_{\text{Ba testnité}} \cdot 1.5 \cdot v_0 \cdot t \cdot e^{-\frac{t - \frac{z}{v_s}}{\tau_{\text{Ba testnité}}}} \cdot e^{-\frac{\sqrt{R^2 - z^2 - v_0 \cdot t - \frac{z}{v_s}}}{v_w \cdot t - \frac{z}{v_s}}}$$



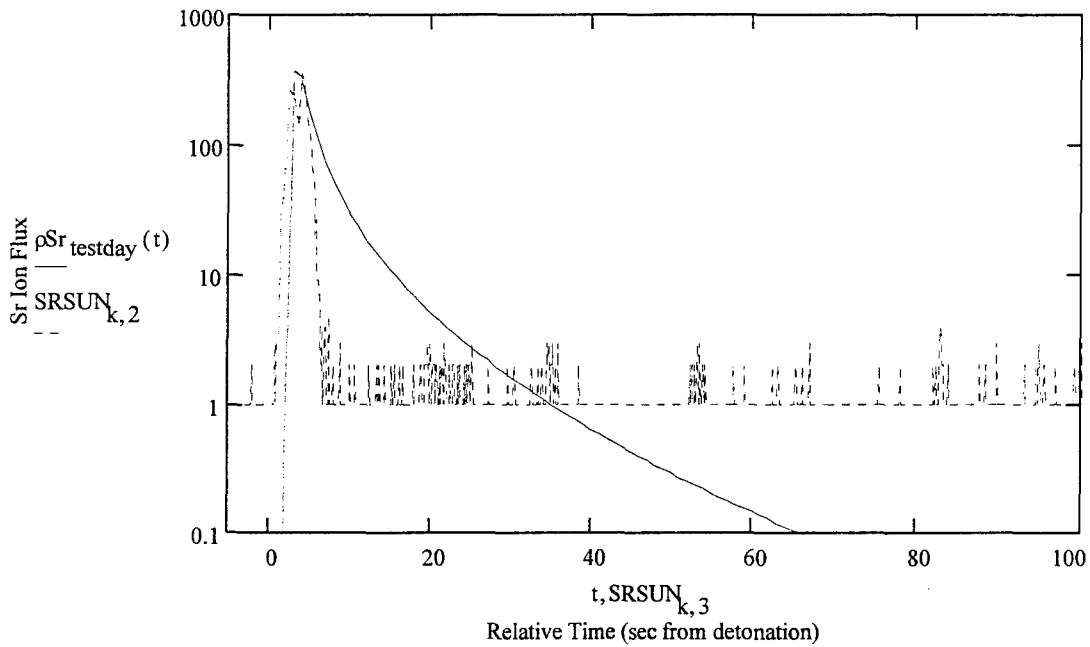
Here, it is a time constant of 260 seconds which makes the barium model fit the dark dat

Search for Time Constants (continued)

Strontium Light (G-1)

$$\tau_{\text{Sr testday}} = 26 \quad k_{\text{Sr testday}} = \frac{1}{\tau_{\text{Sr testday}}} \quad \text{CSr}_{\text{testday}} = \frac{k_{\text{Sr testday}}}{v_s} \cdot \text{CSr}$$

$$\rho_{\text{Sr testday}}(t) = \text{CSr}_{\text{testday}} \cdot e^{-\frac{t - \frac{z}{v_s}}{\tau_{\text{Sr testday}}}} \cdot e^{-\frac{R^2 - z^2 - v_0 \cdot t - \frac{z}{v_s}}{v_w \cdot t - \frac{z}{v_s}} \cdot \frac{1.5 \cdot v_0 \cdot t}{t - \frac{z}{v_s}}}$$



Here the time constant has been changed until the strontium model matches the G-1 data. The result is a constant of 26 seconds.

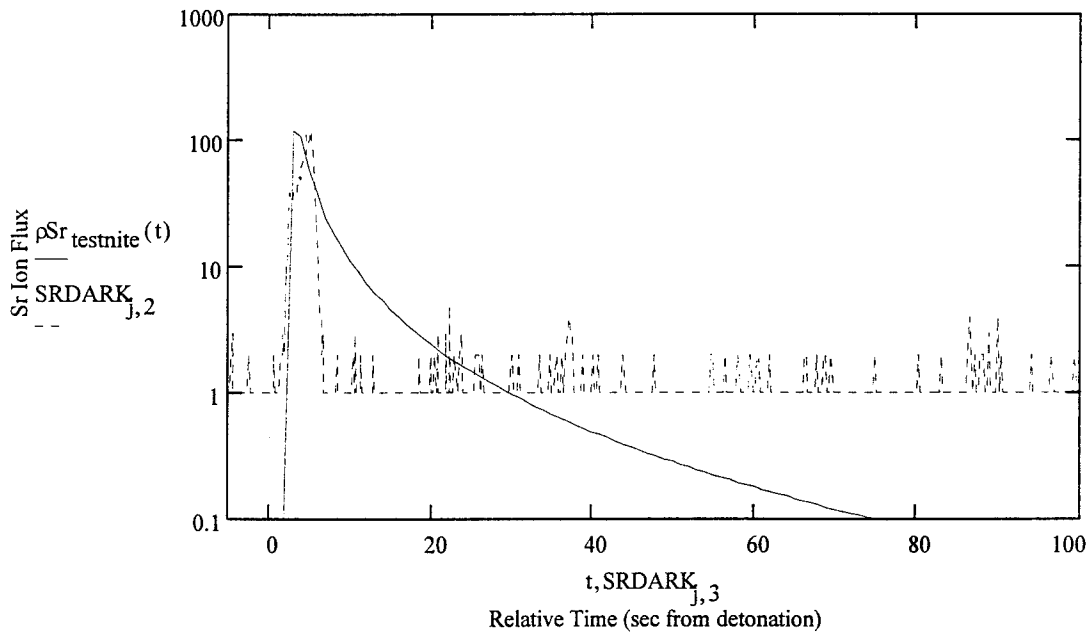
Search for Time Constants (continued)

Strontium Dark (G-11b)

$$\tau_{\text{Sr testnite}} = 90 \quad k_{\text{Sr testnite}} = \frac{1}{\tau_{\text{Sr testnite}}} \quad \text{CSr}_{\text{testnite}} = \frac{k_{\text{Sr testnite}}}{v_s} \cdot \text{CSr}$$

$$\rho_{\text{Sr testnite}}(t) = \text{CSr}_{\text{testnite}} \frac{e^{-\frac{t - \frac{z}{v_s}}{\tau_{\text{Sr testnite}}}} \cdot e^{-\frac{\sqrt{R^2 + z^2 - v_0 t - \frac{z}{v_s}}}{v_w \cdot t - \frac{z}{v_s}}}}{t - \frac{z}{v_s}^3} \cdot d$$

$1.5 \cdot v_0 \cdot t$
 0

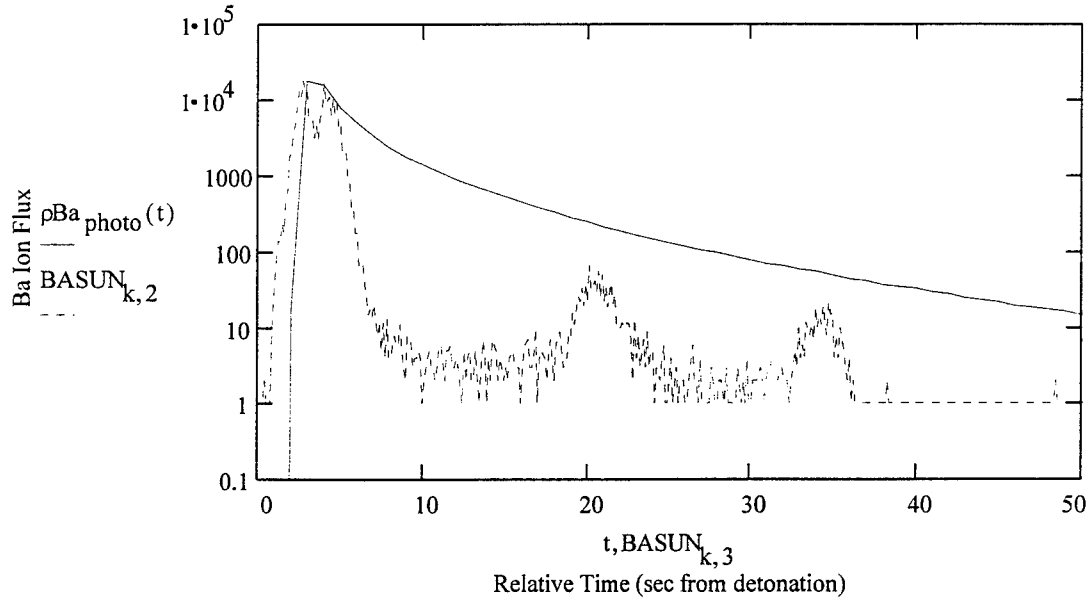


The strontium model requires a time constant of around 90 sec to match the G-11b data.

Barium Photoionization

$$C_{Ba \text{ photo}} = \frac{k_{Ba \text{ photo}}}{v_s} \cdot C_{Ba}$$

$$\rho_{Ba \text{ photo}}(t) = C_{Ba \text{ photo}} \cdot \frac{1.5 \cdot v_0 \cdot t}{e^{-\frac{t - \frac{z}{v_s}}{\tau_{Ba \text{ photo}}}} \cdot e^{-\frac{\sqrt{R^2 - z^2} - v_0 \cdot t - \frac{z}{v_s}}{v_w \cdot t - \frac{z}{v_s}}} \cdot \left(t - \frac{z}{v_s}\right)^3} \quad d$$

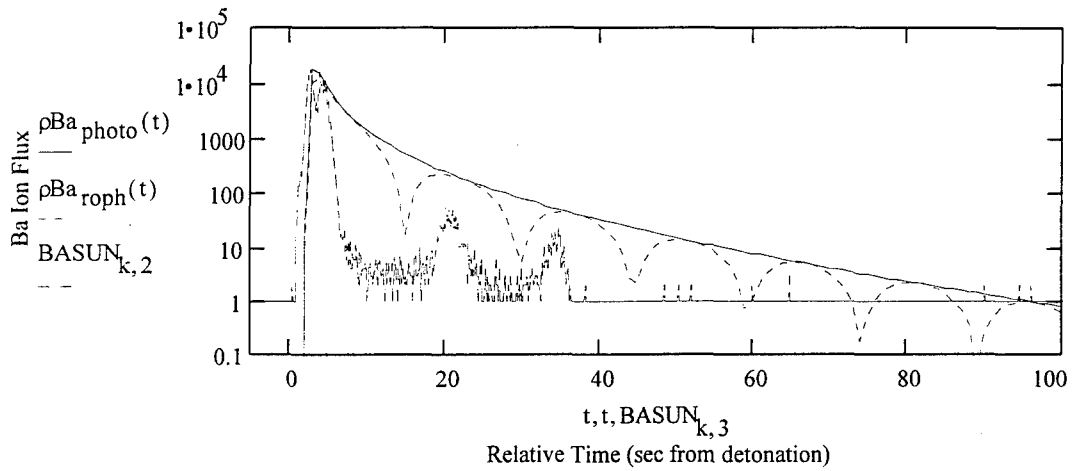


Rotation of Spacecraft

CRRES spun at a rate of 2.02 rpm during the experiment. Thus QIMS will count through ion field in the form of a sine function.

$$\omega = \frac{2.02}{60} \cdot 2 \cdot \pi$$

$$\rho_{Ba_roph}(t) = \rho_{Ba_photo}(t) \cdot \sin(\omega \cdot t)$$

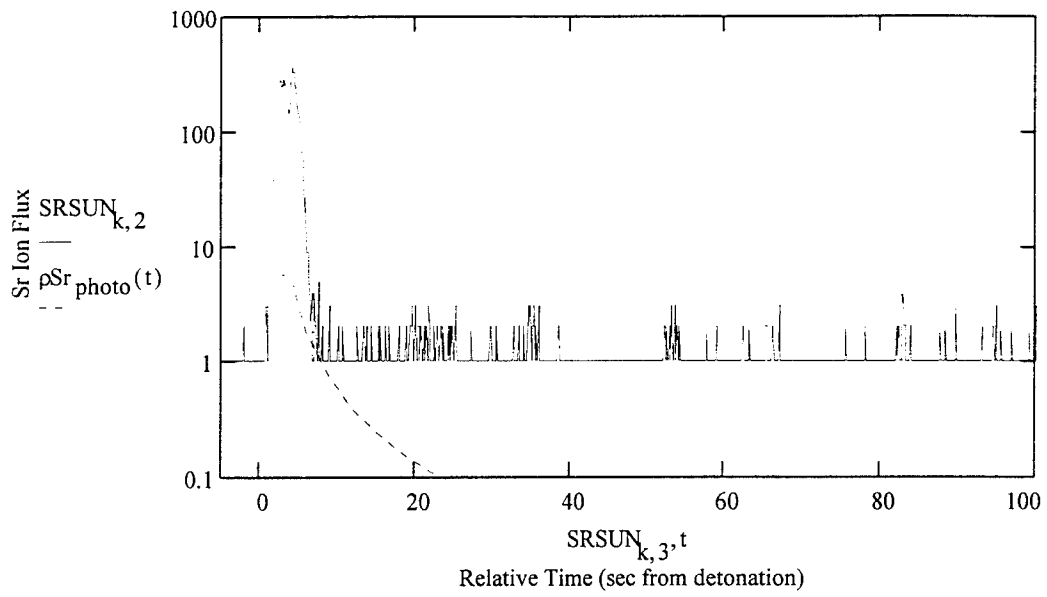


Strontium Photoionization

From Wescott et al. (1990), the Sr photoionization time constant is 1920 sec.

$$\tau_{Sr_photo} = 1920 \quad k_{Sr_photo} = \frac{1}{\tau_{Sr_photo}} \quad CSr_photo = \frac{k_{Sr_photo}}{v_s} \cdot CSr$$

$$\rho_{Sr_photo}(t) = CSr_photo \cdot \frac{e^{-\frac{t - \frac{z}{v_s}}{\tau_{Sr_photo}}} \cdot e^{-\left[\frac{\sqrt{R^2 + z^2} - v_0 \cdot t - \frac{z}{v_s}}{v_w \cdot t - \frac{z}{v_s}} \right]^2}}}{\left(t - \frac{z}{v_s} \right)^3} \cdot d$$



As can be seen, photoionization does not nearly account for the data taken by QIM. There must be another process.

Barium Charge Exchange

Let's now account for the production of ions due to charge exchange reactions. The average velocity of particles in the cloud will first be defined. Using the velocity we can obtain a cross section from a graph in Wolf (1995a). Densities for both night and day will be defined and then constants for both can be calculated.

$$v = 1.133 \cdot 10^4 \implies \sigma_{Ba_{ce}} = 7 \cdot 10^{-20} \text{ cross section for charge exchange between ground states of } O^+ \text{ and Ba}$$

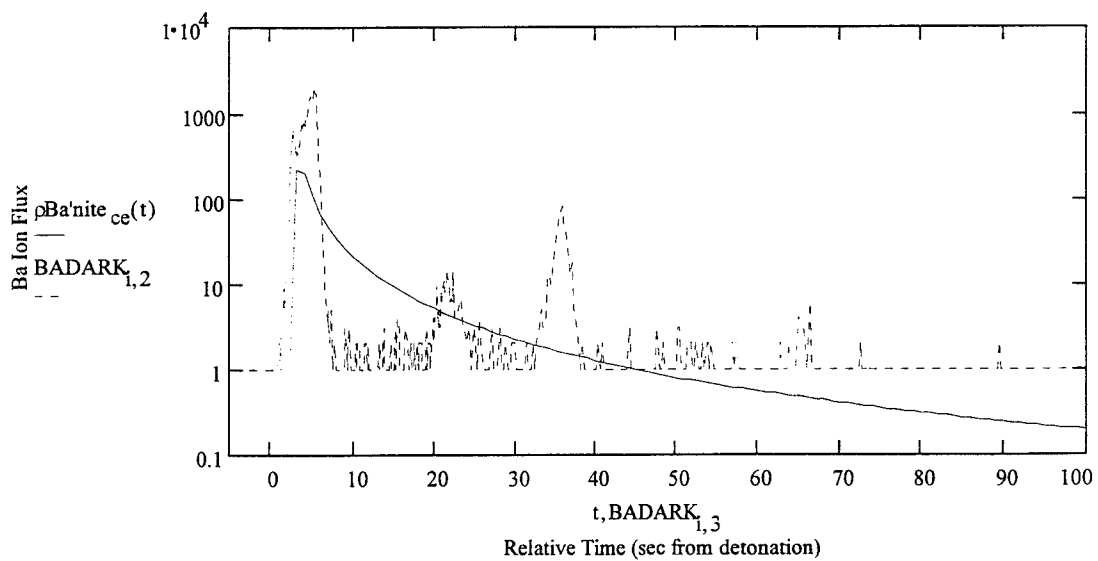
Nighttime ionosphere values:

$$n'_{nite_{Oplus}} = 5 \cdot 10^{11}$$

$$k_{Ba'nite_{ce}} = \sigma_{Ba_{ce}} \cdot v \cdot n'_{nite_{Oplus}} \quad \tau_{Ba'nite_{ce}} = \frac{1}{k_{Ba'nite_{ce}}} \quad C_{Ba'nite_{ce}} = \frac{k_{Ba'nite_{ce}}}{v_s} \cdot C_{Ba}$$

First look at charge exchange in the nighttime ionosphere and compare it with G-11b:

$$\rho_{Ba'nite_{ce}}(t) = C_{Ba'nite_{ce}} \int_0^{1.5 \cdot v_0 \cdot t} e^{-\left[\frac{t - \frac{z}{v_s}}{\tau_{Ba'nite_{ce}}} \right]} \cdot e^{-\left[\frac{\sqrt{R^2 - z^2} - v_0 \cdot t - \frac{z}{v_s}}{v_w \cdot t - \frac{z}{v_s}} \right]^2} dz$$



Barium Charge Exchange (continued)

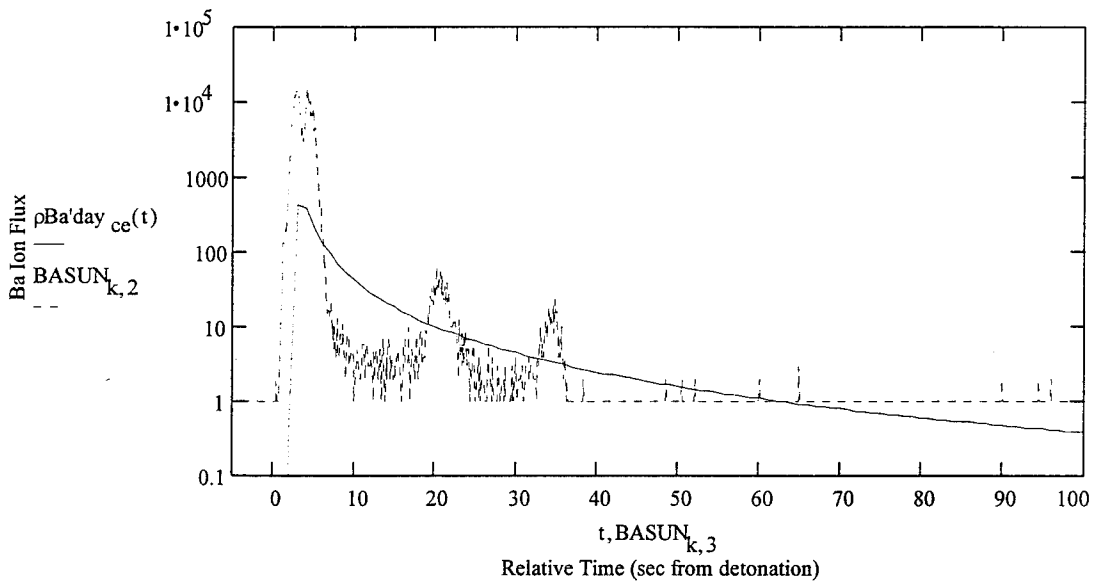
Now the higher daytime ionosphere plasma density will be considered to compare charge exchange with the G-1 release.

Daytime ionosphere values:

$$n_{\text{day Oplus}} = 10^{12}$$

$$k_{\text{Ba'day ce}} = \sigma_{\text{Ba ce}} \cdot v \cdot n_{\text{day Oplus}} \quad \tau_{\text{Ba'day ce}} = \frac{1}{k_{\text{Ba'day ce}}} \quad C_{\text{Ba'day ce}} = \frac{k_{\text{Ba'day ce}}}{v_s} \cdot C_{\text{Ba}}$$

$$\rho_{\text{Ba'day ce}}(t) = C_{\text{Ba'day ce}} \cdot \frac{1.5 \cdot v_0 \cdot t}{e^{\left[\frac{t - \frac{z}{v_s}}{\tau_{\text{Ba'day ce}}} \right]} \cdot e^{\left[\frac{\sqrt{R^2 - z^2} - v_0 \cdot t - \frac{z}{v_s}}{v_w \cdot t - \frac{z}{v_s}} \right]^2} dz}$$



Strontium Charge Exchange

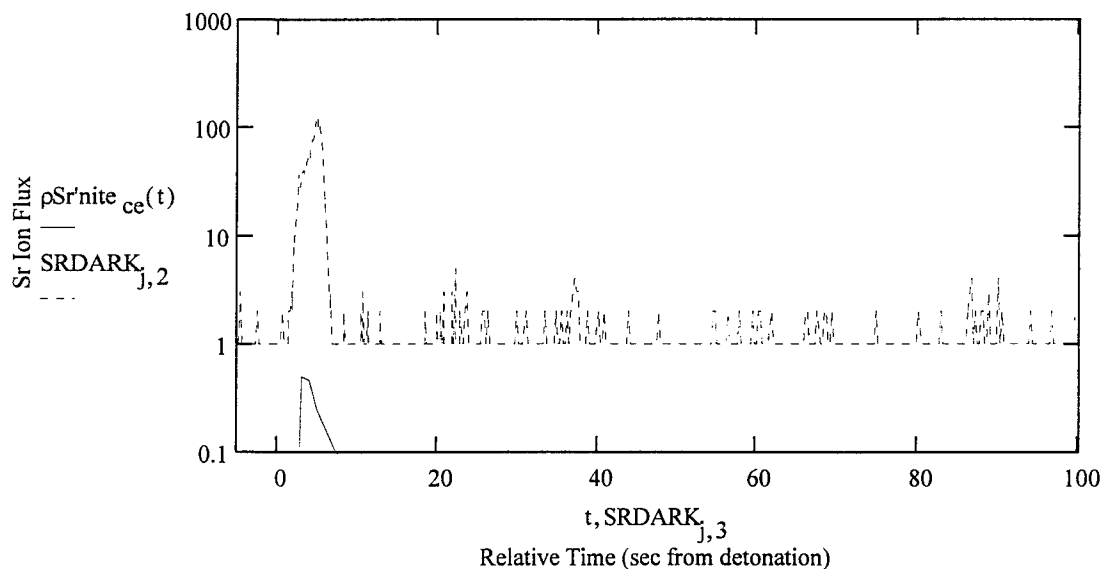
Using the particle velocity and the graph from Wolf (1995a), the charge exchange constant for interaction between the ground states of O⁺ and Sr is found.

$$v = 1.133 \cdot 10^4 \text{ m/s} \implies \sigma_{\text{Sr ce}} = 8 \cdot 10^{-21} \text{ m}^2 \text{ cross section for charge exchange between ground states of O}^+ \text{ and Sr}$$

Nighttime:

$$k_{\text{Sr'nite ce}} = \sigma_{\text{Sr ce}} \cdot v \cdot n_{\text{Oplus}} \quad \tau_{\text{Sr'nite ce}} = \frac{1}{k_{\text{Sr'nite ce}}} \quad C_{\text{Sr'nite ce}} = \frac{k_{\text{Sr'nite ce}}}{v_s} \cdot C_{\text{Sr}}$$

$$\rho_{\text{Sr'nite ce}}(t) := C_{\text{Sr'nite ce}} \cdot \int_0^{1.5 \cdot v_0 \cdot t} e^{-\frac{t - \frac{z}{v_s}}{\tau_{\text{Sr'nite ce}}}} \cdot \left[\frac{R^2 - z^2 - v_0 \cdot t - \frac{z}{v_s}}{v_w \cdot t - \frac{z}{v_s}} \right]^2 \cdot e^{-\frac{z}{v_s}} dz$$

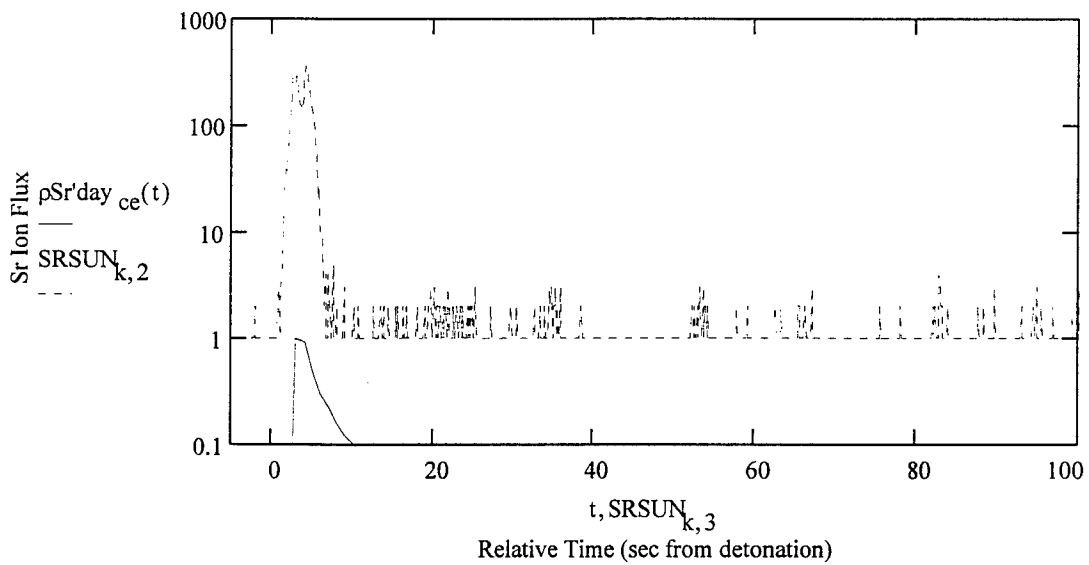


Strontium Charge Exchange (continued)

Daytime:

$$kSr'day_{ce} = \alpha Sr_{ce} \cdot v \cdot n'_{day} O_{plus} \quad \tau Sr'day_{ce} = \frac{1}{kSr'day_{ce}} \quad CSr'day_{ce} = \frac{kSr'day_{ce}}{v_s} \cdot CSr$$

$$\rho Sr'day_{ce}(t) = CSr'day_{ce} \cdot \int_0^{1.5 \cdot v_0 \cdot t} e^{-\left[\frac{t - \frac{z}{v_s}}{\tau Sr'day_{ce}} \right] \cdot \frac{\sqrt{R^2 - z^2} - v_0 \cdot t - \frac{z}{v_s}}{v_w \cdot t - \frac{z}{v_s}}} \cdot \frac{dz}{t - \frac{z}{v_s}^3}$$



Barium Electron Impact (EI)

Now, using Vainshtein et al.'s (1972) and McFarland's (1967) cross section results, we can come up with model output for EI results. This would be used in the case of CIV, where high energy electrons (energized by fast neutrals) ionize neutrals. Assuming an electron energy of 10 eV, an average between the two papers results in a cross section for Ba EI of:

$$\sigma_{Ba_{ei}} = 1.1 \cdot 10^{-19}$$

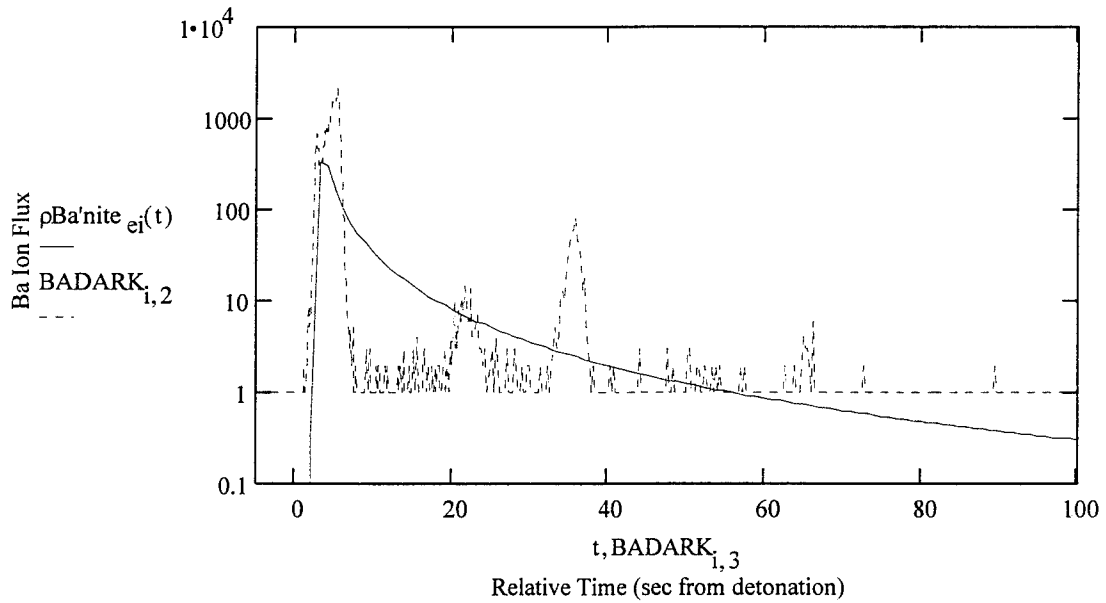
$$n'_{nite_e} = n'_{nite_{Oplus}}$$

$$n'_{day_e} = n'_{day_{Oplus}}$$

Note: Total e densities are set equal to the daytime and nighttime O+ densities. However, an energy source is required to elevate even close to this many into the "hot" tail. This is probably an unrealistic estimate, since in typical CIV experiments, only 10% of the electron population is "hot".

$$kBa'_{nite_{ei}} = \sigma_{Ba_{ei}} \cdot v \cdot n'_{nite_e} \quad \tau_{Ba'_{nite_{ei}}} = \frac{1}{kBa'_{nite_{ei}}} \quad CBa'_{nite_{ei}} = \frac{kBa'_{nite_{ei}}}{v_s} \cdot CB$$

$$\rho_{Ba'_{nite_{ei}}}(t) = CBa'_{nite_{ei}} \int_0^{1.5 \cdot v_0 \cdot t} \frac{e^{-\left[\frac{t - \frac{z}{v_s}}{\tau_{Ba'_{nite_{ei}}}} \right]} \cdot e^{-\left[\frac{\sqrt{R^2 - z^2} - v_0 \cdot t - \frac{z}{v_s}}{v_w \cdot t - \frac{z}{v_s}} \right]^2}}}{\left(t - \frac{z}{v_s} \right)^3} dz$$



Barium Electron Impact (continued)

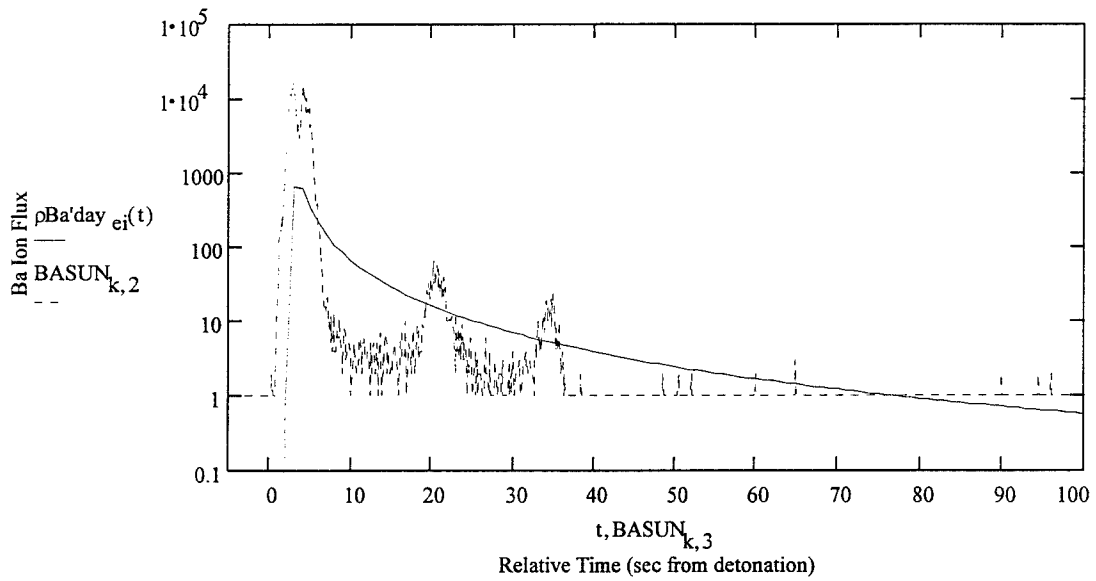
Now the higher daytime ionosphere plasma density will be considered to compare EI w the G-1 release.

$$kBa'day_{ei} = \sigma Ba_{ei} \cdot v \cdot n \cdot day_e \quad \tau Ba'day_{ei} = \frac{1}{kBa'day_{ei}} \quad C Ba'day_{ei} = \frac{kBa'day_{ei}}{v_s} \cdot C Ba$$

$$\rho Ba'day_{ei}(t) = C Ba'day_{ei} \int_0^{1.5 \cdot v_0 \cdot t} e^{-\frac{t - \frac{z}{v_s}}{\tau Ba'day_{ei}}} \cdot e^{-\frac{\sqrt{R^2 - z^2 - v_0 \cdot t - \frac{z}{v_s}}}{v_w \cdot t - \frac{z}{v_s}}} dz$$

$$t - \frac{z}{v_s}$$

$$t - \frac{z}{v_s}$$



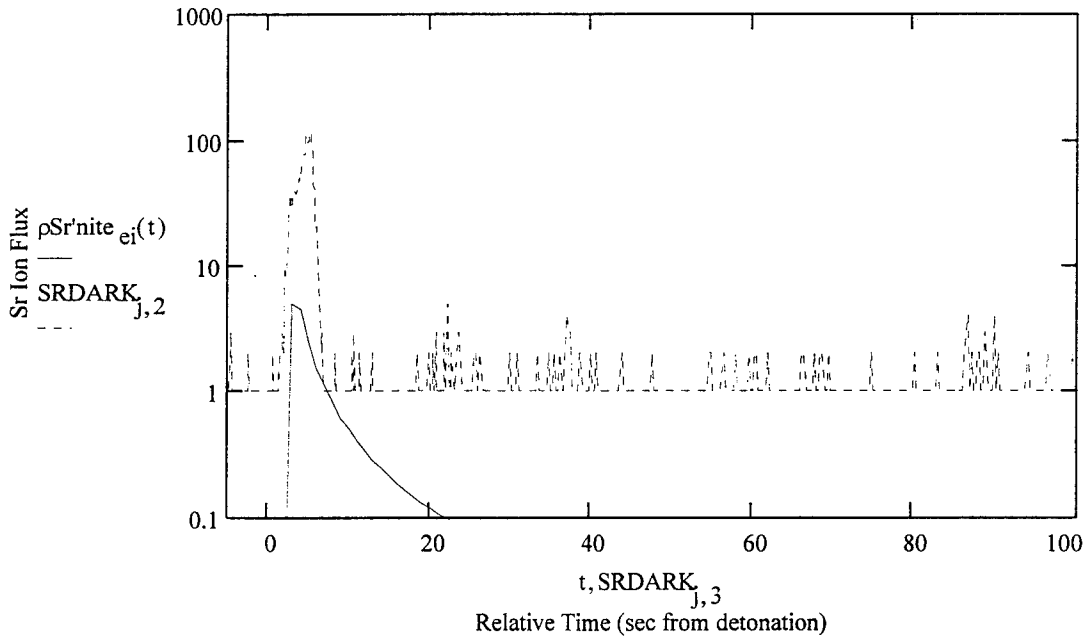
Strontium Electron Impact (EI)

Using Vainshtein et al.'s (1972) and McFarland's (1967) cross section results, we can al come up with model output for Sr EI. Again assuming an electron energy of 10 eV, an average between the two papers results in a cross section for Sr EI of:

$$\sigma_{Sr\ ei} = 8 \cdot 10^{-20}$$

$$k_{Sr'nite_{ei}} = \sigma_{Sr\ ei} \cdot v \cdot n_{nite_e} \quad \tau_{Sr'nite_{ei}} = \frac{1}{k_{Sr'nite_{ei}}} \quad CS_{Sr'nite_{ei}} = \frac{k_{Sr'nite_{ei}}}{v_s} \cdot CSr$$

$$\rho_{Sr'nite_{ei}}(t) = CS_{Sr'nite_{ei}} \int_0^{1.5 \cdot v_0 \cdot t} e^{-\frac{t-z}{v_s} \tau_{Sr'nite_{ei}}} \cdot e^{-\left[\frac{\sqrt{R^2 + z^2} - v_0 \cdot t - \frac{z}{v_s}}{v_w \cdot t - \frac{z}{v_s}} \right]^2} dz$$

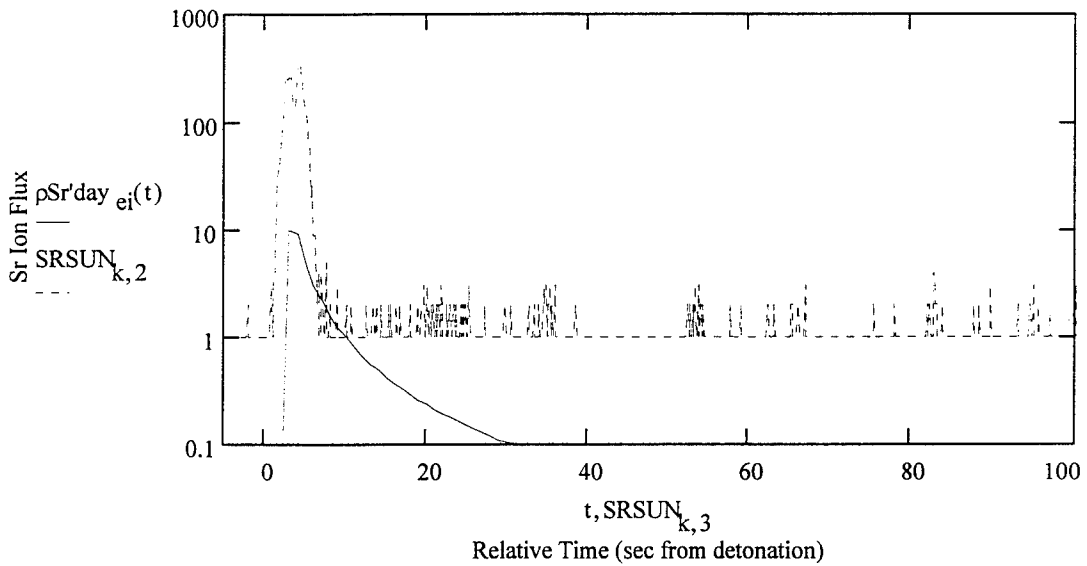


Strontium Electron Impact (continued)

Now the higher daytime ionosphere plasma density will be considered to compare EI w the G-1 data.

$$kSr'day_{ei} = \sigma Sr_{ei} \cdot v \cdot n'day_e \quad \tau Sr'day_{ei} = \frac{1}{kSr'day_{ei}} \quad CSr'day_{ei} = \frac{kSr'day_{ei}}{v_s} \cdot CSr$$

$$\rho Sr'day_{ei}(t) = CSr'day_{ei} \int_0^{1.5 \cdot v_0 \cdot t} \frac{e^{-\left[\frac{t-z}{v_s} + \frac{\sqrt{R^2 - z^2} - v_0 \cdot t - \frac{z}{v_s}}{v_w \cdot t - \frac{z}{v_s}} \right]^2}}{t - \frac{z}{v_s}} dz$$



Now, given that electron impact does not match the data using the above numbers, what kind of electron densities are required to do so?

$$\tau Ba_{testnite} = 2.6 \cdot 10^2 \quad nBa'nite_{test'e} := \frac{1}{\tau Ba_{testnite} \cdot \sigma Ba_{ei} \cdot v} \quad nBa'nite_{test'e} = 3.08605781 \cdot 10^{12}$$

$$\tau Sr_{testnite} = 90 \quad nSr'nite_{test'e} := \frac{1}{\tau Sr_{testnite} \cdot \sigma Sr_{ei} \cdot v} \quad nSr'nite_{test'e} = 1.22585074 \cdot 10^{13}$$

$$\tau Sr_{testday} = 26 \quad nSr'day_{test'e} := \frac{1}{\tau Sr_{testday} \cdot \sigma Sr_{ei} \cdot v} \quad nSr'day_{test'e} = 4.24332949 \cdot 10^{13}$$

Barium Charge Stripping

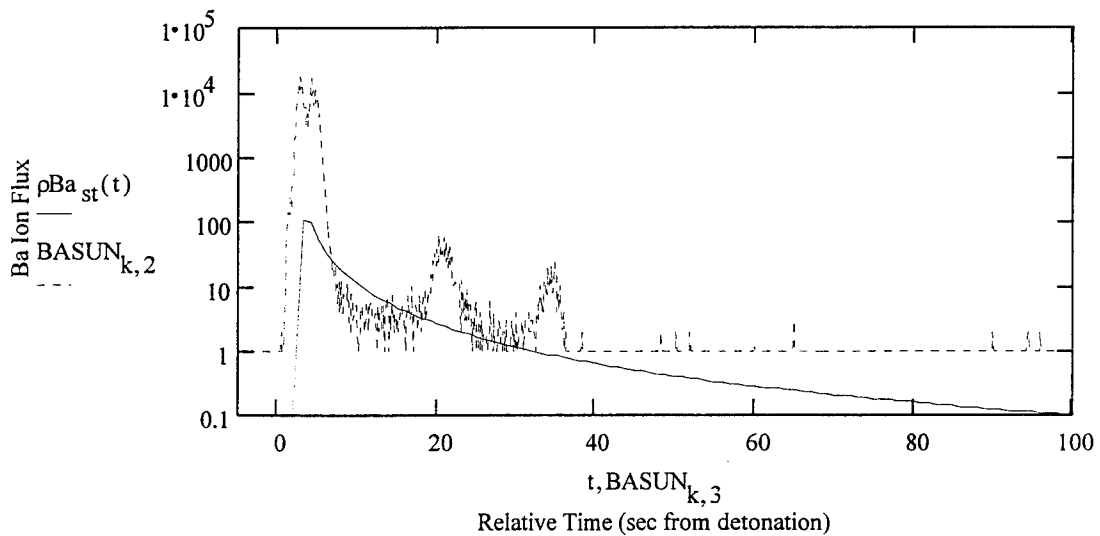
Not much is known about stripping reactions. However the two extreme guesses from literature will be used to see how the resultant ion production compares to the experimental data.

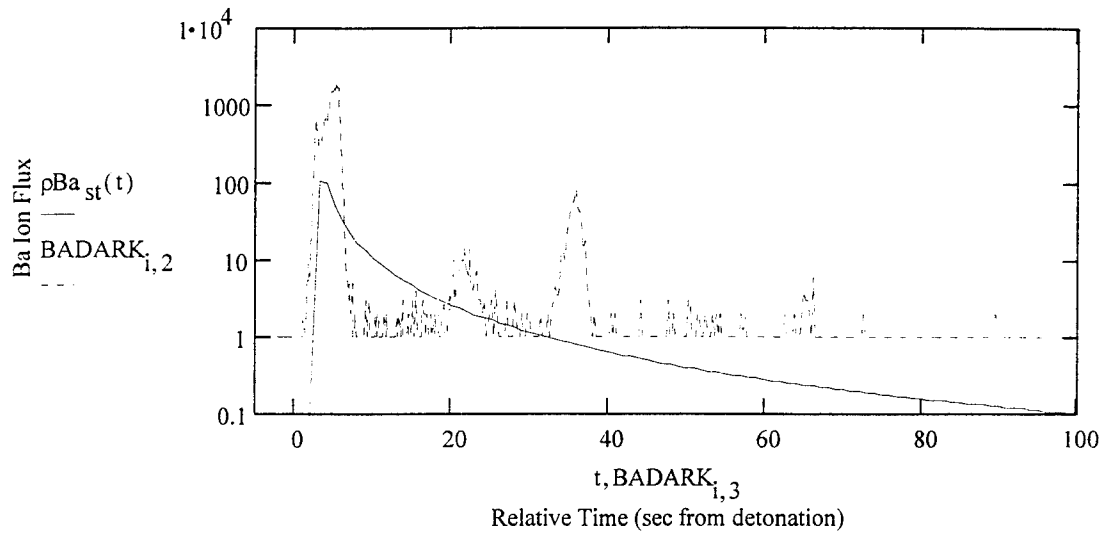
Here the low estimate for barium charge stripping cross section (Wescott et al., 1994) is:

$$\sigma_{Ba_{st}} = 3.5 \cdot 10^{-23} \quad \text{and the Oxygen density is: } n_O = 5 \cdot 10^{14}$$

$$k_{Ba_{st}} = \sigma_{Ba_{st}} \cdot v \cdot n_O \quad \tau_{Ba_{st}} = \frac{1}{k_{Ba_{st}}} \quad C_{Ba_{st}} = \frac{k_{Ba_{st}}}{v_s} \cdot C_{Ba}$$

$$\rho_{Ba_{st}}(t) = C_{Ba_{st}} \int_0^{1.5 \cdot v_0 \cdot t} e^{-\left[\frac{t - \frac{z}{v_s}}{\tau_{Ba_{st}}} \right]} \cdot e^{-\left[\frac{\sqrt{R^2 + z^2} - v_0 \cdot t - \frac{z}{v_s}}{v_w \cdot t - \frac{z}{v_s}} \right]^2} dz$$





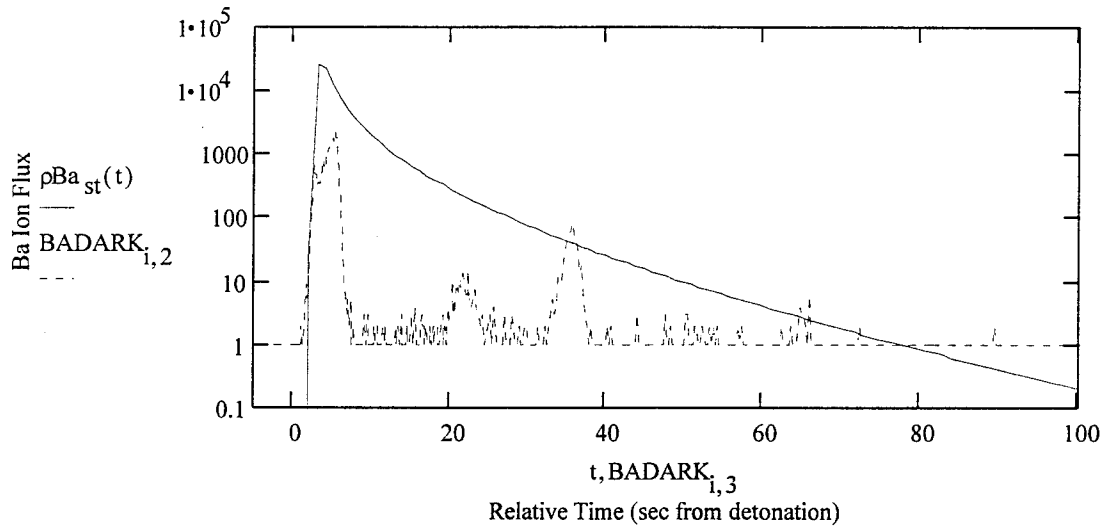
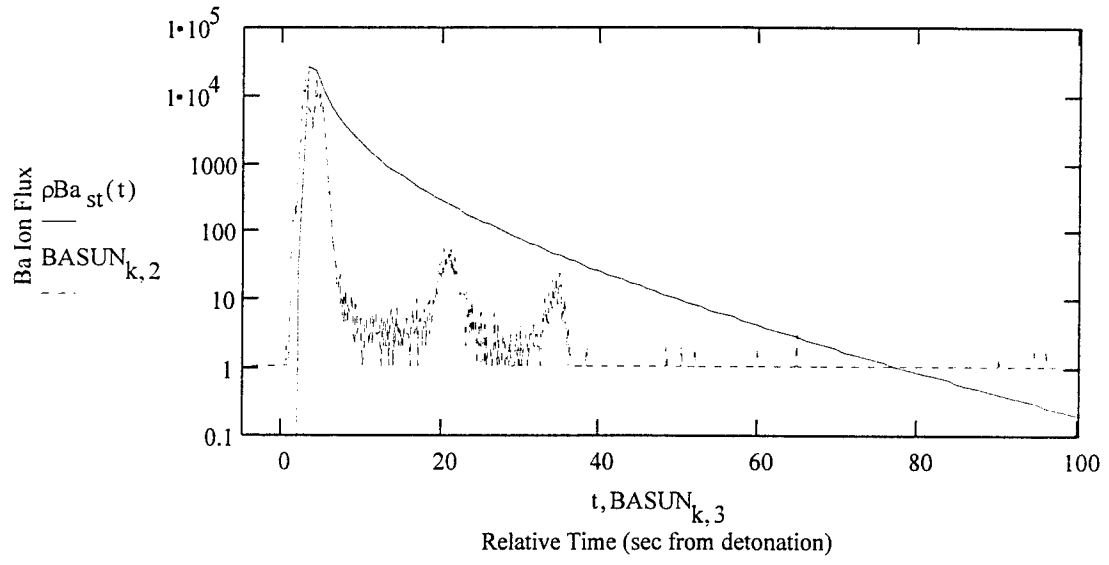
Barium Charge Stripping (continued)

Now using a high estimate for the stripping cross section (Lai and Murad, 1989)

$$\sigma_{Ba_{st}} = 1 \cdot 10^{-20}$$

$$k_{Ba_{st}} = \sigma_{Ba_{st}} \cdot v \cdot n_O \quad \tau_{Ba_{st}} := \frac{1}{k_{Ba_{st}}} \quad C_{Ba_{st}} := \frac{k_{Ba_{st}}}{v_s} \cdot C_{Ba}$$

$$\rho_{Ba_{st}}(t) = C_{Ba_{st}} \int_0^{1.5 \cdot v_0 \cdot t} e^{-\left[\frac{t - \frac{z}{v_s}}{\tau_{Ba_{st}}} \right]} \cdot e^{-\left[\frac{\left[\frac{\sqrt{R^2 + z^2} - v_0 \cdot t - \frac{z}{v_s}}{v_w \cdot t - \frac{z}{v_s}} \right]^2}{t - \frac{z}{v_s}} \right]} dz$$



Barium Charge Stripping (continued)

Using the time constants required to match the data calculated above, a stripping cross section can be found which would match the data.

Barium Dark (G-11b):

$$\tau_{\text{Ba testnite}} = 2.6 \cdot 10^2 \quad \sigma_{\text{Ba stripnite}} = \frac{1}{\tau_{\text{Ba testnite}}^{v \cdot n} O} \quad \sigma_{\text{Ba stripnite}} = 6.78932718 \cdot 10^{-22}$$

Strontium Light(G-1):

$$\tau_{\text{Sr testday}} = 26 \quad \sigma_{\text{Sr stripday}} = \frac{1}{\tau_{\text{Sr testday}}^{v \cdot n} O} \quad \sigma_{\text{Sr stripday}} = 6.78932718 \cdot 10^{-21}$$

StrontiumDark (G-11b):

$$\tau_{\text{Sr testnite}} = 90 \quad \sigma_{\text{Sr stripnite}} = \frac{1}{\tau_{\text{Sr testnite}}^{v \cdot n} O} \quad \sigma_{\text{Sr stripnite}} = 1.96136118 \cdot 10^{-21}$$

Thus the cross sections calculated here easily fall within the bounds of the charge stripping cross section range above. This does not prove stripping to have occurred. It simply states that given the current knowledge of these reactions, stripping is a hypothesized solution to the problem of reproducing the CRRES ion flux data.

Total Data Fit for Barium Dark (G-11b)

Now the model will be adapted to fit the whole data set for the barium dark release, in which photoionization does not start until the cloud crosses the UV terminator. This is not required for the other data sets, since for strontium photoionization is not a factor and in the G-1 release, solar radiation dominates all other ionization processes for barium. In order to simulate the ionizing UV radiation steadily growing as the satellite moves from dark to light and not abruptly "turning on," the photoionization rate constant is linearly stepped from 0 to its maximum value.

$$k_{\text{Ba}' \text{ photo}_t} = \frac{1}{\tau_{\text{Ba}' \text{ photo}}} \quad \text{sets the value of the photoionization rate at all times before the rates at early times are changed in the next line}$$

$$t1 = 1..17 \quad k_{\text{Ba}' \text{ photo}_{t1}} = 0 \quad \text{sets the rate constant equal to 0 for the first 17 seconds}$$

The following statements step the rate constant linearly up to its maximum value:

$$\begin{aligned}
 kBa'_{photo_{18}} &= 0.08 \cdot \frac{1}{\tau Ba_{photo}} & kBa'_{photo_{19}} &= 0.16 \cdot \frac{1}{\tau Ba_{photo}} & kBa'_{photo_{20}} &= 0.24 \cdot \frac{1}{\tau Ba_{photo}} \\
 kBa'_{photo_{21}} &= 0.32 \cdot \frac{1}{\tau Ba_{photo}} & kBa'_{photo_{22}} &= 0.40 \cdot \frac{1}{\tau Ba_{photo}} & kBa'_{photo_{23}} &= 0.48 \cdot \frac{1}{\tau Ba_{photo}} \\
 kBa'_{photo_{24}} &= 0.56 \cdot \frac{1}{\tau Ba_{photo}} & kBa'_{photo_{25}} &= 0.64 \cdot \frac{1}{\tau Ba_{photo}} & kBa'_{photo_{26}} &= 0.72 \cdot \frac{1}{\tau Ba_{photo}} \\
 kBa'_{photo_{27}} &= 0.80 \cdot \frac{1}{\tau Ba_{photo}} & kBa'_{photo_{28}} &= 0.88 \cdot \frac{1}{\tau Ba_{photo}} & kBa'_{photo_{29}} &= 0.96 \cdot \frac{1}{\tau Ba_{photo}} \\
 CBa'_{photo_t} &= \frac{kBa'_{photo_t}}{v_s} \cdot CBa
 \end{aligned}$$

The next task is to calculate ion densities produced in the dark. The time and rate constant required to match the dark data are used.

$$\rho_{Banit_t} = CBa_{testnit_t} \int_0^{1.5 \cdot v_0 \cdot t} \frac{e^{-\left[\frac{t - \frac{z}{v_s}}{\tau Ba_{testnit}} \right]} \cdot e^{-\left[\frac{\left[\sqrt{R^2 + z^2} - v_0 \cdot t - \frac{z}{v_s} \right]^2}{v_w \cdot t - \frac{z}{v_s}} \right]}}{\left(t - \frac{z}{v_s} \right)^3} dz$$

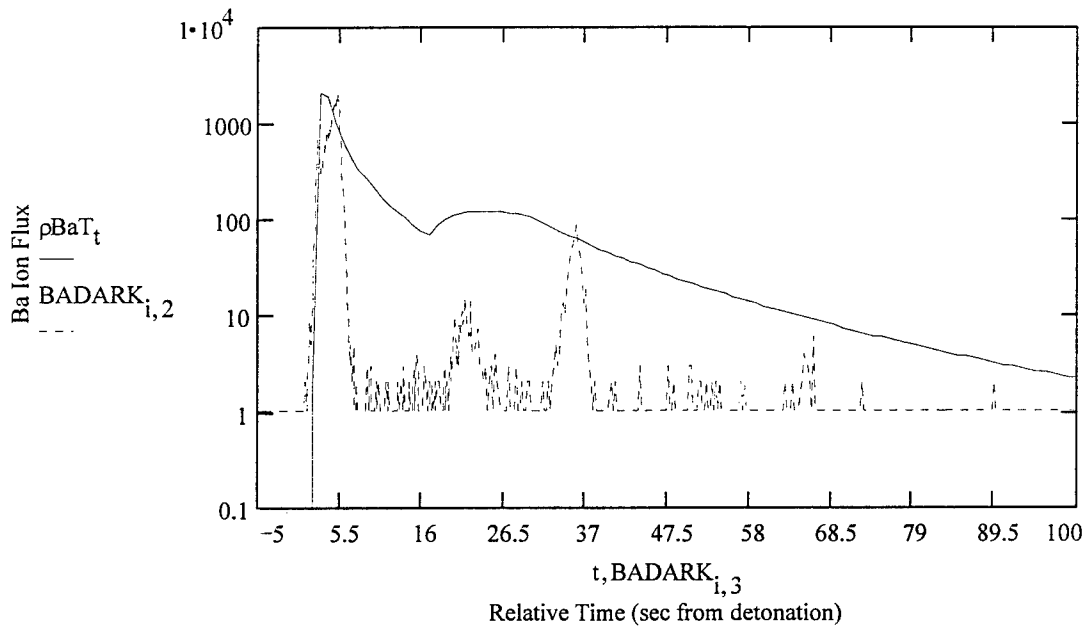
Next, the photoionization portion of the model is calculated. Due to how the rate constant w defined above, this density integral will yield zero until UV radiation enters the picture and k becomes nonzero.

$$\rho_{Baday_t} = CBa'_{photo_t} \int_0^{1.5 \cdot v_0 \cdot t} \frac{e^{-\left[\frac{t - \frac{z}{v_s}}{\tau Ba_{photo}} \right]} \cdot e^{-\left[\frac{\left[\sqrt{R^2 + z^2} - v_0 \cdot t - \frac{z}{v_s} \right]^2}{v_w \cdot t - \frac{z}{v_s}} \right]}}{\left(t - \frac{z}{v_s} \right)^3} dz$$

Total Data Fit for Barium Dark (continue)

The total ion count is that for the nighttime processes, which continue into the sunlight, plus photoionization, starting once the cloud receives sunlight. The oxygen ion density is also changed after crossing the UV terminator, representing the increase in plasma density on the daytime side of the ionosphere.

$$\rho_{\text{BaT}_t} = \rho_{\text{Banite}_t} - \rho_{\text{Baday}_t}$$



Two Processes Producing Double Peak--Barium Dark

All of the data sets demonstrate two miniature peaks within the first maximum. The following work represents the effort to model the double peak with two processes, one being delayed by some characteristic of the releases.

First the initial minor peak will be reproduced using charge exchange:

$$n'day_{Oplus} := 10^{12} \quad n'nite_{Oplus} := 10^{11} \quad v := 1.133 \cdot 10^4 \implies oBa_{ce} = 7 \cdot 10^{-20}$$

$$kBa'day_{ce} := oBa_{ce} \cdot v \cdot n'day_{Oplus} \quad \tau Ba'day_{ce} := \frac{1}{kBa'day_{ce}} \quad C Ba'day_{ce} = \frac{kBa'day_{ce}}{v_s} \cdot C Ba$$

$$kBa'nite_{ce} := oBa_{ce} \cdot v \cdot n'nite_{Oplus} \quad \tau Ba'nite_{ce} := \frac{1}{kBa'nite_{ce}} \quad C Ba'nite_{ce} = \frac{kBa'nite_{ce}}{v_s} \cdot C Ba$$

$$\rho Ba_{ce}(t) := C Ba'nite_{ce} \int_0^{1.5 \cdot v_0 \cdot t} \exp\left[\frac{t - \frac{z}{v_s}}{\tau Ba'nite_{ce}}\right] \cdot \exp\left[\frac{v_w \cdot t - \frac{z}{v_s}}{v_w \cdot t - \frac{z}{v_s}}\right] \cdot \exp\left[\frac{R^2 + z^2 - v_0 \cdot t - \frac{z}{v_s}}{v_w \cdot t - \frac{z}{v_s}}\right] dz$$

Next the 2nd minor peak is reproduced using a changing neutral atomic oxygen population. Some mechanism would be required to evacuate the cloud region of ambient particles for the first few seconds, which is probably not very realistic.

$$\sigma_{Ba_{st}} := 9 \cdot 10^{-22} \text{ charge stripping cross section}$$

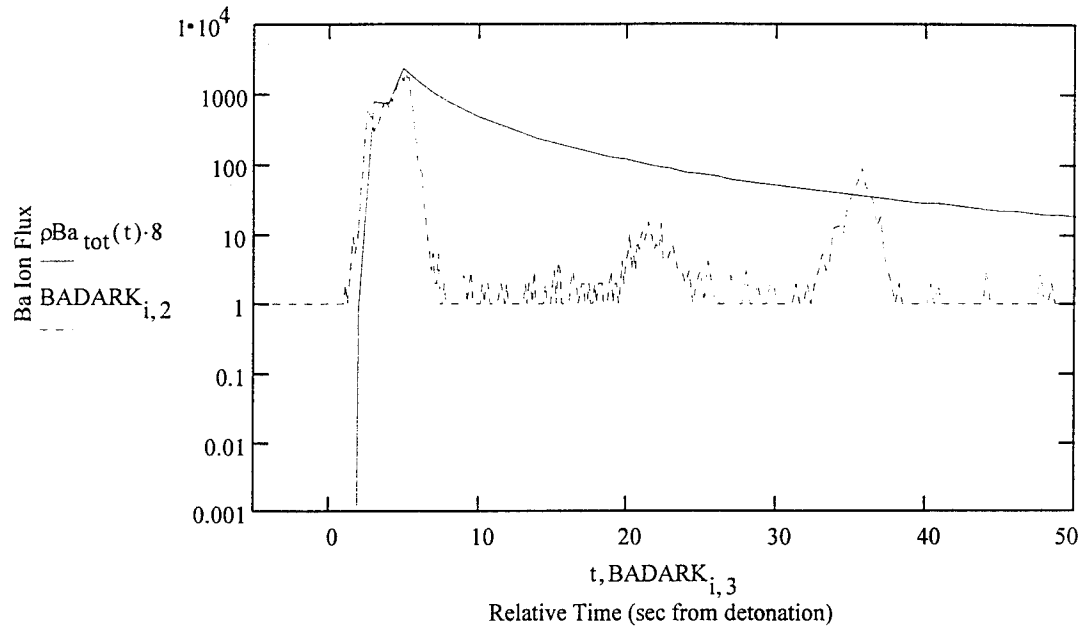
$$n_O(t) = \text{if } t < 5, 10^{13}, 10^{14} \text{ O density is lower for first 4 seconds, then increases}$$

$$k_{Ba_{st}}(t) = \sigma_{Ba_{st}} \cdot v \cdot n_O(t) \quad \tau_{Ba_{st}}(t) := \frac{1}{k_{Ba_{st}}(t)} \quad C_{Ba_{st}}(t) = \frac{k_{Ba_{st}}(t)}{v_s} \cdot C_{Ba}$$

$$\rho_{Ba_{st}}(t) = C_{Ba_{st}}(t) \cdot \int_0^{1.5 \cdot v_0 \cdot t} \exp\left[-\frac{t - \frac{z}{v_s}}{\tau_{Ba_{st}}(t)}\right] \cdot \exp\left[-\frac{\sqrt{R^2 - z^2} - v_0 \cdot t - \frac{z}{v_s}}{v_w \cdot t - \frac{z}{v_s}}\right]^2 dz$$

$$\rho_{Ba_{tot}}(t) := \rho_{Ba_{ce}}(t) + \rho_{Ba_{st}}(t)$$

Now the result from assuming a charge exchange process plus a stripping process delayed by a temporary decrease in the neutral atomic oxygen density is compared to the QIMS counts.



Barium Dark--2 Processes Producing Double Peak (continue)

Now an attempt is made to model the double peak using the concept that the stripping cross section at the satellite might increase drastically as the as QIMS encounters particles of decreasing velocity:

$$\rho_{Ba_{ce}}(t) = C_{Ba_{day_{ce}}} \cdot \int_0^{1.5 \cdot v_0 \cdot t} \frac{\exp\left[-\frac{t - \frac{z}{v_s}}{\tau_{Ba_{day_{ce}}}}\right] \cdot \exp\left[-\frac{\sqrt{R^2 + z^2} - v_0 \cdot t - \frac{z}{v_s}}{v_w \cdot t - \frac{z}{v_s}}\right]^2}{\left(t - \frac{z}{v_s}\right)^3} dz$$

$$\sigma_{Ba_{st_t}} := 3 \cdot 10^{-20}$$

$$\sigma_{Ba_{st_1}} := 10^{-22} \quad \sigma_{Ba_{st_2}} := 10^{-22} \quad \sigma_{Ba_{st_3}} := 10^{-22} \quad \sigma_{Ba_{st_4}} := 10^{-22}$$

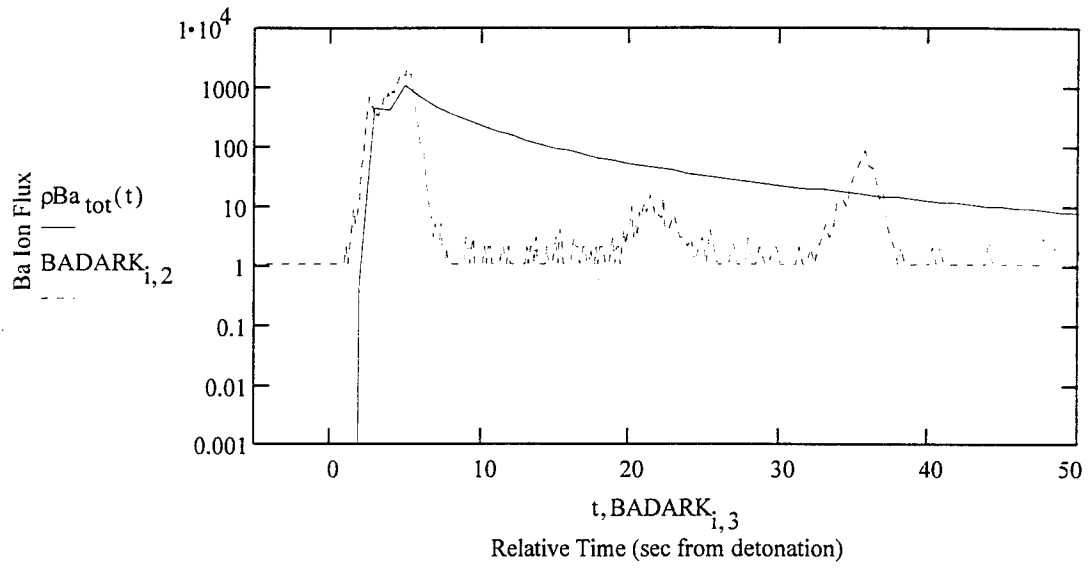
$$v_t := 1.133 \cdot 10^4 \quad v_2 := 1.2 \cdot 10^4 \quad v_3 := 1.17 \cdot 10^4 \quad v_4 := 1.12 \cdot 10^4 \quad v_5 := 1.08 \cdot 10^4$$

$$n_O = 10^{13} \quad \text{Oxygen density}$$

$$k_{Ba_{st}}(t) := \sigma_{Ba_{st_t}} \cdot v_t \cdot n_O \quad \tau_{Ba_{st}}(t) := \frac{1}{k_{Ba_{st}}(t)} \cdot C_{Ba_{st}}(t) := \frac{k_{Ba_{st}}(t)}{v_s} \cdot C_{Ba}$$

$$\rho_{Ba_{st}}(t) = C_{Ba_{st}}(t) \cdot \int_0^{1.5 \cdot v_0 \cdot t} \frac{\exp\left[-\frac{t - \frac{z}{v_s}}{\tau_{Ba_{st}}(t)}\right] \cdot \exp\left[-\frac{\sqrt{R^2 + z^2} - v_0 \cdot t - \frac{z}{v_s}}{v_w \cdot t - \frac{z}{v_s}}\right]^2}{\left(t - \frac{z}{v_s}\right)^3} dz$$

$$\rho_{Ba_{tot}}(t) := \rho_{Ba_{ce}}(t) - \rho_{Ba_{st}}(t)$$



Barium Sun--2 Processes Producing Double Peak

First photoionization is defined, assuming it starts from the time of detonation.

$$\rho_{\text{Ba photo}}(t) = C_{\text{Ba photo}} \int_0^{1.5 \cdot v_0 \cdot t} \frac{\exp\left[-\frac{t - \frac{z}{v_s}}{\tau_{\text{Ba photo}}}\right] \cdot \exp\left[-\frac{\sqrt{R^2 + z^2} - v_0 \cdot t - \frac{z}{v_s}}{v_w \cdot t - \frac{z}{v_s}}\right]^2}{\left(t - \frac{z}{v_s}\right)^3} dz$$

Then the delay in charge stripping is again attributed to a rapidly increasing cross section as slow particles are encountered.

$$\sigma_{\text{Ba st}_t} := 3 \cdot 10^{-20}$$

$$\sigma_{\text{Ba st}_1} := 10^{-22} \quad \sigma_{\text{Ba st}_2} := 10^{-22} \quad \sigma_{\text{Ba st}_3} := 10^{-22} \quad \sigma_{\text{Ba st}_4} := 10^{-22}$$

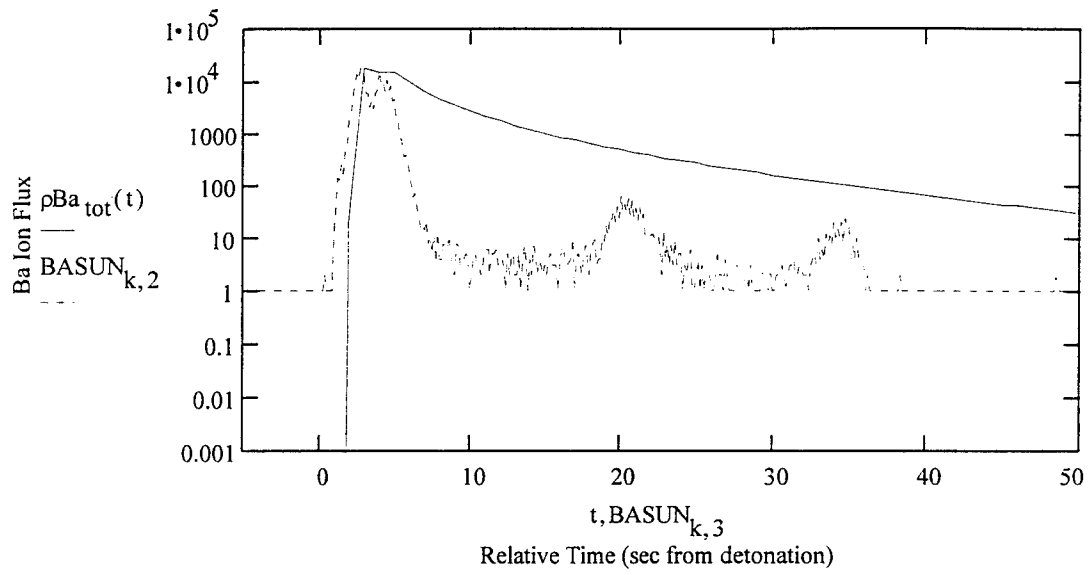
$$v_1 := 1.133 \cdot 10^4 \quad v_2 := 1.2 \cdot 10^4 \quad v_3 := 1.2 \cdot 10^4 \quad v_4 := 1.17 \cdot 10^4 \quad v_5 := 1.12 \cdot 10^4 \quad v_6 := 1.08 \cdot 10^4$$

$$n_{\text{O}} := 10^{14} \quad \text{Oxygen density}$$

$$k_{\text{Ba st}_t}(t) := \sigma_{\text{Ba st}_t} \cdot v_t \cdot n_{\text{O}} \quad \tau_{\text{Ba st}}(t) := \frac{1}{k_{\text{Ba st}}(t)} \quad C_{\text{Ba st}}(t) := \frac{k_{\text{Ba st}}(t)}{v_s} \cdot C_{\text{Ba}}$$

$$\rho_{\text{Ba st}}(t) = C_{\text{Ba st}}(t) \int_0^{1.5 \cdot v_0 \cdot t} \frac{\exp\left[-\frac{t - \frac{z}{v_s}}{\tau_{\text{Ba st}}(t)}\right] \cdot \exp\left[-\frac{\sqrt{R^2 + z^2} - v_0 \cdot t - \frac{z}{v_s}}{v_w \cdot t - \frac{z}{v_s}}\right]^2}{\left(t - \frac{z}{v_s}\right)^3} dz$$

$$\rho_{\text{Ba tot}}(t) := \rho_{\text{Ba photo}}(t) + \rho_{\text{Ba st}}(t)$$



Appendix C: Calculation of Basic Parameters

In this section, all basic parameters of the CRRES experiments are calculated.

Definition of Constants, Environmental Values and Equations:

$$e = 1.602 \cdot 10^{-19} \cdot \text{coul} \quad B = 3.15 \cdot 10^{-5} \cdot \text{tesla} \quad v_{\text{perp}} = 10000 \cdot \frac{\text{m}}{\text{sec}}$$

Cyclotron Radius

$$r_c = \frac{m \cdot v_{\text{perp}}}{e \cdot B}$$

Cyclotron Frequency

$$\omega_c = \frac{e \cdot B}{m}$$

Cyclotron Period

$$P_c = \frac{2 \cdot \pi \cdot r_c}{v_{\text{perp}}}$$

Parameters for Barium:

$$m_{\text{Ba}} = 2.28 \cdot 10^{-25} \cdot \text{kg}$$

Cyclotron Radius

$$r_{\text{Ba}_c} = \frac{m_{\text{Ba}} \cdot v_{\text{perp}}}{e \cdot B}$$

$$r_{\text{Ba}_c} = 4.52 \cdot 10^2 \cdot \text{m}$$

Cyclotron Frequency

$$\omega_{\text{Ba}_c} = \frac{e \cdot B}{m_{\text{Ba}}}$$

$$\omega_{\text{Ba}_c} = 22.13 \cdot \text{sec}^{-1}$$

Cyclotron Period

$$P_{\text{Ba}_c} = \frac{2 \cdot \pi \cdot r_{\text{Ba}_c}}{v_{\text{perp}}}$$

$$P_{\text{Ba}_c} = 0.28 \cdot \text{sec}$$

Parameters for Strontium:

$$m_{\text{Sr}} = 1.45 \cdot 10^{-25} \cdot \text{kg}$$

Cyclotron Radius

$$r_{\text{Sr}_c} = \frac{m_{\text{Sr}} \cdot v_{\text{perp}}}{e \cdot B}$$

$$r_{\text{Sr}_c} = 2.87 \cdot 10^2 \cdot \text{m}$$

Cyclotron Frequency

$$\omega_{\text{Sr}_c} = \frac{e \cdot B}{m_{\text{Sr}}}$$

$$\omega_{\text{Sr}_c} = 34.8 \cdot \text{sec}^{-1}$$

Cyclotron Period

$$P_{\text{Sr}_c} = \frac{2 \cdot \pi \cdot r_{\text{Sr}_c}}{v_{\text{perp}}}$$

$$P_{\text{Sr}_c} = 0.18 \cdot \text{sec}$$

Parameters for Atomic Oxygen Ions:

$$m_{\text{Oplus}} = 2.66 \cdot 10^{-26} \cdot \text{kg}$$

Cyclotron Radius

$$r_{\text{Oplus}_c} = \frac{m_{\text{Oplus}} \cdot v_{\text{perp}}}{e \cdot B}$$

$$r_{\text{Oplus}_c} = 52.71 \cdot \text{m}$$

Cyclotron Frequency

$$\omega_{\text{Oplus}_c} = \frac{e \cdot B}{m_{\text{Oplus}}}$$

$$\omega_{\text{Oplus}_c} = 1.9 \cdot 10^2 \cdot \text{sec}^{-1}$$

Cyclotron Period

$$P_{\text{Oplus}_c} = \frac{2 \cdot \pi \cdot r_{\text{Oplus}_c}}{v_{\text{perp}}}$$

$$P_{\text{Oplus}_c} = 0.03 \cdot \text{sec}$$

Calculation of Mean Free Path for Charge Exchange between CRRES Particles and O^+ .

From Kittel (1969), the definition of the mean free path is:

$$l = \frac{1}{\pi \cdot d^2 \cdot n}$$

where n is the number density of the target species and $\pi \cdot d^2$ is the cross sectional area.

For barium or strontium interacting with ambient oxygen ions, n is the number density of O^+ and the area is the charge exchange cross section.

Barium:

$$\sigma_{Ba} = 7 \cdot 10^{-20} \cdot m^2 \quad n_{Oplus} = 10^{12} \cdot m^{-3}$$

$$l_{Ba} = \frac{1}{\sigma_{Ba} \cdot n_{Oplus}} \quad l_{Ba} = 1.43 \cdot 10^7 \cdot m$$

Strontium

$$\sigma_{Sr} = 8 \cdot 10^{-21} \cdot m^2 \quad n_{Oplus} = 10^{12} \cdot m^{-3}$$

$$l_{Sr} = \frac{1}{\sigma_{Sr} \cdot n_{Oplus}} \quad l_{Sr} = 1.25 \cdot 10^8 \cdot m$$

These are both very large distances and are bigger than the cloud diame

Bibliography

- Alfven, Hannes, On the Origin of the Solar System, The International Series of Monographs on Physics, Clarendon Press, Oxford, 1954.
- Axnas, I. and N. Brenning, Experiments on the Magnetic Field and Neutral Density Limits on CIV Interaction, Advances in Space Research, 10(7), (7)27-(7)30, 1990.
- Axnas, I. and N. Brenning, CIV Interaction: Laboratory Experiments on the Magnetic Field and Neutral Density Limits, Plasma Physics and Controlled Fusion, 33(1), 1-27, 1991.
- Bernhardt, P.A., Probing the Magnetosphere Using Chemical Releases from the Combined Release and Radiation Effects Satellite, Phys. Fluids B, 4(7), 2249-2256, 1992.
- Biasca, Rodger and Daniel Hastings, Upper Bound Estimates of Anomalous Ion Production in Space-Based Critical Ionization Velocity Experiments, Journal of Geophysical Research, 98(A10), 17569-17581, 1993.
- Brenning, N., Experiments on the Critical Ionization Velocity Interaction in Weak Magnetic Fields, Plasma Physics, 23(10), 967-977, 1981.
- Brenning, N., Limits on the Magnetic Field Strength for Critical Ionization Velocity Interaction, Physics of Fluids, 28(11), 3424-3426, 1985.
- Brenning, Nils, Review of the CIV Phenomenon, Space Science Reviews, 59(3/4), 209-314, 1992a.
- Brenning, Nils, A Comparison Between Laboratory and Space Experiments on Alfven's CIV Effect, IEEE Transactions on Plasma Science, 20(6), 778-786, 1992b.
- Carlsten, J.L., Photoionization of Barium Clouds via the ³D Metastable Levels, Planetary Space Science, 23, 53-60, 1975.
- Delamere, P.A., H.C. Stenbaek-Nielsen, D.L. Hampton, and E.M. Wescott, Optical Observations of the Early ($t < 5$ s) Ion Dynamics of the CRRES G1, G9, and G11A Releases, to be published in Journal of Geophysical Research, 1995.
- Drapatz, S.W., The Radiative Transfer Problem in Freely Expanding Gaseous Clouds and its Application to Barium Cloud Experiments, Planetary Space Science, 20, 663-682, 1972.

- Dyke, J.M., M. Feher, B.W.J. Gravenor, and A. Morris, High-Temperature Photoelectron Spectroscopy: A Study of the Alkaline Earth Oxides SrO and BaO, Journal of Physical Chemistry, 91, 4476-4481, 1987.
- Goertz, C. K., S. Machida, and G. Lu, On the Theory of CIV, Advances in Space Research, 10(7), 33-45, 1990.
- Hallinan, Thomas J., Observed Rate of Ionization in Shaped-Charge Releases of Barium in the Ionosphere, Journal of Geophysical Research, 93(A8), 8705-8712, 1988.
- Hargreaves, J. K., The Solar-terrestrial Environment, Cambridge University Press, Cambridge, Great Britain, 1992.
- Huba, J.D., H.G. Mitchell, J.A. Fedder, and P.A. Bernhardt, 'Skidding' of the CRRES G-9 Barium Release, Geophysical Research Letters, 19(11), 1085-1088, 1992.
- Hunton, D. E., Charge Transfer Reactions of Metastable Ba(I) and Sr(I) in the CRRES G-11b Chemical Release Experiment, unpublished, 1994.
- Hunton, D. E., Long-term Expansion Characteristics of CRRES Barium Release Clouds, Geophysical Research Letters, 20(7), 563-566, 1993.
- Johnson, M.H. and John Kierein, Combined Release and Radiation Effects Satellite (CRRES): Spacecraft and Mission, Journal of Spacecraft and Rockets, 29(4), 556-562, 1992.
- Kelley, Michael C., The Earth's Ionosphere: Plasma Physics and Electrodynamics, Academic Press, Inc., San Diego, 1989.
- Kittel, Charles, Thermal Physics, John Wiley & Sons, Inc., New York, 1969.
- Lai, Shu, William J. McNeil, and Edmond Murad, The Role of Metastable States in Critical Ionization Velocity Discharges, Journal of Geophysical Research, 93(A6), 5871-5878, 1988.
- Lai, Shu T., Edmond Murad, and William J. McNeil, An Overview of Atomic and Molecular Processes in Critical Velocity Ionization, IEEE Transactions on Plasma Science, 17(2), 124-134, 1989a.
- Lai, Shu T. and Edmond Murad, Critical Ionization Velocity Experiments in Space, Planetary Space Science, 37(7), 865-872, 1989b.
- Lai, Shu T., Edmond Murad, and William J. McNeil, Critical Ionization Velocity in a Mixture of Species, Planetary Space Science, 38(8), 1011-1016, 1990.

- Lai, Shu T., Edmond Murad, and William J. McNeil, Effects of Altitude on Critical Ionization Velocity Experiments in Space, Planetary Space Science, 39(12), 1707-1713, 1991.
- Lai, Shu T., Edmond Murad, and William J. McNeil, Amplification of Critical Velocity Ionization by Associative Ionization, Journal of Geophysical Research, 97(A4), 4099-4107, 1992a.
- Liou, K. and R. B. Torbert, On Ba^+ Production in the CRIT II Experiment, Journal of Geophysical Research, 100(A4), 5811-5818, 1995.
- Ma, T.Z. and R.W. Schunk, Ionization and Expansion of Barium Clouds in the Ionosphere, Journal of Geophysical Research, 98(A1), 323-336, 1993.
- McFarland, Robert H., Electron-Impact Ionization Measurements of Surface-Ionizable Atoms, Physical Review, 159(1), 20-26, 1967.
- McNeil, William J., Shu T. Lai, and Edmond Murad, Interplay Between Collective and Collisional Processes in Critical Velocity Ionization, Journal of Geophysical Research, 95(A7), 10345-10356, 1990.
- Mitchell, H.G. Jr., J.A. Fedder, J.D. Huba, and S.T. Zalesak, Transverse Motion of High-Speed Barium Clouds in the Ionosphere, Journal of Geophysical Research, 90(A11), 11091-11095, 1985.
- Mobius, E., K. Papadopoulos, and A. Piel, On the Turbulent Heating and the Threshold Condition in the Critical Ionization Velocity Interaction, Planetary Space Science, 35(3), 345-352, 1987.
- National Oceanic and Atmospheric Administration, National Aeronautics and Space Administration, and United States Air Force. U.S. Standard Atmosphere, 1976. Washington, D.C.: GPO, October, 1976.
- Newell, Patrick T. and R. B. Torbert, Competing Atomic Processes in Ba and Sr Injection Critical Velocity Experiments, Geophysical Research Letters, 12(12), 835-838, 1985.
- Parks, George K., Physics of Space Plasmas: An Introduction, Addison-Wesley Publishing Company, Redwood City, California, 1991.
- Person, James C., David Resendes, and Harry Petschek, Effects of Collisional Processes on the Critical Velocity Hypothesis, Journal of Geophysical Research, 95(A4), 4039-4055, 1990.
- Reasoner, David L., Chemical-Release Mission of CRRES, Journal of Spacecraft and Rockets, 29(4), 580-584, 1992.

- Rishbeth, Henry, and Owen K. Garriott, Introduction to Ionospheric Physics, Academic Press, New York, 1969.
- Rodriguez, P., Overview of the LASSII Experiment on the Combined Release and Radiation Effects Satellite, Journal of Spacecraft and Rockets, 29(4), 564-565, 1992.
- Stenbaek-Nielsen, H.C., E.M. Wescott, D. Rees, A. Valenzuela, and N. Brenning, Non-Solar UV Produced Ions Observed Optically from the "CRIT I" Critical Velocity Ionization Experiment, Journal of Geophysical Research, 95(A6), 7749-7757, 1990a.
- Stenbaek-Nielsen, H.C., E.M. Wescott, and T.J. Hallinan, Observed Barium Emission Rates, Journal of Geophysical Research, 98(A10), 17491-17500, 1993.
- Swenson, G.R., S.B. Mende, R.E. Meyerott, and R.L. Rairden, Charge Exchange Contamination of CRIT-II Barium CIV Experiment, Geophysical Research Letters, 18(3), 401-403, 1991.
- Szuszczewicz, E.P., D.E. Hunton, J.R. Wygant, and R.W. Schunk, Observations and Model Comparisons of Early-time Expansion Characteristics of a Satellite-borne Barium-Lithium Release at F-region altitudes, Geophysical Research Letters, 20(19) 2031-2034, October 8, 1993.
- Tascione, Thomas F., Introduction to the Space Environment, Orbit Book Company, Inc., Malabar, Florida, 1988.
- Torbert, R.B. and Patrick T. Newell, A Magnetospheric Critical Velocity Experiment: Particle Results, Journal of Geophysical Research, 91(A9), 9947-9955, 1986.
- Trzcinski, E., J. F. Borghetti, L. Wlodyka, G. Federico, and D. E. Hunton, NRL-701 LASSII/QIMS Quadrupole Ion Mass Spectrometer on CRRES, Journal of Spacecraft and Rockets, 29(4), 604-606, 1992.
- Vainshtein, L.A., V.I. Ochkur, V.I. Rakhovskii, and A.M. Stepanov, Absolute Values of Electron Impact Ionization Cross Sections for Magnesium, Calcium, Strontium and Barium, Soviet Physics JETP, 34(2), 271-275, 1972.
- Vampola, A.L., Combined Release and Radiation Effects Satellite, Journal of Spacecraft and Rockets, 29(4), 555, 1992.
- Weast, Robert C., ed. CRC Handbook of Chemistry and Physics. Cleveland, Ohio: CRC Press, Inc., 55th ed., 1974-1975.

Wescott, Eugene M., Hans Stanbaek-Nielsen, and Daniel W. Swift, Sr90, Strontium Shaped-Charge Critical Ionization Velocity Experiment, Journal of Geophysical Research, 95(A12), 21069-21075, 1990.

Wescott, E.M., H.C. Stenbaek-Nielsen, D.L. Hampton, and P.A. Delamere, Results of Critical Velocity Experiments with Barium, Strontium, and Calcium Releases from CRRES Satellite, Journal of Geophysical Research, 99(A2), 2145-2158, 1994.

Wolf, Paul J., Calculation of Charge Exchange Cross Sections for Barium and Strontium with Atomic Oxygen Ions, unpublished, 1995a.

Wolf, Paul J., Rate of Equilibrium Calculations for Barium and Strontium, unpublished, 1995b.

Vita

Capt Timothy M. Shadid [REDACTED] He graduated from Woodruff High School in 1986 and received an appointment to enter the United States Air Force Academy in Colorado Springs, Colorado. He finished his studies there and earned a Bachelor of Science in Engineering Physics, graduating and receiving a commission in the United States Air Force as a second lieutenant on 30 May 1990. He entered the weather career field and was required to complete studies at Texas A & M University as part of the Basic Meteorology Program. He graduated with a second Bachelor of Science in meteorology in December 1991 and subsequently reported to Shaw AFB, South Carolina for duty as wing weather officer. While there he deployed to Southwest Asia in support of Operation Southern Watch in the summer of 1993. In May 1994, he entered the School of Engineering Physics, Air Force Institute of Technology.

Permanent Address: [REDACTED]

[REDACTED]
[REDACTED]

REPORT DOCUMENTATION PAGE

Form Approved
OMB No. 0704-0188

Public reporting burden for this collection of information is estimated to average 1 hour per response, including the time for reviewing instructions, searching existing data sources, gathering and maintaining the data needed, and completing and reviewing the collection of information. Send comments regarding this burden estimate or any other aspect of this collection of information, including suggestions for reducing this burden, to Washington Headquarters Services, Directorate for Information Operations and Reports, 1215 Jefferson Davis Highway, Suite 1204, Arlington, VA 22202-4302, and to the Office of Management and Budget, Paperwork Reduction Project (0704-0188), Washington, DC 20503.

1. AGENCY USE ONLY (Leave blank)	2. REPORT DATE Dec 95	3. REPORT TYPE AND DATES COVERED
----------------------------------	--------------------------	----------------------------------

4. TITLE AND SUBTITLE Analysis and Interpretation of Ion Data Associated with Neutral Gas Releases in the Earth's Ionosphere	5. FUNDING NUMBERS
---	--------------------

6. AUTHOR(S) Capt Tim Shadid	
-------------------------------------	--

7. PERFORMING ORGANIZATION NAME(S) AND ADDRESS(ES) AFIT/ENP WPAFB, OH Lt Col Paul Wolf	8. PERFORMING ORGANIZATION REPORT NUMBER AFIT/GAP/ENP/95D-12
---	---

9. SPONSORING / MONITORING AGENCY NAME(S) AND ADDRESS(ES) Dr Don E Hunton Phillips Laboratory GPID Hanscom AFB, MA 01731	10. SPONSORING / MONITORING AGENCY REPORT NUMBER DSN: 478-4057 Comm: 617-377-4057
--	---

11. SUPPLEMENTARY NOTES

12a. DISTRIBUTION / AVAILABILITY STATEMENT Unlimited distribution	12b. DISTRIBUTION CODE
--	------------------------

13. ABSTRACT (Maximum 200 words)

Barium and strontium release experiments were conducted throughout 1991 from the Combined Release and Radiation Effects Satellite (CRRES) to study both natural and man-made disturbances in the earth's ionosphere. A mass spectrometer on the spacecraft counted the Ba and Sr ions as the cloud expanded. In this study, data from the G-1 (in sunlight) and G-11b (in darkness) releases were modeled to understand the source of the ion signals. The model reproduced the Ba⁺ sun data well assuming photoionization ($\tau = 28$ s) was the primary ionization mechanism. However, it was not able to account for the remaining ion data: (a) Sr has a very long photoionization time constant ($\tau = 1920$ s) and model/data comparisons showed that the Sr ionization rate must be ≈ 60 times greater than the photoionization rate to account for the observed signals. (b) The charge transfer ionization process between Sr/Ba and ambient O⁺ was not sufficient to reproduce the ionization rates for Sr sun data and Sr/Ba dark data. Processes potentially responsible for the CRRES data include charge stripping and critical velocity ionization (CIV). Split peaks in the ion data were also investigated and found to be due to either an instrument sensitivity feature or a two-process mechanism.

14. SUBJECT TERMS CRRES, ionosphere, barium, strontium, charge exchange, photoionization, charge stripping, electron impact, critical ionization velocity	15. NUMBER OF PAGES 146
	16. PRICE CODE

17. SECURITY CLASSIFICATION OF REPORT unclassified	18. SECURITY CLASSIFICATION OF THIS PAGE unclassified	19. SECURITY CLASSIFICATION OF ABSTRACT unclassified	20. LIMITATION OF ABSTRACT unlimited
---	--	---	---